Nanoscale quantum transport for quantum information processing

by

Farzad Qassemi Maloomeh

A thesis
presented to the University of Waterloo
in fulfillment of the
thesis requirement for the degree of
Doctor of Philosophy
in
Physics-Quantum Information

Waterloo, Ontario, Canada, 2012

I hereby declare that, with the exception of the material in the chapter 5, which is explicitly noted as the work of experimental collaborators, I am the sole author of this thesis. This is a true copy of the thesis, including any required final revisions, as accepted by my examiners.

I understand that my thesis may be made electronically available to the public.

Abstract

In this thesis, I study quantum transport of electron (e.g., current and noise) in quantum dots exploring microscopic processes responsible for spin-relaxation in double quantum dots in Pauli spin blockade regime. This is a regime where current is blocked due to the spin configuration of electrons in the dot. The Pauli spin blockade provides a means for preparation, manipulation and readout in spin qubits. Hence, understanding the underlying mechanism which lifts this blockade is extremely important.

First, I have developed a theory of spin-flip cotunneling (higher order tunneling) processes in double quantum dots in the Pauli spin blockade regime. Utilizing this theory, I have calculated the full analytical dependence of the stationary current on applied magnetic fields, gate voltages, and an inter-dot tunnel coupling in Pauli spin blockade. This work is important for understanding the nature of leakage, especially in systems where other spin-flip mechanisms (due, e.g., hyperfine coupling to nuclear spins or spin-orbit coupling) are weak, including silicon and carbon-nanotube or graphene quantum dots. This theory explains recent experiments on carbon nanotubes and silicon double quantum dot.

In addition, I propose a new scheme based on the current noise to probe spin-relaxation mechanisms in double quantum dot in the Pauli spin blockade regime, where spin-selection rule applies. As a result, I provide a simple closed-form expression which can be used to fit experimental data to extract multiple spin-relaxation rates, even at very low energy splitting. This method allows for the characterization of different aspects of decay process in these systems.

Acknowledgements

It is an honor to acknowledge here all of those who contributed to this thesis and made this work possible. I apologize if I have overlooked some names.

First and formest, I would like to thank my adviser, Prof. Frank Wilhelm, for giving me a chance to join the Quantum Device Theory group at the University of Waterloo. His enormous contribution to my thesis, in form of ideas and guidance, provided me with better understanding of my research. I am deeply grateful for being part of his group that comprises some of the best students and researchers in my field of study. I would especially thank Prof. Xuedang Hu, Prof. Tonny Leggett, Prof Jonathan Baugh, and Prof. Anton Burkov who chaired my defense committee.

Since I started my PhD, Bill Coish, former post-doctoral fellow at IQC, took me under his wings, taught me not only physics but also how to communicate and write physics. His physics intuition and skills in different mathematical techniques helped me immensely in my thesis. I especially appreciate his patience on occasions when I had to frequently ask him questions. He also became a good friend, with whom I could discuss various events happening in our group or in my life. I am also indebted to my colleagues: Peter Groszkowski, Felix Motzoi, Botan Khani, Jay Gambetta, Emily Pritchett, and Seth Merkel.

Furthermore, I would like to thank Prof. Birgitta Whaley for providing an opportunity for me to visit her group at the University of California, Berkeley. I especially thank her availability and communication resources. Moreover, I am grateful to my former advisers, Prof. Martin Houde who encouraged me to further pursue theoretical physics in my PhD, and Prof. Gerry McKeon whose insightful advices will always be with me.

I did my undergraduate studies at the Shahid Beheshti University of Iran, formerly known as the National University of Iran. There I benefited from lectures given by Prof. Mir Fakhraee, Prof. Azizi, and Prof. Goshtasbpoor. Prof. Goshtasbpoor helped me in an early undergraduate work that led to my first research project, for which I am eternally grateful. I would like to take this opportunity ac-

knowledge all the help and support that my undergraduate teachers, my classmates and the staff at Shahid Beheshti Univ provided me with.

Here, I would like to acknowledge Massoud Borhani who helped me to prepare this manuscript. Furthermore, since I started my graduate studies, Ardeshir Eftekharzadeh has always been available for fruitful discussions and for improving my academic writing. I would like to thank Massoud and Ardeshir for being patient with me and for being good friends. I want to also thank my fantastic friends in Waterloo for providing a warm and friendly environment during my studies. Finally, I cordially thank all of my family members, particularly my wife, Mona Khaleghy Rad, for their continuous support and for being there when I needed their help; When I look through these pages, I see them everywhere.

Dedication

I dedicate this thesis to my parents and my best friend who is also my Wife.

Contents

List of Tables

List of Figures

Chapter 1

Introduction

The rapid progress of nanoengineering in the last decades has enabled the development of wide variety of low dimensional nanostructures. A quantum dot is a confined region in nanostructures, enabling us to trap electrons and holes. At these short scales, quantum mechanical effects in combination with Coulomb interactions, immensely affect the observable physical properties.

There are several experimental realizations of quantum dots, including self assembled [80, 91], vertical [4, 129], and laterally defined quantum dots in semiconductor heterostructures [77], carbon nanotubes [88, 11, 120], and graphene nanostructures [92]. In this thesis, we focus on electron transport in 2D lateral quantum dots in semiconductor heterostructures. In these materials, the band structure causes the conduction electrons to be confined in the direction of heterointerface, however, the electrons can freely move in the transverse direction, and form a two dimensional electron gas (2DEG). In such 2DEGs, a quantum dot is formed by patterning metallic top gates. It is possible to isolate a pool of electrons, a quantum dot, by applying a negative voltage to these gates. The primary advantage of this type of quantum dots is that its properties such as the number of electrons in the dot, or the tunneling rates to the dot, can be tuned by adjusting the gate voltages.

Quantum dots are proven to be useful to investigate physical properties of model Hamiltonians in a controlled environment. For example, recently observed Klein tunneling in Graphene [64], was also demonstrated in tunable double quantum dot

[127]. Normally to observe such phenomena a large electric field is required due to the large rest mass of a free electron, however, the low effective rest mass of the electrons in small-band gap nanotubes makes the observation of Klein tunneling in carbon nanostructures possible [64, 127]. As another example, quantum dots have provided a framework to experimentally test theoretical predictions about the Kondo model [89, 48, 93, 24, 69, 70, 2].

The range of applications of quantum dots is not limited to test model systems. Additionally, quantum dots provide a unique framework as future quantum devices. Semiconductor-based quantum electronics are extremely appealing, due to their commonalities with current classical electronics [85, 62]. Quantum dot can be used, as a spin filter [55], spin pump [133], or as a spin memory [112, 78].

Another important application of quantum dots is, as building blocks of quantum information processing, where this thesis is devoted to. For quantum information purposes a quantum two level system, a qubit, is desired. The basic requirements for experimentally feasible realization of a qubit are, high-fidelity initialization, coherent manipulation and read-out. The electron spin is a true two-level quantum system, which is a natural candidate for realization of a qubit. In 1998, Loss and DiVincenzo in their seminal paper [85] have shown that all the necessary steps toward building a quantum computer can be achieved, using single electron rotation, and two electron spin coupling through exchange interaction. Since the original proposal by Loss and DiVincenzo, significant experimental progress has been made. The first experimental demonstration of single electron manipulation was achieved by Koppens et al [73] in 2006. Petta et al [102] successfully realized coherent coupling of two spins in two neighboring quantum dots. Moreover, Elzerman et al [33], and Hanson et al [54], performed different measurement schemes to detect the spin orientation in a quantum dot.

Pauli spin blockade [98], where current through a double quantum dot is blocked conditional on the microscopic spin state of electrons due to Pauli exclusion principle, is useful in initialization, manipulation and read-out. The Pauli spin blockade is, however, imperfect; any source of spin-flip can lift this blockade. Different

mechanisms which can induce spin-flip include, spin-orbit interaction , hyperfine interaction, or dot-lead higher order tunneling (cotunneling) [109, 79, 84]. One of the major issues in heterostructures, is the presence of nuclear spins in (some of) the host material, leading to relatively short spin relaxation and coherence times [40, 39, 65, 99, 1, 74, 18]. However, recently several methods have been suggested to suppress the effect of hyperfine interaction [68, 47, 43]. Interplay of nuclear spin and electron spin offer an interesting platform to study quantum many body effects in real systems [115, 104, 116, 86, 117]

The spin-orbit interaction causes spin relaxation by providing a mechanism for coupling electron spin to electric fluctuations in the leads [67, 50, 118, 51]. This coupling induces spin-relaxation and since the relaxation necessarily destroys superposition, it sets an upper bound on the decoherence time through $T_2 \leq 2T_1$.

In order to avoid spin relaxation by nuclear spin and spin-orbit interaction one can use materials with small spin-orbit coupling and no net nuclear spin such as carbon or silicon [18, 79]. Even in these materials, spin-mixing occurs due to natural interaction of electron spins with leads through cotunneling [83, 132, 109]. Usually, cotunneling is relatively small compared to the other spin-flip mechanisms, however, recent theoretical studies have shown that cotunneling could be important to better understand the electron transport in quantum dots [83, 132, 109, 22]. These theoretical studies have recently been supported by experimental observation of leakage current in silicon double dot [79], and carbon nanotubes [138].

Although all necessary steps toward quantum computation using electron spins are provided, yet the full control over electron spin requires a through understanding of interactions between the electron spin and its environment. For example, a complete theoretical picture of spin decay in quantum dots is still missing [18, 138].

The organization of this thesis is as follows. In chapter 2 we review the basic physics of lateral double quantum dots. We also briefly review the spin-orbit and hyperfine mediated relaxation in quantum dots. In chapter 3, we discuss the spin-flip cotunneling in double quantum dot in the Pauli spin blockade. This chapter is published in the Physical Review Letters [109]. In chapter 4, we extend our previous

studies to develop an analytical equations for leakage current at finite temperature, magnetic field and detuning. This chapter is published in Physical Review B [22]. In chapter 5, the theoretical and experimental aspects of singlet-triplet spin qubit in silicon qubits are studied. This chapter is published in Nature, Scientific Reports [79]. In chapter 6, we present a novel method to probe different relaxation rates in a double quantum dot using finite frequency current autocorrelation. Finally in chapter 7, we summarize the work presented in this thesis and possible future research directions.

As a main author in the first two papers, I was responsible to carry out calculations, develop the texts, and create figures. In the third paper, I analyzed and discussed the experimental data with the experimental group. Additionally, I was responsible to develop the theory for this experiment, and I have also contributed in writing the manuscript. The details for my contribution is stated at the end of this paper.

Chapter 2

Double quantum dots

In this chapter, we provide the background information necessary to follow the rest of this thesis. We briefly review the physical features of lateral quantum dots. There are many excellent reviews on quantum dots (e.g. see Ref. [53]), which we frequently refer to. First, we provide a cursory introduction to the physical properties of a two dimensional electron gas (2DEG). In sec. 2.2 we go over the transport properties in the Coulomb blockade regime. In sections 2.3 and 2.4, we explain the double quantum dot charge stability and Pauli spin blockade, respectively. Finally, in sec. 2.5, hyperfine and spin-orbit mediated spin relaxation in quantum dots are discussed.

2.1 Lateral quantum dots

In a typical lateral quantum dot in semiconductor heterosctures, electrons are confined between two semiconductor layers which have different band gaps. For example, in a AlGaAs/GaAs heterostructure a 2DEG is formed between undoped GaAs and AlGaAs. Additionally, such structures consist of dopant atoms (e.g., Silicon donors), which are placed at some distance away from the interface. Silicon is an n-type dopant, and the electrons move from AlGaAs to GaAs, leaving behind the positively charged ions. Due to the separation between positive and negative charges, an electric field is produced in the direction of charge transfer, which limits

the amount of transferred electrons. Since there is an offset between AlGaAs and GaAs bandgap, the electrons remain trapped at the interface (See Fig. 2.1). Due to large level spacing in the direction of material growth, the electrons are confined at the interface, while they are free to move in the transverse direction. A set of gates are patterned on the surface of heterostructure, which are capacitively coupled to the electron distribution in the 2DEG underneath. Finally, a quantum dot is formed by isolating electrons in a small region of 2DEG (typically less than 100 nm) by applying negative voltages to the gate electrodes.

Several energy scales are relevant to the understanding of the general properties of the charge states in the quantum dots in 2DEG. The first is the temperature, T, which determines the broadening of the Fermi distribution in the leads. Typically, an electron temperature between 50mk-150mk is achieved in dilution refrigerators. The second important energy scale is the orbital level energy spacing, due to spatial confinement of electrons. Similar to a particle in a box, this energy spacing is roughly $\Delta E \sim \frac{\hbar^2}{2m^* a}$, where a is the length scale of the confining potential, m^* is the effective electron mass, and $\hbar$ is the Plank constant. For example, for GaAs, $m^* = 0.067 m_e$, where m_e is the electron free mass. Typically, this level spacing in quantum dots is in the order of a few meV. If the electrons were non-interacting, they would fill energy levels according to the Hund's rule, with two electrons (with opposite spins) in each orbital, until all the energy levels below the Fermi level are filled. However, due to electron-electron Coulomb repulsion, it takes a certain amount of energy, the so-called charging energy, to add the second electron in the dot. In constant-interaction model, charging energy is characterized by $U \sim \frac{e^2}{C}$, where C is the sum of all capacitance to the dot.

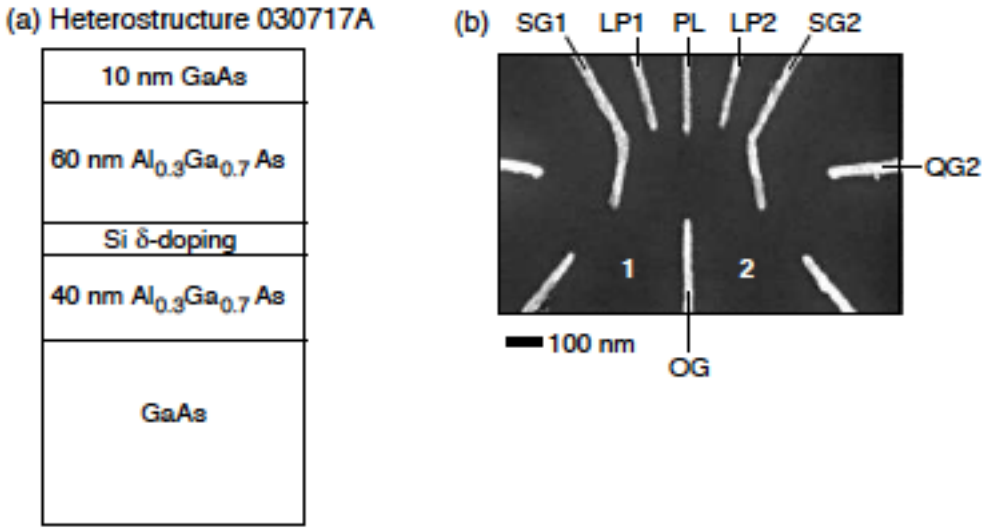

Figure 2.1: a) Schematic of heterostructure materials used for the fabrication of 2DEGs. b) Electron micrograph of the gates geometry in a lateral quantum dot [3]. The gates SG1, LP1, PL, LP2, SG2, and OG are used to form a quantum dot coupled to the source and the drain (labeled 1 and 2), by two tunnel barriers. A quantum point contact (QPC) is formed by applying a negative voltage to the gate QG2.

2.2 Electron transport in a single dot: Coulomb blockade

A common method for probing a quantum dot is to apply a source-drain voltage across the quantum dot, and then measure the electron transport through the quantum dot. The interplay between different energy scales mentioned in the previous section leads to interesting phenomena in quantum dots. In particular, Coulomb blockade corresponds to the regime where charging energy, U, dominates over other energy scales, i.e., $U \gg \Delta E \gg kT$. In this regime, the linear conductance (the measured current divided by the applied gate voltage) exhibits sharp resonances, where between these conductance peaks the measured current is exponentially suppressed, see fig. 2.2 b. This oscillatory feature is called, the Coulomb blockade oscillation. The Coulomb blockade can also be observed in measurements of nonlinear current characteristics of quantum dots. Coulomb blockade provides information about the orbital level spacing, charging energy, and spin states of single quantum dots [131, 53].

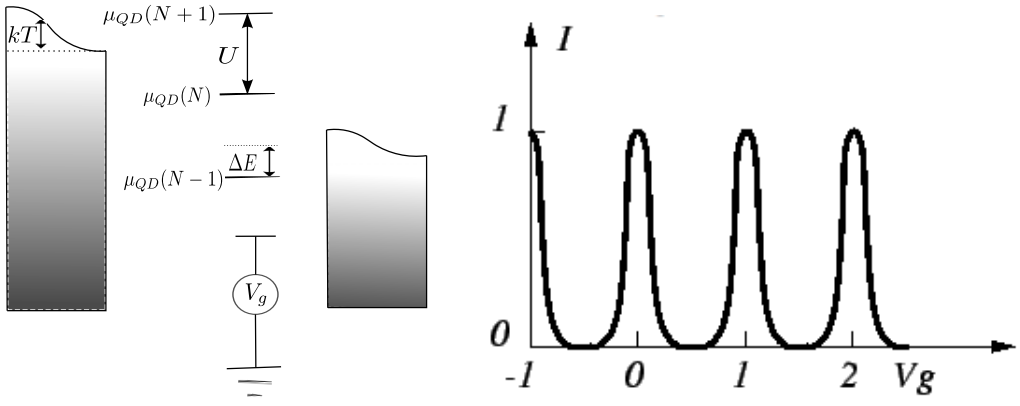

(a) (b)

Figure 2.2: (a) Energy diagram for a single electron in a quantum dot. All relevant energy scales namely the temperature, kT, confining energy ΔE, and charging energy U are depicted in this picture. By changing the gate voltage V_g, the electron chemical potential, $\mu_Q(N)$, in the dot changes, where N is the total number of electrons in the quantum dot. Once the dot chemical potential is placed between the left and right leads Fermi energy, electrons can hop on and off the dot. (b) Schematic plot of current vs. gate voltage in Coulomb blockade regime.

We use a simple, yet general and intuitive way, to explain Coulomb blockade in quantum dots. For this purpose, consider a quantum dot coupled to a source and a drain, Fig. 2.2 a. First, we focus on the occurrence of conductance peaks, as a function of the applied gate voltage. Here, we consider only (first-order) energy-conserving processes. Starting from an empty quantum dot, electrons can only tunnel through the dot when the chemical potential of QD falls within the bias window, i.e. when $\mu_s \geq \mu_{QD}(N) \geq \mu_d$. Here μ_s and μ_d are the source and drain chemical potentials. μ_{QD} is the quantum dot chemical potential, which depends linearly on the gate voltage. Hence, we can control the number of electrons in quantum dots by changing the gate voltage.

To better understand the dot chemical potential quantitatively, we model the quantum Hamiltonian of an isolated quantum dot using the Hubbard model, where the details of the electron's wave function are neglected and the Coulomb interaction is given only in terms of on-site interaction [53],

$$H_{QD} = \sum_{k,\sigma} \epsilon_{k\sigma} n_{k\sigma} + \frac{1}{2} UN(N-1) - eV_g N, \tag{2.1}$$

where $\epsilon_{k\sigma}$ is the kth orbital energy, and $n_{k\sigma} = d^\dagger_{k\sigma} d_{k\sigma}$ gives the number of electrons in level k with spin σ, and $d_{k\sigma}/d^\dagger_{k\sigma}$ annihilates/creates electron in orbital level k with spin σ. $N = \sum_{k,\sigma} n_{k\sigma}$ counts the total number of electrons in the quantum dot, where N commutes with the quantum dot Hamiltonian. We can therefore, label the quantum dot energy levels by the number of electrons in the dot $E_{QD}(N) = \sum_{n=1}^{N} \epsilon_n + UN(N-1) - eV_g N$, where $\sum_{n=1}^{N} \epsilon_n$ is the sum over the occupied single-particle energy levels. Hence, the quantum dot chemical potential is given by $\mu_{QD}(N) = E_{QD}(N) - E_{QD}(N-1) + \epsilon_N$, where the single particle occupation energy ϵ_N is irrelevant in our discussion.

At large negative gate voltages, the dot contains zero number of electrons. Since the one electron state is above the Fermi energy of the leads, this energy offset forbids the electron tunneling. We can adjust one-electron chemical potential in the dot, via lowering the dot energy level by changing the electrode gate voltages on

the top. Once the dot chemical potential is within the bias window, $\mu_s \geq \mu_{QD} \geq \mu_d$, electrons can tunnel through the quantum dot. Thus, by shifting the gate voltage we can move the whole ladder of the electrochemical potential levels up or down, which leads to appearance of conductance peaks.

2.3 Charge stability diagrams

Consider two serially coupled quantum dots labeled by 1 (left) and 2 (right), whose electrochemical potential is controlled by independent gate voltages, V_1, V_2, applied locally to each quantum dot. Similar to the single quantum dot case, physical characteristics (energy levels, tunneling rates, etc) of double quantum dots can be probed by electron transport through the double dot. The primary tool used to understand double quantum dots is the charge stability diagram. The stability diagram is a two-dimensional plot of current, or differential conductance, through the double dot, or through a neighboring QPC, given as a function of applied gate voltages V_1, V_2 (See Fig. 2.3). This two-dimensional plot visualizes the equilibrium charge states of double quantum dots, which consists of regions where the double-dot has a charge configuration (N_1, N_2), for various N_1, N_2 (see fig. 2.3). Transport through double quantum dots, and the relevant charge stability diagram have been discussed thoroughly in [131].

To study differential conductance through the double dot, we start from a model Hamiltonian to obtain the electron state configurations in double quantum dots. Similar to the single quantum dot case, we use the Hubbard Hamiltonian to investigate properties of the isolated double quantum dot [23, 139],

$$H^C_{DQD} = \sum_{l,k\sigma} \epsilon_{lk\sigma} n_{lk\sigma} + \frac{1}{2} \sum_l U N_l (N_l - 1) + U' N_1 N_2 - \sum_l e V_l N_l \quad (2.2)$$

where U is the on-site Coulomb interaction for each dot, and U' is the interdot electrostatic repulsion in the double quantum dot. The effect of local top gate po-

tential is given by $V_{1(2)}$. The total number of electrons in each dot is represented by $N_{1(2)} = \sum_{k\sigma} n_{1(2)k\sigma}$, where $n_{1(2)k\sigma}$ is the left(right) dot occupation number operator. The Hamiltonian in equation 2.2 conserves the number of electrons on each dot, i. e., $[H^C_{DQD}, N_i] = 0$ for $i = 1, 2$, therefore, we label the ground state by the two-dot occupation numbers (N_1, N_2), where $N_1(2)$ is the number of electrons on the left(right) dot.

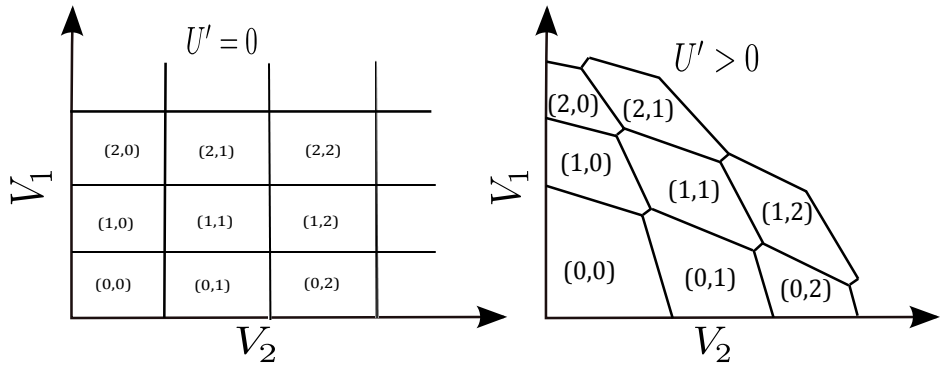

Figure 2.3: Charge stability diagrams for (a) capacitively decoupled and (b) coupled double quantum dots, labelled by the equilibrium electron numbers (N_1, N_2) in dots 1 and 2, respectively. The lines indicate the gate voltage values at which the electron number changes.

At each vertex, in the charge stability plot at finite interdot electrostatic Coulomb energy ($U' \neq 0$), three different charge states are energetically degenerate. These points are called triple points. At low source-drain bias voltages, electron transport through the double dot is only possible at these triple points. Transport at these triple points is extensively studied in [53].

2.4 Spin to charge conversion: Pauli spin blockade

In laterally confined double quantum dots, electrons can be moved from one dot to the other, by changing the gate voltages applied locally to each dot. The interdot

tunneling, which is due to electrons wave functions overlap at two quantum dots, is generally spin independent. Hence, in situations where initial and final spin states are orthogonal, the transition is forbidden by spin selection rules, leading to a phenomenon called Pauli spin blockade. To understand Pauli spin blockade, we first examine the spin states in the isolated (from source and drain leads) double dot, and the possible transitions between these spin states, neglecting spin-flip processes. These spin-flip mechanisms will be studied in the next section.

We work in the region of the charge stability diagram where the occupancy of the double dot changes from $(0,1) \rightarrow (1,1) \rightarrow (0,2) \rightarrow (0,1)$. For (0,1) and (0,2) charge configurations, the spin physics is identical to the single dot case since the left quantum dot is not occupied. In the (0,1) charge state, the two spin states are degenerate at zero magnetic magnetic field. However, an external magnetic field, B, induces a Zeeman splitting in the spin states, $\Delta E_Z = E_\uparrow - E_\downarrow$, where $\Delta E_Z = g\mu_B B$ is the Zeeman energy splitting (g is the electron gyromagnetic ratio and μ_B is the electron Bohr magneton). In the (0,2) charge state, there are four possible spin states: the singlet, denoted by $S(0,2) = (|(0,\uparrow\downarrow)\rangle - |(0,\downarrow\uparrow)\rangle)/\sqrt{2}$ and the three triplets $T_+(0,2) = |(0,\uparrow\uparrow)\rangle, T_-(0,2) = |0,\downarrow\downarrow\rangle$, and $T_0(0,2) = (|(0,\uparrow\downarrow)\rangle + |(0,\downarrow\uparrow)\rangle)/\sqrt{2}$. At zero magnetic field, the three spin triplets are degenerate, which are separated from spin singlet ground state by $U \sim meV$. Since most of experiments are performed in the bias regime that (0,2) spin triplets are energetically inaccessible, and in this thesis, we do not study their contributions to the transport through double quantum dot.

In the (1,1) charge state, the two-electron states are also form spin singlets and triplets, namely, $S(1,1) = (|(\uparrow,\downarrow)\rangle - |(\downarrow,\uparrow)\rangle)/\sqrt{2}$, $T_+(1,1) = |(\uparrow,\uparrow)\rangle, T_-(1,1) = |\downarrow,\downarrow\rangle$, and $T_0(1,1) = (|(\uparrow,\downarrow)\rangle + |(\downarrow,\uparrow)\rangle)/\sqrt{2}$. However, in this case electrons are localized in different dots. Here, the energy difference between the lowest-energy singlet and unpolarized spin triplet state depends on the tunneling and the single dot charging energy.

Recall that we are working at a triple point, where electrons are transferred through the double quantum dot $(0,1) \rightarrow (1,1) \rightarrow (0,2) \rightarrow (0,1)$. In this cycle the

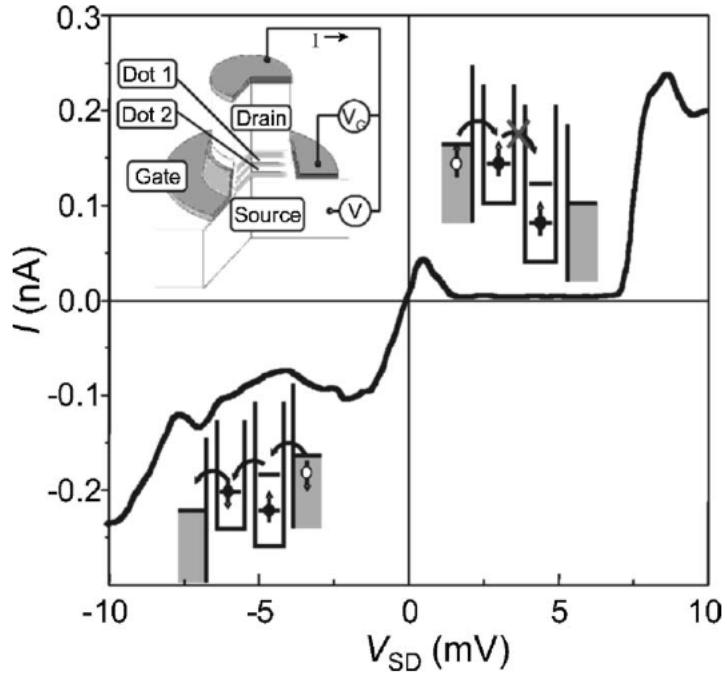

Figure 2.4: Current (I) as a function of source-drain voltage (V) in a vertical double dot system. Nonzero current is measured over the entire range of negative voltages. For positive bias, current is blocked in the range 2mv-7mV. At bias voltages exceeding 7 mV, the (0,2) triplet state becomes accessible and Pauli blockade is lifted. Insets: Device schematic and energy-level configuration at positive and negative bias voltages. This plot is reproduced from Hanson et al. [53].

right dot always contains at least one electron. Assume this electron is spin up. Once an electron tunnels from the source lead, the double dot can either form a spin triplet $T(1,1)$, or a spin singlet $S(1,1)$. If the two electrons form a singlet state $S(1,1)$, the electron in the left dot can transfer to the right dot forming $S(0,2)$. However, if electrons form one of the triplet states $T(1,1)$, the electron in the left dot will not be able to tunnel to the right dot, because $T(0,2)$ is not energetically favorable. Hence, in the absence of any spin-flip mechanism, the system will remain stuck in a $(1,1)$. Because it is the Pauli exclusion principle that forbids electrons to make a transition from a $T(1,1)$ state to $S(0,2)$, this blockade is also referred to as Pauli blockade. The origin of Pauli blockade is schematically illustrated in the insets of Fig. 2.4.

Pauli spin blockade was first observed in experiments on vertically coupled quan-

tum dots (Ono et al[98]). Later experiments in few-electron lateral dots combined charge sensing and transport to study this effect [60].

2.5 Spin-flip processes: Hyperfine interaction, spin-orbit coupling, and cotunneling processes

Electron spin states in a quantum dot are mixed due to coupling to the environment. As mentioned earlier in the introduction, there are three primary channels that an electron spin can couple to its surrounding, namely, spin-orbit interaction, hyperfine interaction, and cotunneling. The spin-orbit interaction couples the electron spin to its orbital state, and therefore, makes the spin sensitive to the electric fluctuations in the environment (e.g., due to phonons). Additionally, the hyperfine interaction, which couples the electron spin to the bath of nuclear spins of the host material. The hyperfine interaction is the main source of phase randomization (decoherence) in materials with non-zero nuclear magnetic moment, such as GaAs. The spin-orbit and hyperfine interaction strengths depend on the host material specifications. For example, the hyperfine interaction is suppressed in materials with zero net nuclear spin, such as silicon. The electron higher order tunnel coupling to the source and drain leads, also mixes the electron spin states together. It has been shown that in materials with no net nuclear spin, and with small spin-orbit coupling, cotunneling can explain the observed leakage current due to spin state mixing [79, 138].

In this section we give an overview of the spin-relaxation rates due to hyperfine and spin-orbit interactions. The spin-flip relaxation rates due to cotunneling in quantum dots have been explicitly calculated in Chapter 3.

2.5.1 Spin-orbit interaction

The spin-orbit interaction is a relativistic effect, which is caused by the electron motion through electric fields intrinsic to the semiconductor heterostructure [31, 111]. In the electron's rest frame, these electric fields transform to magnetic fields,

which interact with the electron spin.

There are two main contributions to the spin-orbit interaction in semiconductors. The first contribution is caused by the lack of inversion symmetry in the heterostructure, which gives rise to Rashba spin-orbit coupling [111]. The second contribution to the spin-orbit interaction is due to the lack of crystal inversion symmetry, which causes the Dresselhaus spin-orbit coupling [31].

In nearly two dimensional quantum dots, the dominant mechanism for spin-relaxation is due to the linear-in-momentum spin-orbit Hamiltonian given by [50],

$$H_{SO} = (\beta - \alpha)p_y\sigma_x + (\beta + \alpha)p_x\sigma_y, \tag{2.3}$$

where α and β are Rashba and Dresselhaus coupling strength, respectively. While the Dresselhaus coupling is fixed for a given semiconductor layer, the Rashba parameter is externally tunable by changing gate voltages.

The Rashba and Dresselhaus spin-orbit interactions have different symmetries, and this causes the spin relaxation rate to vary by changing the orientation of the applied magnetic field with respect to the heterostructure crystalline axes [50]. For some orientations of the field, the Rashba and Dresselhaus interactions are cooperate, and the relaxation rate is maximized. For other orientations, the interactions oppose one another, and the relaxation rate is suppressed. If the Rashba and Dresselhaus parameters are equal, then the two interactions can cancel one another at the minimum, and the spin relaxation would become dominated by other mechanisms, such as hyperfine-mediated relaxation. A priori the Rashba and Dresselhaus parameters are not necessarily equal.

2.5.2 Hyperfine Interaction

The wavefunction of an electron trapped in quantum dots is spatially extended over many lattice sites of the host crystal lattice. For example in GaAs, the element Ga comes in two stable isotopes in nature, which both have finite nuclear magnetic

moments with nuclear spin 3/2. In addition, the only stable isotope of As has nuclear spin 3/2. Each electron spin, therefore, can interact with a large ensemble of nuclei (typically 10^6). Similar to spin-orbit interaction discussed in the previous section (sec. 2.5.1), electron spin-nuclear spin hyperfine interaction comes naturally out of Dirac equation [42]. Assuming the electron wavefunction is just the product of orbital and spin component, the contact hyperfine interaction in terms of pure spin operator is expressed as,

$$H_{HF} \propto \sum_i A_i \mathrm{I}_i \otimes S, \tag{2.4}$$

where S is the electron spin operator, I_i is the nuclear spin operator at lattice site i, and A_i is the coupling between electron spin and nuclear spin at lattice site i. generally hyperfine interaction also contains an anisotropic part which has been neglected here. The product of spin operators can be rewritten in terms of spin-ladder operators as $\mathrm{I} \otimes S = \frac{1}{2}\left(\mathrm{I}_+ \otimes S_- + \mathrm{I}_- \otimes S_+\right) + S_z I_z$, where $X_\pm = X_x \pm X_y$ for $X = \mathrm{I}, S$. The first terms, $\mathrm{I}_+ \otimes S_- + \mathrm{I}_- \otimes S_+$, correspond to the electron spin-nuclear spin flip-flop term, where the electron spin flip is accompanied by a nuclear spin flop. This flip-flop term is the source of many interesting physical phenomena such as dynamic nuclear polarization [8, 115, 43]. The last term, $S_z I_z$, corresponds to a change in the electron Zeeman term, which due to the stochastic nature of nuclear spins ensemble, will cause decoherence in the electron spin state. The hyperfine interaction has been identified as the main source of decoherence in host materials with nonzero nuclear magnetic moment, such as GaAs [65].

The quantum behavior of the electron spin in the presence of a bath of nuclear spins is the subject of recent studies [114, 86]. However, the action of nuclear spins ensemble can be approximated by a classical magnetic field called Overhauser field, where an electron experiences an effective magnetic field given by [20],

$$B_N = \frac{1}{g\mu_B} \sum_i A_i \left\langle \mathrm{I}_i \right\rangle, \tag{2.5}$$

where $\langle ... \rangle$ indicates the expectation value with respect to the nuclear spin state. For

large electron Zeeman splitting, $\Delta E_Z \gg g\mu_B B_N^{x,y}$, hyperfine interaction effectively does not mix spin states together. However, similar to the spin-orbit interaction, hyperfine interaction leads to mixing of electron spin and orbital states. Then, phonons would cause transitions between perturbed electron spin states.

In the following table spin-relaxation rates in terms of confining potential $\hbar\omega$ and Zeeman splitting $\Delta E_Z = |g|\mu_B B$ are presented at zero temperature limit [3],

Mechanism	W_{sf}
Hyperfine+piezoelectric phonon	$\propto \Delta E_Z^3 (\hbar\omega_0)^{-2}$
Hyperfine+Ohmic fluctuation	$\propto \Delta E_Z (\hbar\omega_0)^{-2}$
Spin-orbit+piezoelectric phonon	$\propto \Delta E_Z^5 (\hbar\omega_0)^{-1}$
Spin-orbit+Ohmic fluctuation	$\propto \Delta E_Z^3 (\hbar\omega_0)^{-1}$

Table 2.1: Summary of spin-orbit and hyperfine induced relaxation mechanism with their dependence on the relevant energy scales at zero temperature limit, are given here. W_{sf} denote spin-flip rates between electron spin states. At high magnetic fields, spin-orbit interaction dominates but at low magnetic fields other mechanisms may contribute. Ohmic fluctuations correspond to voltage fluctuations intrinsic to a conductor, and are present in the gates and the ohmic leads.

Chapter 3

Stationary and Transient Leakage Current in the Pauli Spin Blockade regime

3.1 Outline

We study the effects of cotunneling and a non-uniform Zeeman splitting on the stationary and transient leakage current through a double quantum dot in the Pauli spin blockade regime. We find that the stationary current due to cotunneling vanishes at low temperature and large applied magnetic field, allowing for the dynamical (rapid) preparation of a pure spin ground state, even at large voltage bias. Additionally, we analyze current that flows between blocking events, characterized, in general, by a fractional effective charge e^*. This charge can be used as a sensitive probe of spin relaxation mechanisms and can be used to determine the visibility of Rabi oscillations.

3.2 Introduction

Initialization and readout of well-defined quantum states are necessary for spin coherence measurements [102, 113, 75], single-spin resonance [73, 97, 107], and quan-

tum information processing. Single electron spins in quantum dots show promise for quantum information tasks [85] due to their long coherence times, but their quantum states can be difficult to initialize (relying on slow spin relaxation processes) and read out. The Pauli spin blockade (PSB) [98] partially solves these problems, where current through a double quantum dot (DQD) is blocked conditional on the microscopic spin state of electrons.

The PSB is, however, imperfect; hyperfine interaction between electron and nuclear spins in III-V semiconductors lifts spin selection rules and can lead to a finite leakage current [99, 74, 38, 44, 61, 59, 6]. Very recently, PSB has been observed in DQDs made from silicon [84, 122] and carbon nanotubes [18, 19], in which the majority isotope has no nuclear spin. Even in these systems, the PSB can be lifted through spin exchange with the leads due to, e.g., cotunneling processes [83, 134, 132]. Significantly, cotunneling events have been shown to be essential even in nuclear-spin-carrying quantum dots to describe nuclear-spin polarization in the PSB regime [8, 115], and therefore should be taken into account.

Single-spin resonance measurements often rely on the transient current that flows before current is blocked as a probe of the electron spin state [73, 97, 107]. An anomalously large transient current has recently been found [73], characterized by an effective charge e^* that passes through a DQD between blocking events. Without a complete understanding of this additional leakage, it may not be possible to determine the visibility of Rabi oscillations in these systems.

3.3 Our model

Here, we evaluate both the stationary and transient leakage current through a DQD, giving simple analytical expressions for the stationary current and the transient effective charge e^*. We find that e^* reaches universal fractional values and that a measurement of e^* in general can be used to extract valuable information related to slow spin relaxation processes.

We consider a series-coupled DQD in a magnetic field gradient (Fig. 3.1(a)).

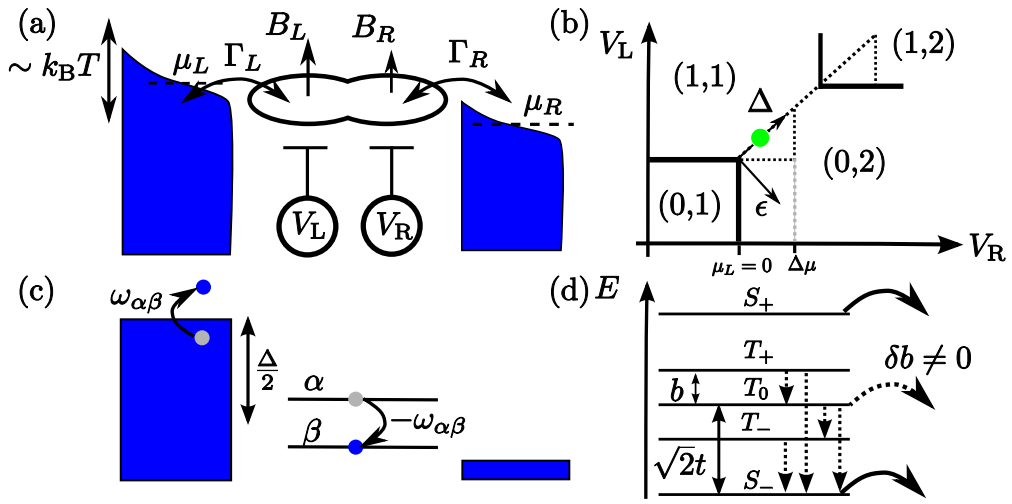

Figure 3.1: A DQD coupled to leads (a). The charge stability diagram is shown in (b). At low temperature, inelastic cotunneling (c) induces transitions to lower-energy dot levels. Two-electron states at $\epsilon = 0$ are shown in (d) with allowed $T = 0$ cotunneling transitions indicated with straight dashed arrows and curved arrows indicating sequential-tunneling processes.

A field gradient is important in spin resonance experiments for local addressing, and may arise from the stray field of a nanomagnet [107] or the Overhauser field due to non-uniformly polarized nuclear spins [73]. We work in a regime where only the $(0,1)$, $(1,1)$, and $(0,2)$ charge states are relevant (the triangular region in Fig. 3.1(b)). Here, (n_L, n_R) indicates n_l electrons in dot orbitals $l = \{L, R\}$. The Hamiltonian in this projected subspace is $H = H_0 + V$, where

$$H_0 = \sum_j E_j \left|j\right\rangle \left\langle j\right| + \sum_{lk\sigma} \epsilon_{lk} c^\dagger_{lk\sigma} c_{lk\sigma}, \tag{3.1}$$

$$V = \delta b \left|S\right\rangle \left\langle T_0\right| + \sum_{kl\sigma jj'} t_l A^{jj'}_{l\sigma} c_{lk\sigma} \left|j\right\rangle \left\langle j'\right| + \text{h.c.} \tag{3.2}$$

The first term in H_0 describes the eigenstates $\left|j\right\rangle = \{\left|\sigma\right\rangle, \left|\alpha\right\rangle\}$ of the unperturbed DQD, with single-electron states labeled by spin $\sigma = \{\uparrow, \downarrow\}$ and two-electron states labeled with α, shown in Fig. 3.1(d) (three spin triplets, ($\alpha = T_{m_s}$, $m_s = 0, \pm$) and two spin singlets, ($\alpha = S_\pm$), giving hybridized $(1,1)$ and $(0,2)$ charge states due to an interdot tunnel coupling t [1]). The second term in H_0 gives the energy

[1]Explicitly, the double-dot eigenstates are $\left|T_+\right\rangle = \left|\uparrow\uparrow\right\rangle$, $\left|T_-\right\rangle = \left|\downarrow\downarrow\right\rangle$, $\left|T_0\right\rangle = (\left|\uparrow\downarrow\right\rangle + \left|\downarrow\uparrow\right\rangle)/\sqrt{2}$, $\left|S_+\right\rangle = \cos\left(\frac{\theta}{2}\right)\left|S\right\rangle - \sin\left(\frac{\theta}{2}\right)\left|S(0,2)\right\rangle$, and $\left|S_-\right\rangle = \sin\left(\frac{\theta}{2}\right)\left|S\right\rangle + \cos\left(\frac{\theta}{2}\right)\left|S(0,2)\right\rangle$, where $\left|S\right\rangle =$

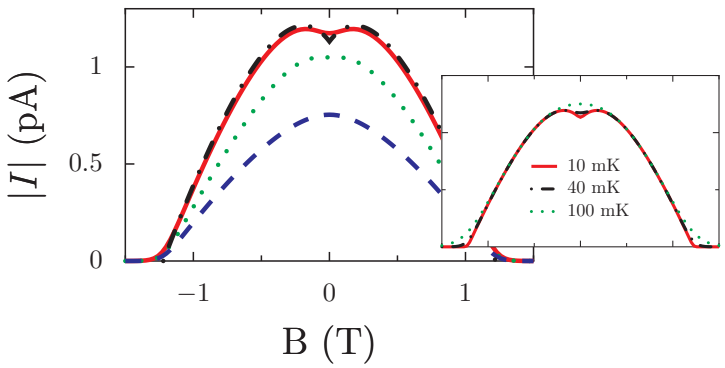

Figure 3.2: Leakage current in the PSB regime due to inelastic cotunneling processes. We have taken $\epsilon = 0$, $\Gamma_L = \Gamma_R = 10\,\mu eV$, $t = 100\,\mu eV$, $\Delta = 1\,meV$, and $g = 2.0$. We show the evolution of $I(B)$ as δB is varied from 0 mT (dashed line), to 20 mT (dotted line), 200 mT (solid line), and for $W_{T_0\to\sigma} \gg W_{\alpha\to\beta}$, $T = 0$ (dash-dotted line, from Eq. (3.7)). Evolution of the curve for $\delta B = 200\,\mathrm{mT}$ as temperature is raised is shown in the inset.

of Fermi-liquid leads. The Zeeman gradient $\delta b = g\mu_B(B_L - B_R)/2$ couples the $(1,1)$-singlet $|S\rangle$ and $m_s = 0$ triplet $|T_0\rangle$ (here, g is the g-factor and B_l is a local magnetic field in dot l). The second term in V describes hopping processes from dot l to lead l with coupling t_l and matrix elements $A^{jj'}_{l\sigma} = \langle j|\, d^\dagger_{l\sigma}\, |j'\rangle$. Here, $d^\dagger_{l\sigma}$ creates an electron in dot l with spin σ and $c^\dagger_{lk\sigma}$ creates an electron in lead l and orbital k, with spin σ.

Working from a standard Hubbard model for the DQD, we find the energies $E_{\uparrow(\downarrow)} = -(\epsilon + \Delta)/2 + (-)b/2$, where ϵ is the detuning (energy difference) between the $(1,1)$ and $(0,2)$ charge states and Δ controls the depth of the two-electron levels (see Fig. 3.1(c)). For the two-electron states, we have $E_{T_0} = -\Delta$, $E_{T_\pm} = -\Delta \pm b$, and $E_{S_\pm} = -\Delta - \epsilon/2 \pm \sqrt{\epsilon^2 + 8t^2}/2$, with $b = g\mu_B(B_L + B_R)/2$.

We solve for the diagonal elements of the reduced (DQD) density matrix ρ_i with the Pauli master equation:

$$\dot{\rho}_i = \sum_j (\rho_j W_{j\to i} - \rho_i W_{i\to j}). \tag{3.3}$$

We calculate the transition rates $W_{i\to j} = W^{\mathrm{st}}_{i\to j} + W^{\mathrm{cot}}_{i\to j}$ directly from Fermi's golden

$(|\uparrow\downarrow\rangle - |\downarrow\uparrow\rangle)/\sqrt{2}$, with $|\sigma\sigma'\rangle = d^\dagger_{L\sigma} d^\dagger_{R\sigma'}\,|0\rangle$ and $|S(0,2)\rangle = d^\dagger_{R\uparrow} d^\dagger_{R\downarrow}\,|0\rangle$. Here, $\tan\theta = -2\sqrt{2}t/\epsilon$.

rule. Here, the sequential-tunneling rates ($W^{\rm st}_{i\to j} = \sum_l W^l_{i\to j} \propto |t_l|^2$) describe direct hopping at leading order in the dot-lead coupling and the cotunneling rates ($W^{\rm cot}_{i\to j} \propto |t_l|^\eta$, $\eta > 2$) are higher-order in t_l.

We consider standard initial conditions, with lead l held in thermal equilibrium with Hamiltonian H_0 at chemical potential μ_l. At first order in V, only the second term in Eq. (3.2) contributes to transport, giving the usual sequential-tunneling rates ($\hbar = 1$) [112, 50]:

$$\begin{aligned} W^l_{\sigma\to\alpha} &= \sum_{\sigma'} \Gamma_l |A^{\alpha\sigma}_{l\sigma'}|^2 f_l(\omega_{\alpha\sigma}), \\ W^l_{\alpha\to\sigma} &= \sum_{\sigma'} \Gamma_l |A^{\alpha\sigma}_{l\sigma'}|^2 \left[1 - f_l(\omega_{\alpha\sigma})\right]. \end{aligned} \tag{3.4}$$

Here, $\Gamma_l = 2\pi\nu|t_l|^2$, where $\nu = \sum_k \delta(\epsilon_F - \epsilon_{lk})$ is the density of states per spin at the Fermi level, $f_l(E)$ is a Fermi function at temperature T and chemical potential μ_l, and $\omega_{ij} = E_i - E_j$.

For large bias, $\mu_L - \mu_R = \Delta\mu > |\Delta| > 2k_BT$, the stationary current is given by $I = e\sum_\alpha W^R_{\alpha\to\sigma}\bar{\rho}_\alpha$, where $\bar{\rho}_i$ is a solution to Eq. (3.3) with $\dot{\rho}_i = 0$. At leading order in V, current will be blocked if one of the triplet states is populated, since $W^R_{T_{m_s}\to\sigma} = 0$. This is the PSB effect. In the absence of other spin-relaxation mechanisms, higher-order contributions in V must be considered to explain a finite leakage current. At second order in V we find:

$$W^R_{T_0\to\sigma} = \Gamma_R \frac{\delta b^2}{8t^2}\left[1 - f_R(\omega_{T_0\sigma})\right], \tag{3.5}$$

$$W^{\rm cot}_{\alpha\to\beta} = \frac{2\Gamma_L^2}{\pi(\Delta-\epsilon)^2} \sum_{\sigma\sigma'\sigma''} |A^{\alpha\sigma''}_{L\sigma}|^2 |A^{\beta\sigma''}_{L\sigma'}|^2 F(\omega_{\alpha\beta}, T), \tag{3.6}$$

where $F(\omega, T) = \omega/(1 - e^{-\omega/k_BT})$. Eq. (3.5) gives the rate for field-assisted sequential-tunneling processes, where δb converts T_0 to a singlet, which can then escape from the DQD via first-order (sequential) tunneling to the right lead (see the curved dashed arrow in Fig. 3.1(d)). Eq. (3.6) gives the rate for an inelastic cotunneling process (Fig. 3.1(c)), allowing for conversion of triplets to singlets

(dashed straight arrows in Fig. 3.1(d)). A competition between the two rates in Eqs. (3.5) and (3.6) will determine the leakage current in the PSB regime when other spin relaxation mechanisms due, e.g., to hyperfine and spin-orbit interactions are suppressed. We note that Eq. (3.5) is independent of Γ_L, whereas Eq. (3.6) is independent of Γ_R, so an asymmetric coupling of the DQD to the leads will play a role in determining the relative scales of the two contributions.

At high temperature ($k_BT > |\omega|$) we have $F(\omega, T) \simeq k_BT$, a regime that has been explored previously [83, 132]. In this work, we focus on the low-temperature regime ($k_BT < |\omega|$), where $F(\omega, T) \simeq \omega\theta(\omega)$, giving rates that vanish linearly for small energy separation, with significant consequences (allowing, e.g., for the initialization of a pure spin state – see below). In Eq. (3.6), we have assumed $|\Delta - \epsilon| \gg |\omega_{\alpha\beta}|$ and have neglected resonant cotunneling contributions [71], which are exponentially suppressed for $\Delta/2 > k_BT$. Corrections due to spin exchange with the right lead are smaller in $\Delta/U' \ll 1$, where U' is the interdot charging energy. Additionally, we have considered the resonant tunneling regime [130] ($\epsilon \lesssim t$).

We have numerically solved for the stationary current using the rates given in Eqs. (3.4)-(3.6) and have plotted the result vs. $B = b/g\mu_B$ in Fig. 3.2. There is a sharp cutoff in the leakage current at large b ($|b| > |E_{S_-}|$), which can be understood directly from Fig. 3.1(d). When the lowest-energy triplet state (T_- for $b > 0$) is below the lowest-energy singlet (S_-), current will be blocked as soon as T_- is populated, since the transition from T_- to S_- vanishes as $W_{T_-\to S_-} \propto \omega_{T_-,S_-}\theta(\omega_{T_-,S_-})$. Thus, at low temperature a *pure* spin state can be prepared ($|T_+\rangle$ or $|T_-\rangle$ depending on the sign of b). We note that this preparation can be achieved even in the presence of a large bias $\Delta\mu > k_BT$. This is a nontrivial result, since a large bias will generally drive the DQD out of equilibrium, resulting in a stationary state that is *not* determined by thermal equilibrium with the leads [2]. Moreover, using this method a pure spin state can be dynamically prepared on a time scale $\tau_{\rm prep} \sim t^{-1}\left(\Delta/\Gamma_L\right)^2 \sim 0.1\,\mu$s (using parameter values from the caption of Fig. 3.2)

[2] We find that processes leading to DQD excitation in our considered large-bias regime are, however, suppressed by the small parameter $\Delta/U \ll 1$ A, where U is the single-dot charging energy.

without the need to wait for slow spin relaxation processes.

In Fig. 3.2, we show cuts at $\epsilon = 0$ describing the evolution of $I(B)$ as the field gradient $\delta B = \delta b/g\mu_B$ is increased from zero (see the appendix A, for the dependence on ϵ). For sufficiently large δB, a dip appears near $B = 0$. Similar zero-field dips have been seen experimentally in several DQD systems and have been attributed to effects due to hyperfine [74] or spin-orbit [105, 18] coupling. In the present context, this zero-field dip can be understood from Fig. 3.1(d), without additional spin relaxation mechanisms. When δb (or Γ_R) is large, T_0 has a fast direct escape path by virtue of Eq. (3.5), so only the T_+ and T_- states can block current. At $b = 0$, all triplets are degenerate, resulting in a vanishing inelastic cotunneling rate at low temperature ($W_{T_\pm \to T_0} \simeq 0$); transport can only occur if $T_\pm$ escapes via S_-. However, for a small nonvanishing Zeeman splitting $b > 0$, we have $W_{T_+ \to T_0} \propto b \neq 0$, allowing an additional escape route for T_+. This results in an initial rise in current for small b, which eventually must fall to zero when $b \simeq \sqrt{2}t$, where T_- goes below S_-. In the limit where $W_{T_0 \to \sigma} \gg W_{\alpha \to \beta}$, we find a simple expression for the stationary leakage current:

$$I = \frac{e}{\pi}\left(\frac{\Gamma_L}{\Delta}\right)^2 \frac{(\sqrt{2}t - |b|)(\sqrt{2}t + 3|b|)}{\sqrt{2}t + |b|}\theta(\sqrt{2}t - |b|), \tag{3.7}$$

where we have taken $\epsilon = 0$, and $T = 0$. The current reaches a maximum at $b_{\max} = \pm\sqrt{2}t(2/\sqrt{3} - 1) \approx \pm 0.22t$. Eq. (3.7) is shown as a dash-dotted line in Fig. 3.2. We note that the limit $W_{T_0 \to \sigma} \gg W_{\alpha \to \beta}$ required for Eq. (3.7) can also be achieved for much smaller δb when $\Gamma_R \gg \Gamma_L$. A sufficiently large electron temperature will wash out the zero-field dip, but provided $b_{\max} \gtrsim k_B T$, this feature will still be visible (see the inset of Fig. 3.2). Reaching this regime for $T \simeq 100\,\mathrm{mK}$ should be possible in nanowire [105] or nanotube DQDs [52] where $t \gtrsim 100\,\mu eV$ is common.

3.4 Transient current

We now turn to the transient (time-dependent) current that flows between blocking events. We consider the instant after an electron has tunneled from the DQD to the right lead. With spin-independent tunneling rates, this leaves the dot in an equal mixture of the states $|\uparrow\rangle$ and $|\downarrow\rangle$, setting the initial condition: $\rho_\sigma(0) = 1/2,\ \rho_\alpha(0) = 0$. The transient current into the right lead is then given by $I_R(t) = e\sum_\alpha W^R_{\alpha\to\sigma}\rho_\alpha(t)$. The average number of electrons m that passes through the DQD, given a charge collection (measurement) time T_M is

$$m(T_M) = \frac{1}{e}\int_0^{T_M} d\tau I_R(\tau). \tag{3.8}$$

In Fig. 3.3 we plot $m(T_M)$ found by integration of Eq. (3.3) for a range of parameters when the stationary current is zero (i.e., $k_BT = \epsilon = 0$, $b > \sqrt{2}t$). The accumulated charge shows a series of plateaux at time scales determined by the three types of rates given in Eqs. (3.4), (3.5), and (3.6). To better understand these plateaux, we consider the long-time saturation value $m = \lim_{T_M\to\infty} m(T_M)$, which has been measured experimentally [73] and can be evaluated directly.

We assume a probability P_B for the DQD to be in a blocking state each time an additional electron tunnels onto the DQD. The probability of exactly n electrons passing through the DQD before current is blocked is then $P_n = (1-P_B)^nP_B$, from which we find $m = \sum_n nP_n = (1-P_B)/P_B$. In the simplest case, there may be N_B blocking levels out of N total, giving $P_B = N_B/N$. Assuming the two spin-polarized triplets $|T_\pm\rangle$ are perfect blocking states, we set $P_B = 1/2$ since 2 out of 4 $(1,1)$-states block perfectly, giving $m = 1$ (the expected value in Ref. [73]; the measured value was $m \simeq 1.5$). However, in the presence of some decay mechanism, transitions between the various two-electron states (see the inset of Fig. 3.3) no longer allow for a clear definition of "blocking" levels. Nevertheless, we can still determine P_B from the sum of probabilities for each independent path leading to a blocking state (T_- for the case shown in Fig. 3.3): $P_B = P_{\sigma\to T_-} + P_{\sigma\to T_0\to T_-} + P_{\sigma\to T_+\to T_0\to T_-} = (1+p+qp)/4$, where $P_{A\to B\ldots}$ indicates

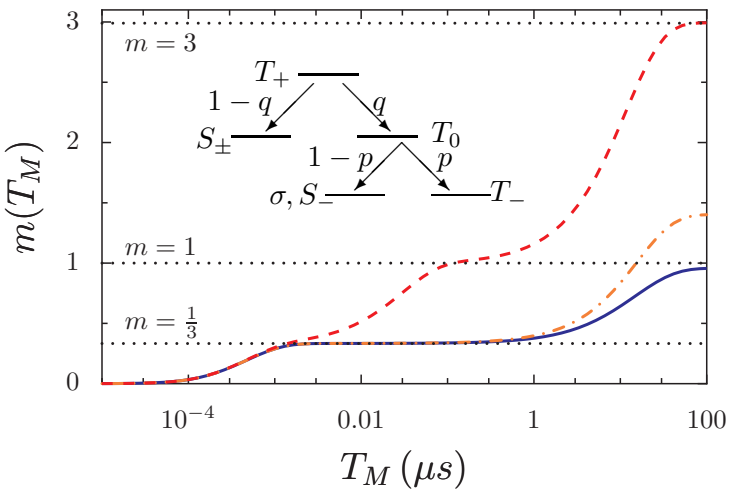

Figure 3.3: Average number $m(T_M)$ of electrons passing through the DQD within measurement time T_M. All values are as in Fig. 3.2 with the addition of $b = 1.01\sqrt{2}t$, $T = 0$, and $\Gamma_R = 10\Gamma_L = 10\,\mu eV$. $m(T_M)$ is shown for $\delta B = 0\,\mathrm{mT}$ (solid line), $\delta B = 3\,\mathrm{mT}$ (dash-dotted line), and $\delta B = 100\,\mathrm{mT}$ (dashed line). The predicted saturation points for 3 of 4 levels blocking ($m = 1/3$), 2 of 4 levels blocking ($m = 1$) and 1 of 4 levels blocking ($m = 3$) are shown with dotted lines. The decay cascade (inset) defines the branching ratios p and q.

the probability for a transition from state A to B, etc., and where the branching ratios are given (for $b > 0$) by: $p = W_{T_0\to T_-}/(W_{T_0\to T_-} + W_{T_0\to S_-} + \sum_\sigma W_{T_0\to\sigma})$ and $q = W_{T_+\to T_0}/(W_{T_+\to T_0} + W_{T_+\to S_-} + W_{T_+\to S_+})$. Inserting this result gives:

$$m = \frac{3 - p - pq}{1 + p + pq}. \tag{3.9}$$

The average effective charge transported between blocking events $e^* = (m+1)e$ is non-integral in general, ranging from $e^* = \frac{4}{3}e$ to $e^* = 4e$. Eq. (3.9) allows for a precision measurement of slow spin-relaxation processes characterized by p and q, *independent* of the microscopic mechanism [3]. For concreteness, we consider the effects of cotunneling and field-assisted sequential tunneling below.

In the limit of zero detuning ($\epsilon = 0$), we find $q = 1/2$, independent of b and t,

[3]For example, in the limit of small b, we find $m \simeq 3 - \gamma b^\eta$, where $\eta = 5$, 3, and 1 for spin-orbit, hyperfine-, and cotunneling-mediated spin relaxation, respectively A.

leaving

$$m = \frac{2-p}{\frac{2}{3}+p}; \quad p = \frac{2|b|}{\sqrt{2}t + 2|b| + \frac{\pi}{2}\left(\frac{\Delta\delta b}{\Gamma_L t}\right)^2 \Gamma_R}. \tag{3.10}$$

Thus, at $\epsilon = 0$, m can be tuned from $m = 3/5$ to $m = 3$ by varying b, δb, $\Gamma_{L,R}$, and t. Eq. (3.10) correctly predicts the saturation values at m=0.96, 1.4, and 3.0 for the solid, dash-dotted, and dashed lines, respectively, in Fig. 3.3.

We have analyzed the effects of inelastic cotunneling and a magnetic field gradient on the PSB. We find and explain a zero-field dip in the stationary current, which may help to explain recent experimental results [74, 105, 18]. We have shown that a pure spin state can be dynamically initialized, even at large bias, which is an important step on the way to full control over the quantum states of electron spins. We have offered a possible explanation for an anomalously large value of the effective charge passing through the DQD found in experiments [73], which is important for single-spin resonance studies. Our expression for this effective charge can be used to probe slow spin relaxation processes in the DQD to help understand the underlying physical mechanisms. A fractional effective charge e^* in transport is often taken as evidence of exotic electronic states [121, 30, 110]. Here, we have shown that e^* can reach universal fractional values in a simple system, without many-body correlations.

We thank D. G. Austing, J. Baugh, J. Gambetta, and D. Loss for useful discussions. We acknowledge funding from an NSERC discovery grant, QuantumWorks, IQC, WIN, CIFAR, and an Ontario PDF (WAC).

Chapter 4

Leakage-current lineshapes from inelastic cotunneling in the Pauli spin blockade regime

4.1 Outline

We find the leakage current through a double quantum dot in the Pauli spin blockade regime accounting for inelastic (spin-flip) cotunneling processes. Taking the energy-dependence of this spin-flip mechanism into account allows for an accurate description of the current as a function of applied magnetic fields, gate voltages, and an inter-dot tunnel coupling. In the presence of an additional local dephasing process or nonuniform magnetic field, we obtain a simple closed-form analytical expression for the leakage current giving the full dependence on an applied magnetic field and energy detuning. This work is important for understanding the nature of leakage, especially in systems where other spin-flip mechanisms (due, e.g., to hyperfine coupling to nuclear spins or spin-orbit coupling) are weak, including silicon and carbon-nanotube or graphene quantum dots.

4.2 Introduction

Spin-dependent current blockade effects have been observed in quantum dots [98, 106] as well as in molecular [57] and single-atom transport.[87] These effects are the basis of spin-to-charge conversion schemes, essential for measurements of spin coherence and relaxation [102, 103, 73, 107] as well as the accurate initialization and readout of spin states for spin-based quantum information processing.[85] Blockade effects have further allowed the observation of intriguing slow periodic oscillations in current, dependent on nuclear spins.[99] A detailed microscopic understanding of how this blockade can be lifted is important to develop an accurate description of these effects and to point the way to generate a more robust blockade for the study of further spin-dependent phenomena.

The Pauli spin blockade of current through a double quantum dot occurs when each of two quantum dots in series energetically favors a one-electron configuration (we will refer to this as the $(1,1)$ regime, where (n,m) refers to n electrons on the left dot and m electrons in the right). Restricting to only the lowest non-degenerate single-particle orbital state in each dot, there are four possible spin configurations in the $(1,1)$ subspace: one spin singlet and three spin triplets. To generate sequential transport of electron charge from left to right, the double-dot must pass through the $(0,2)$ charge configuration, but due to the Pauli exclusion principle, the lowest-energy $(0,2)$-state is a spin singlet when only the lowest single-particle orbital state is accessible. An inter-dot tunnel coupling preserves the spin of the two-electron state and therefore couples only the $(1,1)$ singlet to the $(0,2)$ state. After a small number of electrons has passed through the double-dot, eventually one of the spin-triplet states will be occupied by chance, leaving the double dot stuck in a "blocked" configuration. This blockade can be lifted either through the direct hybridization of singlet and triplet states with the addition of spin-non-conserving terms to the Hamiltonian (due, e.g., to the spin-orbit or hyperfine interactions), or through direct energy-conserving transitions between triplet and singlet levels. In spite of this relatively simple explanation for the Pauli spin blockade, the situation

is complicated by several possible microscopic mechanisms that may dominate in determining the leakage current depending on the material and device characteristics. It is therefore important to understand precisely what influence each of the possible microscopic mechanisms may have on the overall leakage current in order to identify the most relevant mechanism and possibly to suppress it.

Most mechanisms that lift spin blockade are particular to the materials used to manufacture a double-dot device; the contact hyperfine interaction between electron and nuclear spins lifts the blockade in GaAs double dots,[99, 74, 61, 59] and a strong spin-orbit interaction plays the predominant role in lifting the blockade in InAs nanowire double dots.[105, 27, 96] Both of these mechanisms can be suppressed by manufacturing double dots using silicon[83, 84, 122, 79] or carbon-based[15, 18] materials, in which the majority isotope has no nuclear spin and the spin-orbit coupling strength $\propto Z^4$ is significantly weaker due to a smaller atomic number Z. One blockade-lifting mechanism that is present in all double-dot devices, independent of the material composition, is exchange of spins with the leads through higher-order tunneling (cotunneling) processes.[46, 83, 132, 109] By understanding and controlling these processes, one can accurately calibrate single-spin readout and improve on rapid spin preparation schemes.[109] Moreover, cotunneling processes have been shown to be significant in determining dynamic nuclear-spin polarization processes, both in experiment[8] and in theory,[8, 115] so a further understanding of cotunneling may allow for the preparation of a more highly-polarized nuclear-spin system.

In this article we derive analytic expressions for leakage-current lineshapes accounting for inelastic cotunneling processes in well-defined and generically accessible limits. Some results of this analysis have recently been shown, experimentally, to be consistent with transport measurements on silicon double quantum dots,[79] and have proven useful in determining microscopic parameters associated with those devices. A similar application of the results presented here to other material systems may shed light on, e.g., unusually broad lineshapes in the magnetic-field-dependent current through isotopically enriched ^{13}C nanotube double dots.[18]

Inelastic (spin-flip) cotunneling has been known as a significant spin-flip mechanism since early measurements of triplet-to-singlet decay in vertical double quantum dots,[45] where the triplet-to-singlet decay rate was shown to be limited by inelastic cotunneling.[46] In the context of the Pauli spin blockade, spin-flip cotunneling rates have been calculated and compared to experimental data in the high-temperature regime where the associated transition rates between energy levels are independent of the energy-level spacing.[83, 132] More recently, the consequence of the full energy dependence of these rates has been calculated[109] and verified in experiment.[79] In this chapter we apply and extend the analysis presented in refs. [109] and [79] to a broader range of parameters and provide a general and intuitive formalism for the calculation of leakage current through blockaded structures. For simplicity, in specific calculations we neglect orbital/valley degeneracy in our treatment, which may be relevant for quantum dots made from graphene, carbon nanotubes, or silicon nanostructures and can lead, in general, to a more complicated spin-valley blockade.[100, 101] However, the general formalism we present can also be applied directly to systems with valley degeneracy and many of the results we present will be qualitatively unchanged in the presence of additional orbital degeneracies.

The remainder of this article is organized as follows: In Sec. 4.3 we present an intuitive and general procedure for the calculation of current through blockaded structures given a set of decay rates obtained from a microscopic calculation. In Sec. 4.4 we specialize to the case of a double quantum dot in the Pauli spin blockade regime. We recall the calculation of sequential-tunneling and spin-flip cotunneling rates from ref. [109] and apply the procedure of Sec. 4.3 to find leakage-current lineshapes as a function of an applied magnetic field and energy detuning (the energy difference between $(1,1)$ and $(0,2)$ charge states). In the limit of a strong local spin dephasing mechanism or nonuniform magnetic field, we then obtain a single simple closed-form analytical expression giving a full two-dimensional map of the current as a function of detuning and magnetic field. In Sec. 4.5 we conclude with a summary of the main results and a discussion of extensions and possible future work.

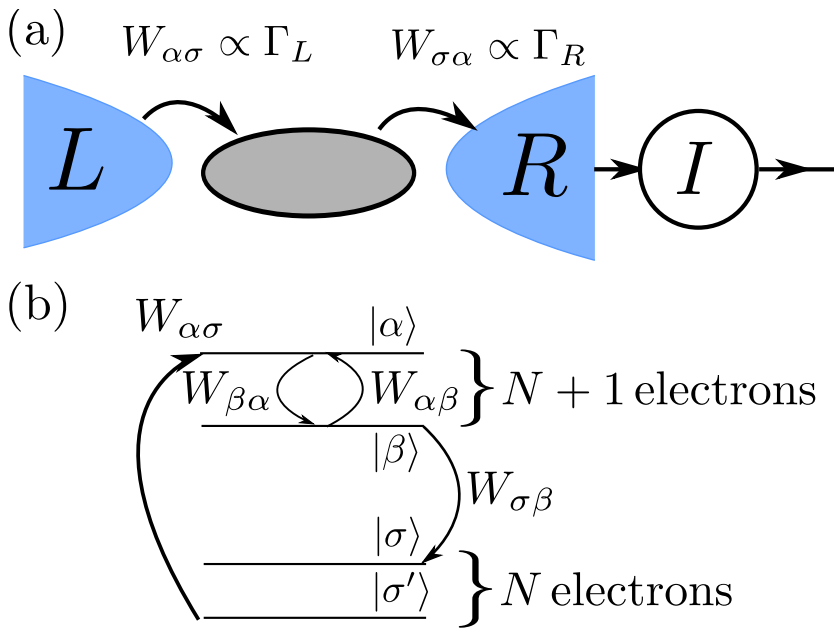

Figure 4.1: (a) A typical transport scenario in the sequential-tunneling regime. In the high-bias limit ($\delta\mu > |E_\alpha - E_\sigma|, T$, where E_j is the energy of level j) electrons hop only in one direction: from the left lead to the dot at a rate $\propto \Gamma_L$, and from the dot to the right lead at a rate $\propto \Gamma_R$. (b) The transport cycle in the sequential tunneling regime is a loop that carries the dot from an N-electron state (labeled with $\{\sigma, \sigma'\}$) to an $N+1$-electron state (labeled here with Greek letters $\{\alpha, \beta\}$). A current blockade will be set up if one or some of the accessible $N+1$-electron states α have negligible transition rates $W_{\sigma\alpha} \simeq 0$, in which case the current may be limited by rates $W_{\beta\alpha}$ inducing transitions within the $N+1$-electron subspace.

4.3 Leakage current through blockaded systems

In this section we establish a generic theory of the current through blockaded nanostructures, incorporating internal transition rates between levels that can lead to a lifting of the blockade. The formalism developed in this section will be used in later sections to derive simple analytical formulas for the dependence of the current on various parameters in the specific case of the Pauli spin blockade of transport through a double quantum dot, accounting for inelastic cotunneling processes. Throughout this chapter, we work in units where $g\mu_{\mathrm{B}} = e = k_{\mathrm{B}} = \hbar = 1$, with electron g-factor g, Bohr magneton μ_{B}, electron charge e, Boltzmann's constant k_{B} and Planck's constant $\hbar$.

We consider a nanoscale system weakly tunnel coupled to leads, set at chemical potentials μ_l and with tunneling rates Γ_l ($l = \mathrm{L}, \mathrm{R}$ for the tunneling rate between the system and the left and right leads, respectively, see Fig. 4.1(a)). In the sequential-tunneling regime, electron charge is transported from left to right through energy-conserving transitions between N-electron states of the system, denoted σ, and $N+1$-electron states, denoted α. These transitions are associated with the exchange of an electron with one of the leads (Fig. 4.1(b)). Finally, we consider the simplifying limit of a large bias $\delta\mu = \mu_L - \mu_R > 0$:

$$|\mu_L - \mu_{\alpha\sigma}| > T, \tag{4.1}$$

$$|\mu_R - \mu_{\sigma\alpha}| > T, \tag{4.2}$$

with chemical potential $\mu_{\alpha\sigma} = E_\alpha - E_\sigma$ (where E_i is the energy of isolated system level i and Latin characters are taken to run over all system eigenstates, independent of the occupation number, i.e.: $i = \{\alpha, \sigma\}$). In this limit, energy-conserving transitions that add one electron to the system $\sigma \to \alpha$ (with rate $W_{\alpha\sigma}$) necessarily involve the removal of an electron from the left lead and transitions that remove an electron from the system, $\alpha \to \sigma$ (with associated rate $W_{\sigma\alpha}$), involve the addition of an electron to the right lead (see Fig. 4.1(a)). Other processes that change the electron number are exponentially suppressed.

The sequential-tunneling current in the high-bias limit (defined by Eqs. (4.1) and (4.2)) is given simply by

$$I = \sum_{\alpha\sigma} W_{\alpha\sigma}\bar{\rho}_\sigma, \tag{4.3}$$

where $\bar{\rho}_i$ solves the (stationary) Pauli master equation for the diagonal elements of the system density matrix:

$$\overline{\dot{\rho}}_i = \sum_j W_{ij}\bar{\rho}_j - W_i\bar{\rho}_i = 0; \quad W_i = \sum_j W_{ji}, \tag{4.4}$$

where we define the average $\overline{\rho(t)} = \lim_{\tau\to\infty} \frac{1}{\tau}\int_0^\tau dt\rho(t)$. The diagonal elements of the stationary density matrix $\bar{\rho}_i$ must satisfy the normalization

$$\sum_i \bar{\rho}_i = 1. \tag{4.5}$$

Use of the classical (Pauli) master equation to describe the diagonal elements of the system density matrix is strictly valid in the high-bias, weak-coupling limit $|\delta\mu| > \Gamma_{L,R}$, where coherences (off-diagonal elements with respect to the isolated system energy eigenbasis) decay to zero on a time scale $\sim 1/|\delta\mu|$ that is short compared to the tunneling time $\sim 1/\Gamma_l$. In Eq. (4.3), we have explicitly assumed that higher-order current-carrying cotunneling corrections $\propto \Gamma_L\Gamma_R$ are small relative to the sequential-tunneling terms $\propto \Gamma_l$. In Sec. 4.4, we will account for cotunneling processes that do not carry current, $\propto \Gamma_l^2$, involving exchange with the same lead. These processes typically dominate over the current-carrying cotunneling processes in the case of a double quantum dot considered in Sec. 4.4.

Solving the linear system given by Eqs. (4.4) and (4.5) for the stationary populations $\bar{\rho}_\sigma$ is sufficient to determine the current I from the set of all rates W_{ij}. However, it is physically intuitive to switch to new variables k_i, defined in terms of the current I, stationary populations $\bar{\rho}_i$ and the total escape rate from state i, $W_i = \sum_j W_{ji}$, as:

$$k_i = \frac{W_i\bar{\rho}_i}{I} = \frac{\text{flux out of state } i}{\text{flux into all states } \alpha}. \tag{4.6}$$

The quantities k_i have a natural physical interpretation: k_i is the number of times state i will be visited, on average, per transport cycle ($\sigma \to \alpha \to \sigma' \to \ldots$, depicted in Fig. 4.1(b)). From the definition (4.6) and normalization (4.5), we find the current

$$I = \left(\sum_i \frac{k_i}{W_i} \right)^{-1}. \tag{4.7}$$

This formula can be understood directly in terms of the interpretation given above for the coefficients k_i. The average time to leave state i if it were occupied is $1/W_i$, while k_i is the number of times (on average) that state i is occupied in each transport cycle. The ratio k_i/W_i is therefore the average time spent in state i per transport cycle and so the total average time per transport cycle (average time to transfer an elementary electron charge) is simply $\sum_i k_i/W_i$. The inverse of this time is the rate at which charge is transferred from left to right, giving the current, Eq. (4.7).

The coefficients k_i can be found systematically in terms of the rates W_{ij} using the identity

$$k_i = \sum_j P_{ij} k_j; \qquad P_{ij} = W_{ij}/W_j, \tag{4.8}$$

where the branching ratios, P_{ij}, give the probability for a transition to state i conditioned on starting in state j. Eq. (4.8) follows directly from Eq. (4.4) and the definition $k_i \propto W_i \bar{\rho}_i$ (Eq. (4.6)). Solving the linear system given in Eq. (4.8) and substituting the result into Eq. (4.7) is formally equivalent to solving for the populations $\bar{\rho}_i$ and substituting the result into Eq. (4.3) for the current. However, for the particular case of blockaded systems, we will find that Eq. (4.8) lends itself better to approximation schemes and often the solution for the k_i can be determined quickly on physical grounds without directly solving the linear system.

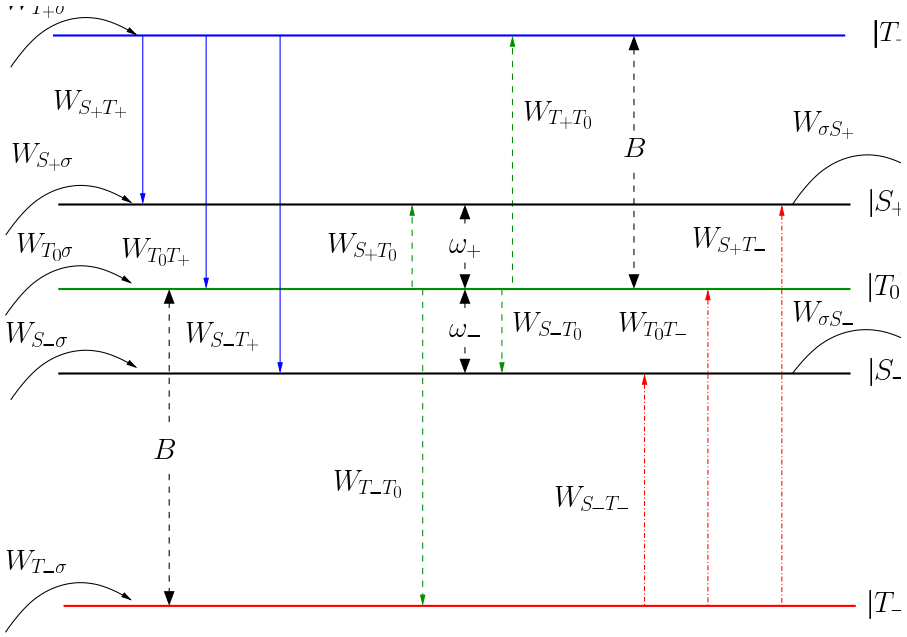

Figure 4.2: Isolated double-quantum-dot energy eigenstates and transition rates between them. The spin-polarized triplet states $|T_\pm\rangle$ are split from the spin-unpolarized triplet $|T_0\rangle$ by an applied magnetic field B and the hybridized spin-singlet states $|S_\pm\rangle$ are split from $|T_0\rangle$ by the detuning-dependent quantities $\omega_\pm$, given in Eq. (4.35), below.

4.4 Inelastic cotunneling and the Pauli spin blockade regime

Here we apply the formalism of Sec. 4.3 to perform an explicit microscopic calculation for the leakage current through a double quantum dot in the Pauli spin blockade regime, accounting for transition rates due to inelastic cotunneling processes. Inelastic cotunneling is a second-order tunneling process associated with a change in energy of the isolated quantum-dot state with a compensating change in energy of the lead state. Since the total energy is conserved, the energy of the combined dot-plus-leads system is, of course, unchanged in this process.

The simple formalism derived in the previous section allows us to efficiently obtain closed-form analytical expressions for the leakage current in terms of all transition rates W_{ij}. We begin by reviewing the calculation of transition rates due to sequential tunneling and inelastic cotunneling, presented in ref. [109].

4.4.1 Transition rates

Our starting point is a Hamiltonian,

$$H = H_0 + \sum_l H_{\mathrm{d}l}, \tag{4.9}$$

where H_0 gives the free Hamiltonian of the double quantum dot and Fermi-liquid leads. In the subspace of $(1,1)$ and $(0,2)$ charge states, the isolated double-dot Hamiltonian eigenstates consist of two spin-singlets $|S_\pm\rangle$, describing $(1,1)$ and $(0,2)$ charge states hybridized due to inter-dot tunneling t, as well as three spin triplets $(|T_\pm\rangle, |T_0\rangle)$, see Fig. 4.2. Sequential transport further involves the $(0,1)$ charge state with spin $\sigma = \uparrow, \downarrow$, denoted: $|\sigma\rangle$. The Hamiltonian $H_{\mathrm{d}l}$ describes the coupling of lead l to dot l ($l = L, R$ for the left and right dot and lead, respectively), with tunneling amplitude t_l (a full specification is given in the appendix B, below).

Transition rates are calculated via Fermi's golden rule:

$$W_{km} = 2\pi \sum_{if} \rho(i) \left|\langle fk| V |im\rangle\right|^2 \delta\left(\mathcal{E}_{fk} - \mathcal{E}_{im}\right), \tag{4.10}$$

where i, f label the initial and final states of the leads, respectively, m, k label the initial and final states of the double dot, $\rho(i)$ describes a product of initial Fermi distributions in the leads, held at electron temperature T and chemical potentials μ_l, and $\mathcal{E}_{im}, \mathcal{E}_{fk}$ give the total initial and final energies of both the double-dot and leads. The effective perturbation V, accounting for transitions up to second order in $H_{\mathrm{d}l}$, is

$$V = \sum_l H_{\mathrm{d}l} + \sum_{abgll'} |a\rangle \langle b| \frac{\langle a| H_{\mathrm{d}l} |g\rangle \langle g| H_{\mathrm{d}l'} |b\rangle}{\mathcal{E}_a - \mathcal{E}_g}, \tag{4.11}$$

where the indices a, b, g describe the collective state of the double dot and leads.

In the high-bias regime (Eqs. (4.1) and (4.2)), we find the sequential tunneling

rates from Eqs. 4.10 and 4.11:

$$W_{\alpha\sigma} = \Gamma_L \sum_{\sigma'} |A_{L\sigma}^{\alpha\sigma}|^2, \tag{4.12}$$

$$W_{\sigma\alpha} = \Gamma_R \sum_{\sigma'} |A_{R\sigma}^{\alpha\sigma}|^2, \tag{4.13}$$

where the tunneling rates Γ_l and transition matrix elements $A_{l\sigma}^{jj'}$ are, respectively,

$$\Gamma_l = 2\pi\nu_l |t_l|^2, \tag{4.14}$$

$$A_{l\sigma}^{jj'} = \langle j | \, d_{l\sigma}^\dagger \, | j' \rangle \, . \tag{4.15}$$

Here, ν_l is the density of states per spin at the Fermi level in lead l. We assume that both ν_l and t_l are approximately energy-independent in our regime of interest.[1] The operator $d_{l\sigma}^\dagger$ creates an electron in single-particle orbital l with spin σ.

The inelastic cotunneling rates $W_{\alpha\beta}$, arising from the second-order term in Eq. (4.11) with $l = l'$, are given by[109]

$$W_{\alpha\beta} = 2cTM_{\alpha\beta}F(\omega_{\beta\alpha}/T), \tag{4.16}$$

with dimensionless prefactor c, matrix elements $M_{\alpha\beta}$, and energy-dependent factor $F(\omega/T)$ given by

$$c = \frac{1}{\pi}\left[\left(\frac{\Gamma_L}{\Delta - \epsilon}\right)^2 + \left(\frac{\Gamma_R}{\Delta + \epsilon - 2U' - 2\delta\mu}\right)^2\right], \tag{4.17}$$

$$M_{\alpha\beta} = \sum_{\sigma\sigma'\sigma''} |A_{L\sigma}^{\alpha\sigma''}|^2 |A_{L\sigma'}^{\beta\sigma''}|^2 = \sum_{\sigma\sigma' j} |A_{R\sigma}^{j\alpha}|^2 |A_{R\sigma'}^{j\beta}|^2, \tag{4.18}$$

$$F(\omega/T) = \frac{\omega/T}{1 - e^{-\omega/T}}. \tag{4.19}$$

The coefficient $c \sim \Gamma_l^2$ in Eq. (4.17) reflects the second-order nature of the cotun-

[1] The tunneling amplitudes t_l will be approximately energy-independent when the bias is small compared to the height of the barrier coupling dot to lead. For a clean system, the density of states ν_l will be independent of energy as long as the bias is small compared to the Fermi energy $E_{\rm F}$.

neling process and we have taken the convention $\mu_L = 0$, $\mu_R = -\delta\mu$ with positive bias $\delta\mu > 0$. Here, the energy detuning $\epsilon = E_{(1,1)} - E_{(0,2)}$ measures the separation in energy between $(1,1)$ and $(0,2)$ charge configurations, and $\Delta = E_{(1,1)} - U$ sets the energy of the $(1,1)$ charge configuration with on-site charging energy U. The transition matrix elements $M_{\alpha\beta}$ arise from processes involving spin exchange with the left lead (associated with virtual states in the $(0,1)$-subspace) or spin exchange with the right lead (associated with virtual states $|j\rangle$ in the $(1,2)$-subspace). The dominant energy and temperature dependence of the cotunneling rates is due to the function $F(\omega/T)$, which arises from an integral over Fermi functions $f_l(E) = 1/(e^{(E-\mu_l)/T} + 1)$:

$$F(\omega/T) = \frac{1}{T}\int_{-\infty}^{\infty} dE f_l(E)\left[1 - f_l(E+\omega)\right]. \tag{4.20}$$

In our analysis, we have neglected resonant cotunneling contributions, which formally lead to a divergence in evaluating rates directly from Eq. (4.11). However, these contributions can be systematically regularized[71] and are suppressed exponentially in the high-bias limit considered here. We have further neglected current-carrying cotunneling processes (those arising from the second-order term with $l \neq l'$ in Eq. (4.11)). We find that these processes are suppressed relative to the considered processes by at least a factor $\sim U'/U$, where U' is the nearest-neighbor charging energy.[109]

Since the energy dependence of the rates $W_{\alpha\beta}$ will play an important role in the following analysis, it is useful to consider $F(\omega/T)$ in the limits of large positive and negative energy difference ω at low T:

$$F(\omega/T) \simeq \frac{\omega}{T}\Theta(\omega/T), \quad \omega > T, \tag{4.21}$$

$$F(\omega/T) \simeq |\omega/T| e^{-|\omega/T|}, \quad \omega < -T. \tag{4.22}$$

Eq. (4.21) reflects the fact that the inelastic relaxation rates increase for large energy-level separation $\omega > T$, as the density of states of the environment increases

and Eq. (4.22) describes exponential suppression of excitation compared to relaxation processes, consistent with detailed balance.

In the high-temperature limit, the inelastic cotunneling rates for both excitation and relaxation approach a constant, energy-independent value since, in this limit,

$$F(\omega/T) \simeq 1, \quad T > |\omega|. \tag{4.23}$$

This high-T limit has been explored in the context of Pauli spin blockade in previous works.[83, 132] In the present work, we are more concerned with the limits where the energy dependence described by Eqs. (4.21) and (4.22) is significant in determining the leakage current.[109]

4.4.2 Leakage current: No local dephasing

Solving the linear system (Eq. (4.8)) for k_i with the rates given in Eqs. (4.12), (4.13), and (4.16) immediately gives the current via the expression in Eq. (4.7). For any set of parameters, one can find the leakage current by solving the full linear system, giving a complex expression in general. However, to understand the physical significance of the results, or in order to perform experimental fits to traces of leakage current vs. magnetic field or energy detuning, it is useful to derive simple analytical expressions, valid in experimentally relevant limits. In this section, we derive expressions for the leakage current in the limit where there is no significant local dephasing mechanism, leading to decay rates that are comparable for all three spin-triplet states, $W_{T_+} \sim W_{T_-} \sim W_{T_0}$. This limit applies to double dots in silicon or carbon when there is no magnetic field gradient. In Sec. 4.4.3 below, we consider the opposite limit of a strong local spin dephasing mechanism or nonuniform magnetic field, leading to $W_{T_0} \gg W_{T_\pm}$, in which case the analysis simplifies considerably.

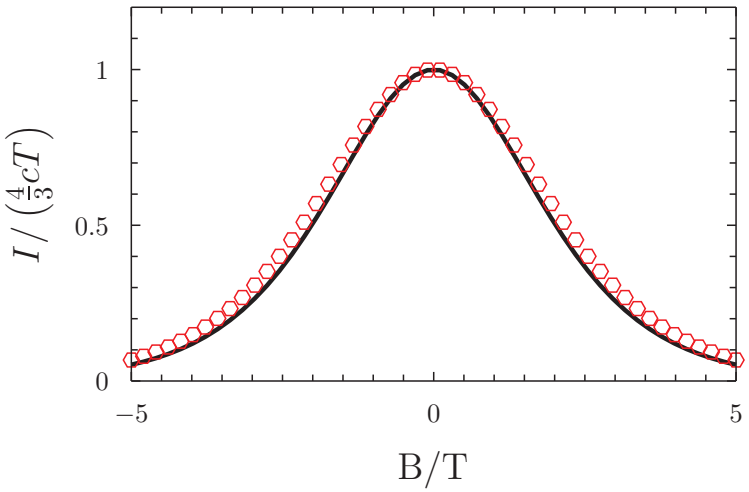

Figure 4.3: Current I vs. magnetic field B at zero detuning ($\epsilon = 0$) from the full expression given in Eq. (4.28) (black solid line) and the approximation, Eq. (4.30) (red circles). This form is valid when the temperature T is large compared to the tunnel coupling t and when the direct dot-lead tunneling rates Γ_l are large compared to inelastic cotunneling rates $W_{\alpha\beta}$, i.e. $T > t$ and $\Gamma_l > W_{\alpha\beta}$. For example, for Silicon ($g = 2$) 100mK corresponds to 75mT.

4.4.2.1 B-field dependence (high-T limit)

First we restrict ourselves to the dependence of the leakage current on an applied magnetic field B, which splits the spin-polarized triplet states $|T_\pm\rangle$ from $|T_0\rangle$ (see Fig. 4.2). We further consider the limit $\Gamma_l \gg W_{\alpha\beta}$ at zero detuning, $\epsilon = 0$, in which the current is dominated by rates of escape from the three spin-triplet states $W_{T_a} \ll W_{S_\pm}, W_\sigma$. Noting that $k_{S_\pm}, k_\sigma \sim O(1)$ in this limit since the singlets $|S_\pm\rangle$ and one-electron states $|\sigma\rangle$ are accessed at most once per transport cycle, Eq. (4.7) simplifies to

$$I \simeq \left(\frac{k_{T_0}}{W_{T_0}} + \frac{k_{T_+}}{W_{T_+}} + \frac{k_{T_-}}{W_{T_-}}\right)^{-1}, \quad \Gamma_l \gg W_{\alpha\beta}. \tag{4.24}$$

We obtain the relevant coefficients k_α from Eq. (4.8), with the cotunneling rates given in Eq. (4.16). We find $k_\sigma = 1/2$, since both spin states, $\sigma = \uparrow, \downarrow$, are equally probable and one of the two is accessed in each transport cycle. For an unpolarized source lead, we find the branching ratios $P_{T_+\uparrow} = P_{T_-\downarrow} = 1/2$, $P_{T_0\sigma} = 1/4$, and finally, directly inserting the relevant rates in the limit $\epsilon = 0$, $t < T$, we find $P_{T_0 T_\pm} = 1/2$. Inserting these results into Eq. (4.8) and solving the linear system in

terms of the two remaining branching ratios gives:

$$k_{T_0} = \frac{1}{2 - p_+ - p_-}, \tag{4.25}$$

$$k_{T_\pm} = \frac{1}{4} + \frac{p_\pm}{2 - p_+ - p_-}, \tag{4.26}$$

with branching ratios

$$p_\pm = P_{T_\pm T_0} = \frac{W_{T_\pm T_0}}{W_{T_0}}. \tag{4.27}$$

Substituting the cotunneling rates given in Eq. (4.16) into Eqs. (4.27), (4.25), and (4.26), and inserting the results for $T > t$ into Eq. (4.24) directly gives an expression for the current vs. B:

$$I(B, \epsilon = 0) = \frac{4}{3} cTG(B/T) \frac{B/T}{\sinh(B/T)}, \tag{4.28}$$

with

$$G(x) = 3\frac{2(\cosh x - 1) + x \sinh x}{2(\cosh x - 1) + 5x \sinh x}. \tag{4.29}$$

Since $G(B/T)$ differs from a constant only at third order in B/T, while $I(B, \epsilon = 0)$ is exponentially suppressed for $B/T \gtrsim 1$, to a very good approximation we take $G(B/T) \simeq G(0) = 1$ leaving the simple expression

$$I(B, \epsilon = 0) \simeq \frac{4}{3} cT \frac{B/T}{\sinh(B/T)}; \quad T > t, \Gamma_l \gg W_{\alpha\beta}. \tag{4.30}$$

The approximate expression, Eq. (4.30), is virtually indistinguishable from the full expression given in Eq. (4.28), see Fig. 4.3.

At zero magnetic field, $B = 0$, Eq. (4.30) simply gives $I \simeq \bar{n} W_{\rm cot}$, where $\bar{n} = 4/3$ gives the average number of electrons that pass through the double dot between "blocking events". This number is 4/3 if three of four $(1, 1)$ charge states block current – in this case, the three spin triplets – see ref. [109]. $W_{\rm cot} = cT$ is the rate at which any one of the triplets converts to a singlet through a cotunneling process in the limit $T > t$.

Physically, the current in Fig. 4.3 falls to zero when $|B| > T$ since the excitation

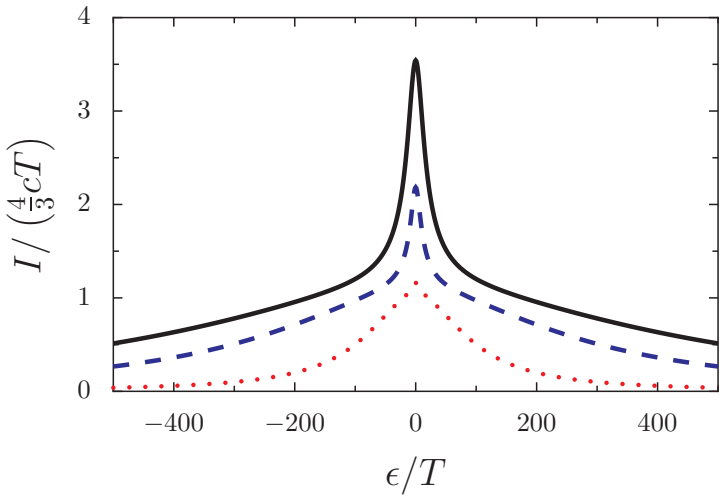

Figure 4.4: Detuning dependence at $B = 0$ from Eq. (4.48) for $\alpha = 100$ and $t = 5T$ (black solid line), $t = 3T$ (blue dashed line), and $t = T$ (red dotted line). The central peak with width $\sim t$ is described by the function $g(\epsilon, t, T)$ and the broad background describes a Lorentzian of width $\delta\epsilon = \alpha t$. (100mK corresponds to 8.6 μeV)

rate out of the ground-state triplet is exponentially suppressed.

4.4.2.2 Detuning dependence

To find the full ϵ-dependence of the current, even in the limit $\Gamma_l \gg W_{\alpha\beta}$ we find that it is necessary to include the escape rates from the singlets $W_{S_\pm}$, which can control the resonant-tunneling current at large detuning, where $W_{S_\pm} \sim W_{T_0}, W_{T_\pm}$.

As in the last section, we aim to find a good approximate solution for the current, starting from the linear equations given in Eq. (4.8). In the limit $\Gamma_l \gg W_{\alpha\beta}$, assumed here, the escape rate from the singlets can be taken to be essentially instantaneous except at sufficiently large detuning $|\epsilon| \gg t$, since $W_{\sigma S_\pm} \propto (t/\epsilon)^2\Gamma_R$ for $\epsilon \to \pm\infty$ (the rate $W_{\sigma S_\pm}$ is limited by the overlap of $|S_\pm\rangle$ with the $(0, 2)$ charge state). It is therefore sufficient to approximate rates by their large-ϵ forms to determine $k_{S_\pm}$. We assume that transition rates between the singlets are small compared to the direct escape rate (i.e., $W_{S_-S_+} \sim (t/\epsilon)^2 c|\epsilon| \ll \min\left(W_{\sigma S_+}, W_{\sigma S_-}\right) \propto (t/\epsilon)^2\Gamma_R$, which simplifies to $c|\epsilon| \ll \Gamma_R$). Provided this is satisfied, in the limit $|\epsilon| \gg t$, we find that only k_{S_+} (k_{S_-}) is relevant for $\epsilon > 0$ ($\epsilon < 0$), allowing us to

introduce a single parameter $k_S = \theta(\epsilon)k_{S_+} + \theta(-\epsilon)k_{S_+}$, where $\theta(x)$ is a Heaviside step function. At $B = 0$, we further find that $k_{T_+} = k_{T_-} = k_T$. The remaining three independent parameters are then given by the linear equations, from Eq. (4.8) after inserting all rates:

$$k_T = \frac{1}{4} + \frac{1}{2+g}k_{T_0} + \frac{1}{3+\eta}k_S, \tag{4.31}$$

$$k_{T_0} = \frac{1}{4} + \frac{2}{1+g}k_T + \frac{1}{3+\eta}k_S, \tag{4.32}$$

$$k_S = \frac{1}{4} + \frac{1}{3}k_{T_0} + k_T, \tag{4.33}$$

with

$$g = g(\epsilon, t, T) = \frac{\omega_+ F(\omega_-/T) + \omega_- F(-\omega_+/T)}{\sqrt{\epsilon^2 + 8t^2}}, \tag{4.34}$$

$$\omega_\pm = \frac{1}{2}\left[\sqrt{\epsilon^2 + 8t^2} \mp \epsilon\right], \tag{4.35}$$

and

$$\eta = \frac{\sum_\sigma W_{\sigma S}}{W_{\rm cot}} \simeq \frac{2\Gamma_R}{cT}\left(\frac{t}{\epsilon}\right)^2 = \frac{16}{3}\left(\frac{\delta\epsilon}{\epsilon}\right)^2, \quad |\epsilon| \gg t. \tag{4.36}$$

Here we have introduced a new energy scale $\delta\epsilon$, giving the value of the detuning at which the inelastic cotunneling rates are comparable to the escape rate from the double dot:

$$\delta\epsilon = \alpha t; \quad \alpha = \sqrt{3\Gamma_R/8cT}. \tag{4.37}$$

As the detuning $\epsilon \to \pm\infty$ is increased, the escape rate from the relevant singlet state $W_{\sigma S_\pm} \propto (t/\epsilon)^2\Gamma_R$ decreases until it becomes smaller than the cotunneling rates $\sim cT$. In the extreme limit, $\eta = 0$ and $g = 1$, Eqs. (4.31), (4.32), and (4.33) only have the singular solution $k_T = k_{T_0} = k_S = \infty$, reflecting the fact that each state is visited an infinite number of times; the system becomes 'stuck' in loops, as depicted between states $|\alpha\rangle$ and $|\beta\rangle$ in Fig. 4.1. To arrive at the leading finite corrections in the limit of large detuning $\epsilon \gg \delta\epsilon$ (equivalently, $\eta \ll 1$), we set $g = 1$, and determine the leading asymptotic solution of Eqs. (4.31), (4.32), and (4.33)

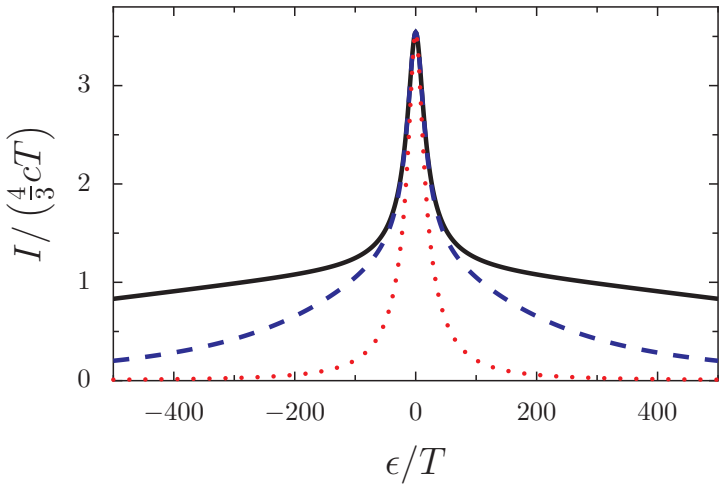

Figure 4.5: Detuning dependence at $B = 0$ from Eq. (4.48) for $t = 5T$ and $\alpha = 200$ (black solid line), $\alpha = 50$ (blue dashed line), and $\alpha = 10$ (red dotted line).

for small η, giving

$$k_T = k_{T_+} = k_{T_-} = \frac{2}{\eta} + \text{const.}, \quad \epsilon \gg \delta\epsilon, \tag{4.38}$$

$$k_{T_0} \simeq k_S = \frac{3}{\eta} + \text{const.}, \quad \epsilon \gg \delta\epsilon. \tag{4.39}$$

In the same large-detuning limit, we have the total decay rates (at any finite temperature T)

$$W_{T_+} = W_{T_-} \simeq 2cT, \quad \epsilon \to \pm\infty, \tag{4.40}$$

$$W_{T_0} \simeq W_{S_\pm} \simeq 3cT, \quad \epsilon \to \pm\infty. \tag{4.41}$$

In the opposite limit of small detuning ($\epsilon \ll \delta\epsilon$, or equivalently $\eta \gg 1$), Eqs. (4.31) and (4.32) decouple from Eq. (4.33). For $|\epsilon| \lesssim t$ and low temperature $T \lesssim t$, it is necessary to keep the g-dependence. The resulting solutions in this limit are

$$k_{T_0} = \frac{1}{4} + \frac{1}{2g}, \quad \epsilon \ll \delta\epsilon, \tag{4.42}$$

$$k_T = k_{T_\pm} = \frac{1}{4} + \frac{1}{4g}, \quad \epsilon \ll \delta\epsilon, \tag{4.43}$$

with corresponding rates given by

$$W_{T_\pm} = cT\,(1+g)\,, \tag{4.44}$$

$$W_{T_0} = cT\,(2+g)\,. \tag{4.45}$$

Combining the above results gives

$$\sum_j \frac{k_j}{W_j} \simeq \frac{4}{cT}\frac{1}{\eta} = \frac{3}{4cT}\left(\frac{\epsilon}{\delta\epsilon}\right)^2, \quad \epsilon \gg \delta\epsilon, \tag{4.46}$$

$$\sum_j \frac{k_j}{W_j} \simeq \frac{3}{4cT} g^{-1}(\epsilon, t, T), \quad \epsilon \ll \delta\epsilon. \tag{4.47}$$

Since the result in Eq. (4.46) vanishes for $\epsilon \ll \delta\epsilon$, but dominates over Eq. (4.47) for $\epsilon \gg \delta\epsilon$, we can simply add the two results to find the appropriate denominator for the current, Eq. (4.7), giving an expression that closely approximates the current everywhere except possibly in a small region around $\epsilon \sim \delta\epsilon$.

The resulting lineshape for the leakage current as a function of detuning ϵ is

$$I(B=0,\epsilon) \simeq \frac{\frac{4}{3}cT}{g^{-1}(\epsilon,t,T) + (\epsilon/\delta\epsilon)^2}, \quad \Gamma_l \gg W_{\alpha\beta}. \tag{4.48}$$

In general, the leakage current lineshape may be dominated by the function $g(\epsilon, t, T)$, due to escape from the triplets at small detuning $\epsilon \lesssim t$, and by a broad Lorentzian with width $\delta\epsilon$, limited by escape from the singlets at large detuning, $\epsilon > t$. Eq. (4.48) is plotted in Fig. 4.4 for various values of the tunnel coupling t, demonstrating the crossover from a narrow central peak dominated by triplet relaxation to a broad Lorentzian background, when each of the states is visited many times before an electron escapes the double dot. The balance between broad Lorentzian and peaked resonant tunneling can be tuned with the ratio of escape rate $\sim \Gamma_R$ to cotunneling rate $\sim cT$, controlled by the parameter α. The evolution of the current vs. detuning as α is varied is shown in Fig. 4.5.

The lineshape given in Eq. (4.48) simplifies considerably in the high-temperature

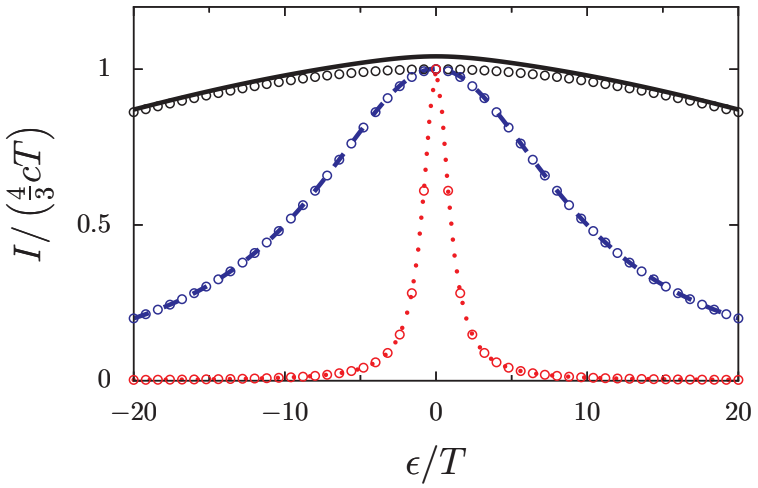

Figure 4.6: Detuning dependence at $B = 0$ from Eq. (4.48) for $\alpha = 100$ and $t = 0.5T$ (black solid line), $t = 0.1T$ (blue dashed line), and $t = 0.01T$ (red dotted line). Open circles give the equivalent curves from Eq. (4.49), valid in the limit $t \lesssim T$.

limit $T > t$, in which case the function $g(\epsilon, t, T) \simeq 1$, leaving a simple Lorentzian:

$$I(B = 0, \epsilon) \simeq \frac{\frac{4}{3}cT}{1 + (\epsilon/\delta\epsilon)^2}, \quad T > t, \Gamma_l \gg W_{\alpha\beta}. \tag{4.49}$$

Eq. (4.49) is plotted in Fig. 4.6 and compared with the full expression given in Eq. (4.48) in the relevant high-temperature limit.

Eq. (4.49) is consistent with recent experiments on silicon double quantum dots.[79]

4.4.3 Leakage current in the strong-dephasing limit

An especially simple and ubiquitous limit occurs when there is a strong local dephasing process[2] or a magnetic field gradient, allowing rapid escape for the spin-unpolarized triplet state $|T_0\rangle$ (i.e., $W_{T_0} \simeq W_{\sigma T_0} \gg W_{\alpha\beta}$). The advantage of this limit is the absence of closed 'loops' that complicated the analysis in Sec. 4.4.2.

At sufficiently small detuning $\epsilon < \delta\epsilon$, the rate of transition from one of the

[2]A spin dephasing process that acts locally on the right and left spins of a double quantum dot will convert the coherent triplet $|T_0\rangle = (|\uparrow\downarrow\rangle + |\downarrow\uparrow\rangle)/\sqrt{2}$ to an incoherent mixture of $|\uparrow\downarrow\rangle$ and $|\downarrow\uparrow\rangle$, both of which have a finite overlap with the singlets $|S_\pm\rangle$, and hence, a finite transition rate to $(0, 1)$ charge states via dot-lead tunneling.

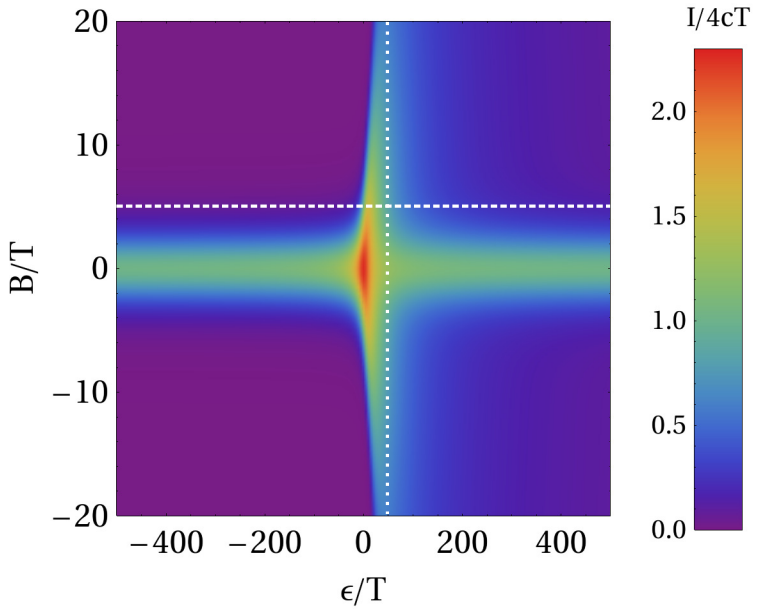

Figure 4.7: Map of the leakage current vs. detuning, ϵ, and magnetic field, B, in the strong-dephasing limit, $W_{T_0} \gg W_{T_\pm}$ from Eqs. (4.50) and (4.51). A tunnel coupling $t = 5T$ was chosen to generate this plot. Cuts vs. B at finite ϵ (dotted line) and vs. ϵ at finite B (dashed line) are shown in Figs. 4.8 and 4.9 below, respectively.

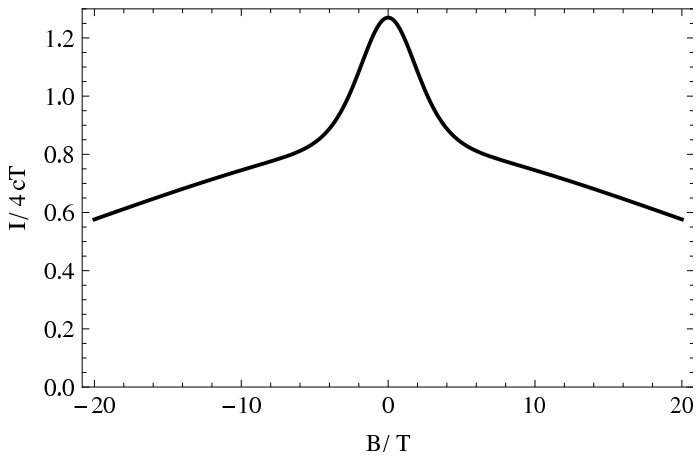

Figure 4.8: Cut of magnetic field dependence at finite detuning $\epsilon/T = 50$ along the dotted vertical line in Fig. 4.7. At finite positive detuning ϵ, the magnetic-field dependence shows a central peak with width set by $\sim T$ due to inelastic escape processes involving the triplet T_0 and excited-state singlet S_+, followed by a long slow decay at larger B, with a width $B \sim \epsilon$, after which the ground state becomes a spin triplet.

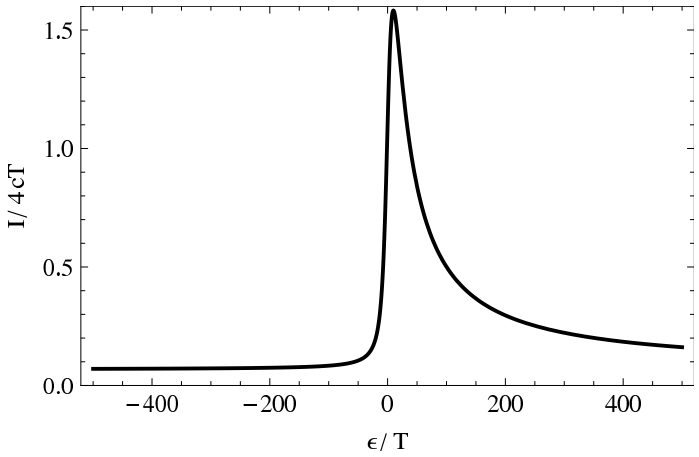

Figure 4.9: Cut of the detuning dependence at fixed finite magnetic field $B/T = 5$, along the dashed horizontal line in Fig. 4.7. At finite magnetic field, the detuning-dependent leakage current due to inelastic cotunneling is asymmetric in ϵ, since the ground state has spin-singlet character for $\epsilon > 0$, but spin-triplet character for $\epsilon < 0$.

singlet states to a triplet is small compared to the singlet escape rate, $W_{\alpha S_\pm} \ll W_{\sigma S_\pm}$. Consequently, the spin-polarized triplets $|T_\pm\rangle$ are visited at most once in each transport cycle, giving $k_{T_\pm} = 1/4$, since each of the four spin states in the $(1,1)$ charge configuration has equal probability of being occupied during a transport cycle. This gives immediately, from Eq. (4.7),

$$I \simeq \frac{4}{W_{T_+}^{-1} + W_{T_-}^{-1}}, \quad \Gamma_l \gg W_{\alpha\beta}, W_{T_0} \gg W_{T_\pm}, W_{\sigma S_\pm} \gg W_{\alpha S_\pm}. \tag{4.50}$$

It is important to emphasize the generality of the simple expression given in Eq. (4.50). In particular, this expression is valid for arbitrary spin-flip processes leading to transitions from the spin-polarized triplet states to the singlets or spin-unpolarized triplet T_0, e.g. $W_{S_+T_\pm} \neq 0$, $W_{T_0T_\pm} \neq 0$, or direct transitions leading to escape from the double dot, $W_{\sigma T_\pm} \neq 0$. These processes can be mediated by coupling to nuclear spins, spin-orbit interaction, or any other mechanism. The existence of a fast local dephasing mechanism (e.g., coupling to nuclear spins) even when spin relaxation rates may be slow is common. Even if there is no dephasing mechanism, a magnetic field gradient across the double dot is sufficient to reach

the limit $W_{T_0} \gg W_{T_\pm}$.[109]

When only inelastic cotunneling processes account for the rate $W_{T_\pm}$, the direct transitions carrying an electron out of the double dot vanish $W_{\sigma T_\pm} = 0$ and the remaining contributions can be found directly from Eq. (4.16):

$$W_{T_\pm}/cT = \left(W_{T_0 T_\pm} + W_{S_+ T_\pm} + W_{S_- T_\pm}\right)/cT$$
$$= F\left(\pm\frac{B}{T}\right) + \frac{\omega_- F\left(\frac{\pm B - \omega_+}{T}\right) + \omega_+ F\left(\frac{\pm B + \omega_-}{T}\right)}{\sqrt{\epsilon^2 + 8t^2}}. \quad (4.51)$$

We recall that the energies $\omega_\pm$ are defined in Eq. (4.35) and the functions $F(x)$ are defined by Eq. (4.19). Inserting the rates given in Eq. (4.51) into Eq. (4.50) immediately gives a complete map of the leakage current, with amplitude determined by the high-temperature cotunneling rate $\sim cT$ and all other features determined by only three dimensionless parameters: the magnetic field, detuning, and tunnel coupling, scaled by the temperature: $B/T, \epsilon/T, t/T$. We show a map of the leakage current as a function of B/T and ϵ/T in Fig. 4.7 for the case of $t = 5T$.

Taking the limit $B = \epsilon = 0$, $T \gg t$, we find that the current saturates at a maximum value:

$$I(B = 0, \epsilon = 0) = 4cT = \bar{n} W_{\mathrm{cot}}, \quad (4.52)$$
$$W_{\mathrm{cot}} = 2cT, \quad T \gg t. \quad (4.53)$$

Here, we find the average number of electrons passing through the double dot for each cotunneling event is $\bar{n} = 2$, in contrast to the situation in Sec. 4.4.2, where $\bar{n} = 4/3$ for the same parameter values. This is due to the fact that now only two out of four of the $(1,1)$ charge states are blocked ($|T_\pm\rangle$), giving $\bar{n} = 4/2 = 2$.

A cut of I vs. B at finite detuning $\epsilon > 0$ is shown in Fig. 4.8. The central peak in this figure has width $\sim T$, due to thermally activated escape from the ground state triplet through the T_0 state. The broad background current falls to zero at $B \simeq \epsilon$, where the ground state becomes a spin-triplet ($|T_-\rangle$ [$|T_+\rangle$] for $B > 0$ [$B < 0$]). A similar effect is shown as a function of ϵ at finite magnetic field $B > T$ in Fig. 4.9.

Here, for $\epsilon < 0$ the ground state becomes a spin triplet and current is suppressed exponentially in B/T, whereas for $\epsilon > 0$ the ground state is a spin-singlet and relaxation processes can still lead to escape with a slow rate $\sim 1/\epsilon$ until ϵ becomes very large. A detuning asymmetry such as this one is often ascribed to phonon-assisted tunneling, but can result (as it does for the inelastic cotunneling mechanism considered here) from any other mechanism for which excitation is exponentially suppressed relative to relaxation.

4.4.3.1 B-field dependence (low-T limit)

In the low-temperature limit, $T \ll t$, we use the approximation given in Eq. (4.21) to find the relevant escape rates from Eq. (4.51). For, e.g., $B > 0$ and $\epsilon = 0$, these rates are

$$W_{T_+} = cB + \frac{c}{2}\left(\sqrt{2}t + B\right)\Theta(\sqrt{2}t + B), \tag{4.54}$$

$$W_{T_-} = \frac{c}{2}\left(\sqrt{2}t - B\right)\Theta(\sqrt{2}t - B). \tag{4.55}$$

Inserting these rates into Eq. (4.50) directly gives the low-temperature expression for the current, previously reported in ref. [109],

$$I = \frac{c(\sqrt{2}t - |B|)(\sqrt{2}t + 3|B|)}{(\sqrt{2}t + |B|)}\Theta(\sqrt{2}t - |B|), \quad T \ll t. \tag{4.56}$$

Eq. (4.56) is plotted in Fig. 4.10. The current falls to zero at $|B| = \sqrt{2}t$ when the ground-state triplet falls below the ground-state singlet $|S_-\rangle$. At larger B, excitation processes are exponentially suppressed and the system becomes locked in the ground-state triplet. The dip at $B = 0$ occurs because relaxation processes from $T_\pm$ to T_0 vanish when the levels become degenerate, while at small finite B, an additional "escape route" is available for the highest-energy triplet through $|T_0\rangle$.

From Eq. (4.50), it is clear that the current will experience a dip at $B = 0$ whenever the rates $W_{T_\pm}$ are reduced at $B = 0$. This effect becomes especially pronounced for contributions to $W_{T_\pm}$ from, e.g., the spin-orbit coupling, which

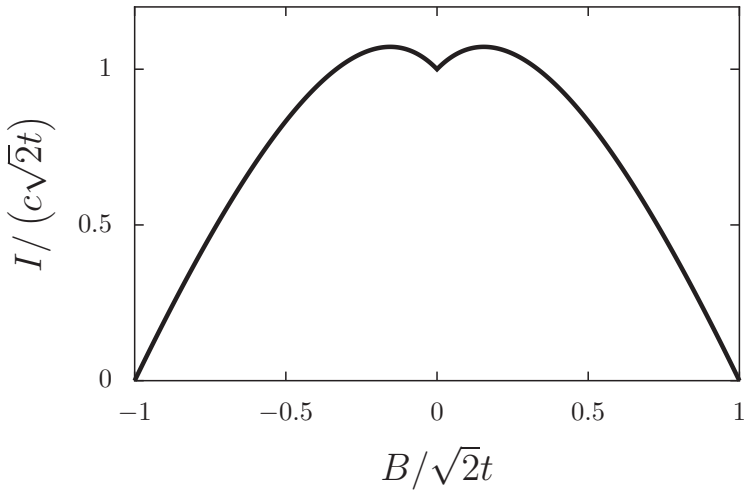

Figure 4.10: $T = 0$ expression for I vs. B (valid for $T < t$).

must necessarily vanish at $B = 0$ due to time-reversal invariance.[51] This effect due to spin-orbit coupling has been demonstrated in the context of the Pauli spin blockade regime using a phenomenological model that preserves time-reversal, but hybridizes the triplet and singlet states.[27] For a microscopic theory, an additional magnetic-field gradient or local spin dephasing process is likely necessary to arrive at this conclusion in general, since the spin triplet state $|T_0\rangle$ does not hybridize with the spin singlets at leading order in the spin-orbit coupling.[51]

4.5 Conclusions

We have presented a generic and simple procedure for calculating leakage current through blockaded structures. Using this generic theory, we found simple analytical expressions for current lineshapes as a function of an applied magnetic field B, energy detuning ϵ, and inter-dot tunnel coupling t. These lineshapes fully account for inelastic cotunneling in two limits: weak-dephasing and strong-dephasing. The results we have found in the weak-dephasing limit are consistent with recent experiments performed on silicon double quantum dots[79] and may be applicable to carbon-based double dots, which are also expected to have weak spin-orbit interactions and only weak dephasing. In the strong-dephasing limit, we have found

a simple expression that gives the full two-dimensional map of leakage current vs. B and ϵ in the presence of inelastic cotunneling. Finally, we have given a general understanding of zero-field current dips in the limit of strong dephasing.

To simplify the analysis directly associated with the Pauli spin blockade in a double quantum dot, we have neglected orbital and valley degeneracy, which may be relevant in silicon and carbon-based double dots. Effects of these degeneracies can, however, be included in a systematic and straightforward way using the general methodology outlined in Sec. 4.3. We leave the details of such an analysis to future study.

We thank H. O. H. Churchill, A. Dzurak, N. S. Lai, C. M. Marcus, A. Morello, and F. Zwanenburg for stimulating discussions. WAC acknowledges funding from the CIFAR JFA, NSERC, FQRNT, and INTRIQ. FQ acknowledges financial support from NSERC, WIN, and QuantumWorks.

Chapter 5

Pauli Spin Blockade in a Highly Tunable Silicon Double Quantum Dot

5.1 Outline

Double quantum dots are convenient solid-state platforms to encode quantum information. Two-electron spin states can be conveniently detected and manipulated using strong quantum selection rules based on the Pauli exclusion principle, leading to the well-know Pauli spin blockade of electron transport for triplet states. Coherent spin states would be optimally preserved in an environment free of nuclear spins, which is achievable in silicon by isotopic purification. Here we report on a deliberately engineered, gate-defined silicon metal-oxide-semiconductor double quantum dot system. The electron occupancy of each dot and the inter-dot tunnel coupling are independently tunable by electrostatic gates. At weak inter-dot coupling we clearly observe Pauli spin blockade and measure a large intra-dot singlet-triplet splitting > 1 meV. The leakage current in spin blockade has a peculiar magnetic field dependence, unrelated to electron-nuclear effects and consistent with the effect of spin-flip cotunneling processes. The results obtained here provide

excellent prospects for realizing singlet-triplet qubits in silicon.

Gate-defined semiconductor quantum dots enable the confinement and manipulation of individual electrons and their spin [53]. Most of the relevant parameters – electron filling, energy splittings, spin states, exchange interaction – can be tuned *in situ* by electric and magnetic fields. Because of this exquisite level of control, quantum dots are being investigated as candidate systems for spin-based quantum information processing [85]. In group III-V semiconductors such as GaAs, the development of highly tunable double quantum dots has allowed the study of both single-electron and two-electron spin dynamics [98, 102, 74, 60, 73]. However, the nuclear spins always present in these materials produce strong decoherence of the electron spin degree of freedom and result in phase coherence times T_2 of below 1 ms [7, 13]. Conversely, group-IV semiconductors such as silicon, silicon-germanium and carbon can be isotopically purified, leaving only spinless isotopes. The weak spin-orbit coupling [128] and the absence of piezoelectric electron-phonon coupling [41] allow for extremely long spin relaxation times T_1 of order seconds, as already demonstrated in several experiments [137, 94, 123]. The phase coherence times have not been measured yet, but they are expected to reach ~ 1 s as well, in highly purified ^{28}Si substrates with low background doping concentration [135].

A widely successful method to observe and control spin phenomena in quantum dots [53] consists of defining a double quantum dot in a series configuration and tuning the potentials such that sequential electron transport requires a stage where two electrons must occupy the same dot. The eigenstates of a two-electron system are singlet and triplet spin states, separated by an energy splitting Δ_{ST} which can be large in tightly confined dots. The electron transport then becomes spin-dependent and can be blocked altogether when the two-electron system forms a triplet state [98, 44]. This phenomenon, known as Pauli spin blockade, has been extensively exploited to investigate the coherence of single-spin [73] and two-spin states [102] in GaAs and InAs [95] quantum dots. Therefore, observing and controlling spin blockade in silicon is a key milestone to unravel the full potential of highly coherent spin qubits. Preliminary success has been obtained in Si [84]

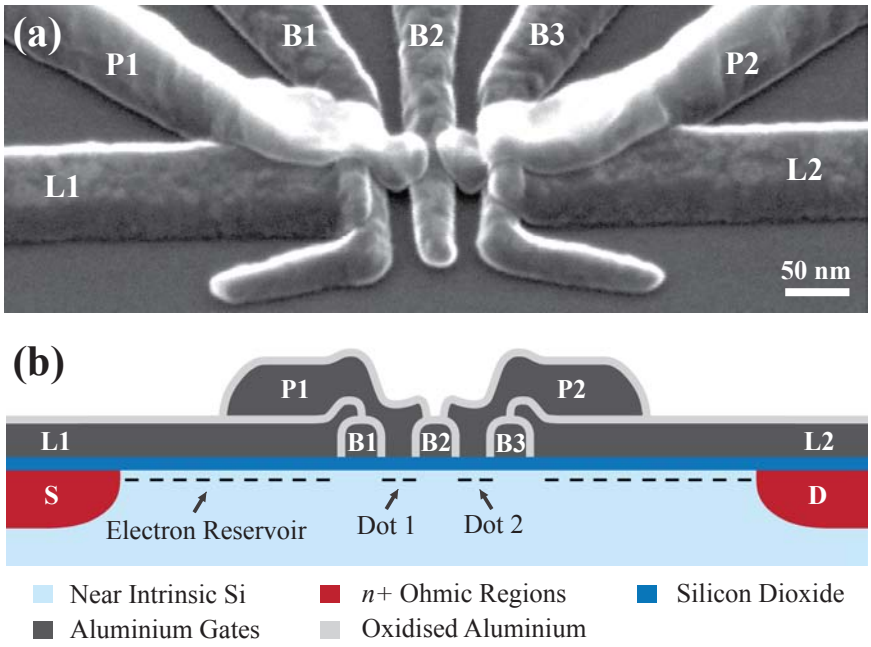

Figure 5.1: **SEM and schematic view of the device**. (a) Scanning electron micrograph of a device identical to that measured. (b) (Not to scale) Schematic cross-section view of the Si MOS double quantum dot. The architecture is defined by B1, B2 and B3 (barrier gates), L1 and L2 (lead gates), and P1 and P2 (plunger gates). The gates are separated by an Al_2O_3 layer (light gray). Positive voltages applied to the lead and plunger gates induce an electron layer (black dashes) underneath the SiO_2. By tuning the barrier gates, Dot 1 and Dot 2 are formed. The coupling of the dots is adjusted using the middle barrier (B2). The regions coloured with red are the n^+ source (S) and drain (D) contacts formed via diffused phosphorus.

and SiGe [122] devices, but in each case the double dot system under study resulted from local variations in the potential of a lithographically-defined single dot, making it difficult to control individual dot occupancies or inter-dot coupling. Spin-based quantum dot qubits require exquisite control of these parameters, so a highly tunable double-dot system in silicon is essential. For singlet-triplet qubits in multivalley semiconductors it is also crucial to ensure that a large valley-orbit splitting is present, to avoid the lifting of Pauli blockade due to valley degeneracy [100, 26].

Here we present an engineered silicon double quantum dot which shows excellent tunability and robust charge stability over a wide range of electron occupancy (m, n). The silicon metal-oxide-semiconductor (MOS) structure utilizes an Al-Al_2O_3-Al multi-gate stack that enables very small dots to be defined, each with independent gate control, together with gate-tunable inter-dot coupling. Such multi-gate stacks have previously been used to construct single Si quantum dots with the ability to achieve single electron occupancy [82]. The double dot presented here exhibits spin blockade in the few-electron regime, from which we are able to extract a large singlet$-$triplet energy splitting and also investigate a new mechanism of singlet$-$triplet mixing in the weak-coupling regime.

5.2 Results

Device architecture. Figure 5.1 shows a scanning electron micrograph (SEM) and cross-sectional schematic of the device, which incorporates 7 independently controlled aluminium gates. When a positive bias is applied to the lead gates (L1 and L2) an accumulation layer of electrons is induced under the thin SiO_2, to form the source and drain reservoirs for the double dot system. A positive voltage on the plunger gate P1 (P2) causes electrons to accumulate in Dot 1 (Dot 2). Independent biasing of P1 and P2 provides direct control of the double-dot electron occupancy (m, n). The tunnel barriers between the two dots and the reservoirs are controlled using the barrier gates: B1, B2 and B3. The middle barrier gate B2 determines the inter-dot tunnel coupling. The electrochemical potentials of the coupled dots

can also be easily tuned to be in resonance with those of the source and drain reservoirs. As shown in Fig. 5.1(b), gates L1 and L2 extend over the source and drain n^+ contacts, and also overlap gates B1 and B3. The upper-layer gates (P1 and P2) are patterned on top of the lead and barrier gates. The lithographic size of the dots is defined by the distance between adjacent barrier gates (∼30 nm) and the width of the plunger gates (∼50 nm), as shown in Fig. 5.1(a).

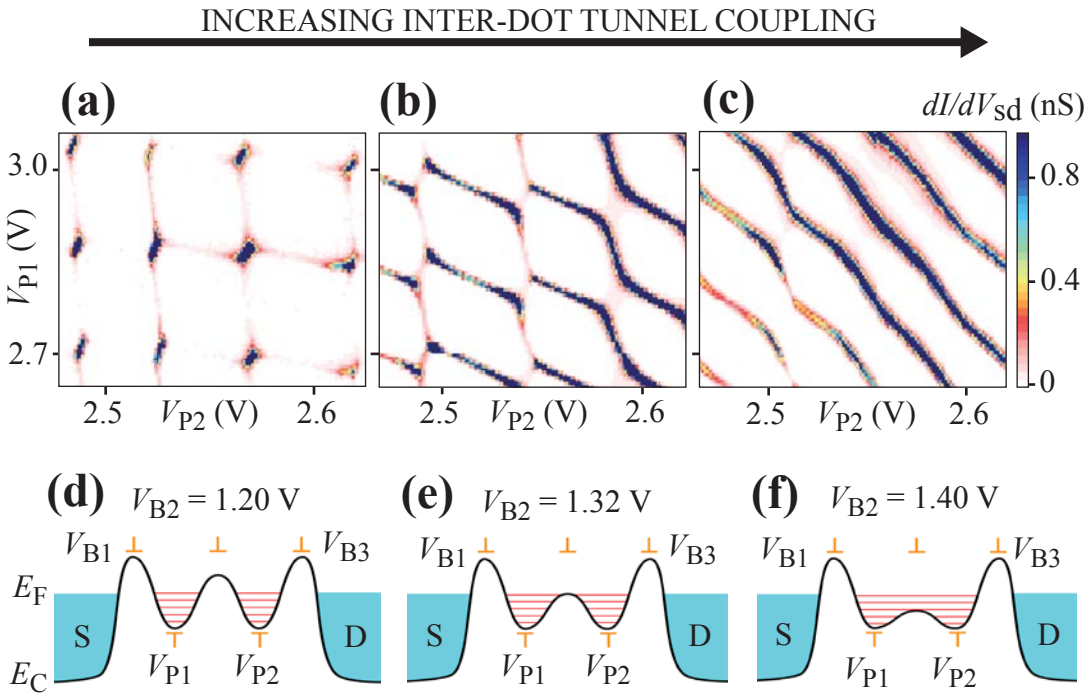

Figure 5.2: **Characteristics at different inter-dot tunnel coupling**. Measured stability diagrams and energy landscape of the double dot system ranging from weak to strong inter-dot tunnel coupling (a)−(c) and (d)−(f) respectively, for $V_{L1} = V_{L2} = 3.0$ V, $V_{B1} = 0.76$ V, $V_{B3} = 1.0$ V and $V_{SD} = 0$. From lower to higher V_{B2}, the tunnel barrier height decreases resulting in stronger inter-dot tunnel coupling. (a) A checker box pattern, (b) honeycomb pattern and (c) diagonal parallel lines indicate that the two dots merge into a single dot as the coupling is increased [131].

Inter-dot tunnel coupling tunability. Figure 5.2 shows the measured differential conductance of the device as a function of the plunger gate voltages, V_{P1} and V_{P2}, with all other gate voltages held constant, together with sketches of the energy landscape of the double dot. The charge-stability maps moving from Fig. 5.2(a) to 5.2(c) clearly show the effects of an increasing inter-dot coupling as the mid-

dle barrier-gate voltage V_{B2} is increased, lowering the tunnel barrier between the dots. Fig. 5.2(b) shows the characteristic honeycomb-shaped stability map representing intermediate inter-dot coupling [131], obtained at $V_{B2} = 1.32$ V. At lower middle barrier-gate voltage, $V_{B2} = 1.20$ V, we observe a checker-box shaped map [Fig. 5.2(a)], since the middle barrier is opaque enough to almost completely decouple the two dots. In contrast, the stability map in Fig. 5.2(c) shows the formation of diagonal parallel lines at $V_{B2} = 1.40$ V. Here the two dots effectively merge into a single dot due to the lowering of the middle barrier [Fig. 5.2(f)]. The transport measurements shown here do not allow a precise determination of the electron occupancy $(m,\ n)$ in the dots, since it is possible that electrons remain in the dots even when I_{SD} is immeasurably small. For the regime plotted in Fig. 5.2 there were at least 10 electrons in each dot, based on our measurement of Coulomb peaks as we further depleted the system. An absolute measurement of dot occupancy would require integration of a charge sensor into the system [60]. These results nevertheless demonstrate that the multi-gated structure provides excellent tunability of coupling while maintaining charge stability over a wide range of electron occupancy.

Capacitances and charging energies. Application of a DC source-drain bias V_{SD} causes the triple-points in the weakly-coupled regime [Fig. 5.2(a)] to extend to form triangular shaped conducting regions [Fig. 5.3(a)] from which the energy scales of the double dot system can be determined [131]. From a triangle pair, we extract the conversion factors between the gate voltages and energy to be $\alpha_1 = eV_{SD}/\delta V_{P1} = 0.089e$ and $\alpha_2 = eV_{SD}/\delta V_{P2} = 0.132e$, where δV_{P1} and δV_{P2} are the lengths of the triangle edges, as shown in Fig. 5.3(a). The total capacitances of Dot-1 and Dot-2 can then be calculated [131], giving $C_1 = 16.3$ aF and $C_2 = 14.5$ aF. The charging energies of the two dots are then $E_{C,1} = e^2/C_1 = 9.8$ meV and $E_{C,2} = e^2/C_2 = 11$ meV, indicating that the left dot is slightly larger than the right dot.

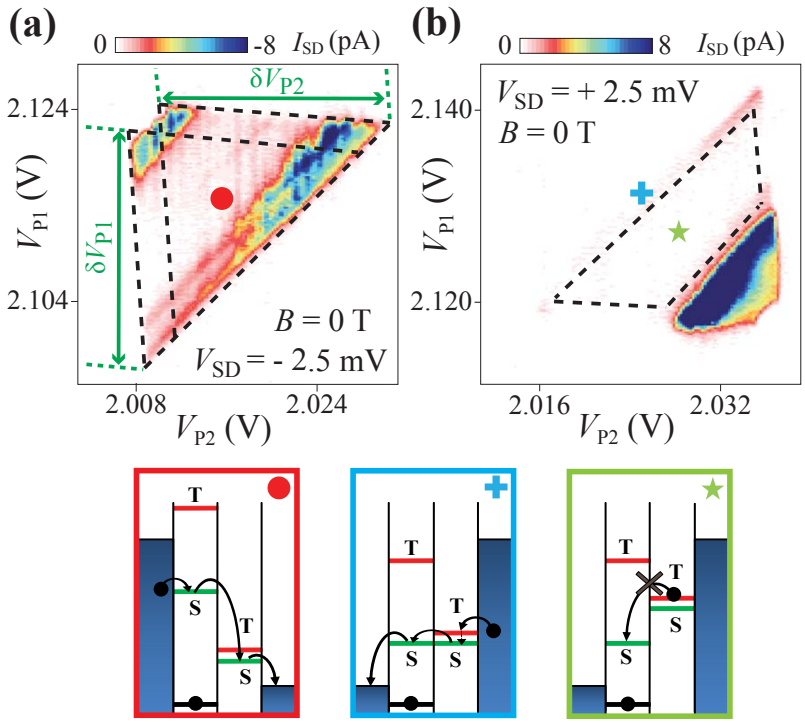

Figure 5.3: **Pauli spin blockade at weakly coupled regime**. Current I_{SD} as a function of V_{P1} and V_{P2} for $B = 0$ T. The lead and barrier gate voltages were fixed at $V_{L1} = V_{L2} = 3.2$ V, $V_{B1} = 0.656$ V, $V_{B2} = 1.176$ V and $V_{B3} = 0.940$ V throughout the experiment. (a) For $V_{SD} = -2.5$ mV, the ground state and excited states of a full bias triangle are shown. The current flows freely at the S(0,2)−S(1,1) transition as illustrated in the box marked by red dot. (b) The same configuration at $V_{SD} = +2.5$ mV, the current between the singlet and triplet states is fully suppressed by spin blockade (green star box) except on the bottom (blue cross box) of the bias triangle. The blue cross box shows how a leakage current arises the Pauli spin blockade region.

Pauli spin blockade. Figure 5.3 shows the current I_{SD} through the double dot as a function of the two plunger gate voltages when measured with both positive [Fig. 5.3(a)] and negative [Fig. 5.3(b)] source-drain biases. Here we observe a suppression of current at one bias polarity, the characteristic signature of Pauli spin blockade [74, 60]. At $V_{SD} = -2.5$ mV we observe a pair of overlapping full bias triangles, as shown in Fig. 5.3(a). Resonant transport through the ground state and the excited states in the double dot occurs when the states within the dots are exactly aligned, leading to peaks in the current which appear as straight lines parallel to the triangle base in Fig. 5.3(a). The non-resonant background current

level at the centre of the triangle is attributed to inelastic tunneling. The non-zero current throughout the triangular region indicates that electrons from the reservoir can tunnel freely from the S(0,2) singlet state to the S(1,1) singlet state, as depicted in the cartoon (red box in Fig. 5.3). Note that here we define (m, n) as the *effective* electron occupancy [84], while the *true* electron occupancy is (m+m_0, n+n_0). The Pauli blockade expected for two-electron singlet and triplet states occurs when the total electron spin of each dot is zero in the (m_0, n_0) state.

At the complementary positive bias of $V_{\mathrm{SD}} = +2.5$ mV we observe strong current suppression in the region bounded by the dashed lines in Fig. 5.3(b). The suppression arises because the transition from T(1,1) to S(0,2) is forbidden by spin conservation during electron tunneling. Once the T(1,1) triplet state is occupied, further current flow is blocked until the electron spin on the right dot reverses its orientation via a relaxation process (green star box in Fig. 5.3) [74, 60].

Singlet-triplet splitting. In a magnetic field B there are four accessible spin states: the singlet S; and three triplets T_-, T_0 and T_+, corresponding to $S_{\mathrm{Z}} = -1$, 0, $+1$. The singlet$-$triplet splitting Δ_{ST} is the energy difference between the blockaded ground state S(0,2) and the excited state T_-(0,2) [60, 84]. Here we study Δ_{ST} as a function of B, applied parallel to the substrate, by measuring spin blockade at a positive bias. Figures 5.4(a$-$c) show the bias triangles in the spin blockade regime at increasing magnetic fields $B = 2$, 4 and 6 T, with the splitting Δ_{ST} marked in Fig. 5.4(a). The measured splitting Δ_{ST} decreases linearly with increasing B [Fig. 5.4(d)], as expected, since the triplet states split linearly by the Zeeman energy, $E_{\mathrm{Z}} = \pm S_{\mathrm{Z}}|g|\mu_B B$, where μ_B is the Bohr magneton and S_{Z} is -1, 0, $+1$. A linear fit through $\Delta_{\mathrm{ST}}(B)$ yields a Landé g-factor of 2.1 ± 0.2, consistent with electrons in silicon.

We observe an exceptionally large value of the (0,2) singlet-triplet splitting at $B = 0$, $\Delta_{\mathrm{ST}} \approx 1.4$ meV. This result is striking because it implies that the nearest valley-orbit state must be at least 1.4 meV above the ground state. The first excited valley-orbit state should be a combination of the $\pm z$ valleys. It would lift the spin blockade [100, 26], and show no remarkable energy shift in a magnetic field, in

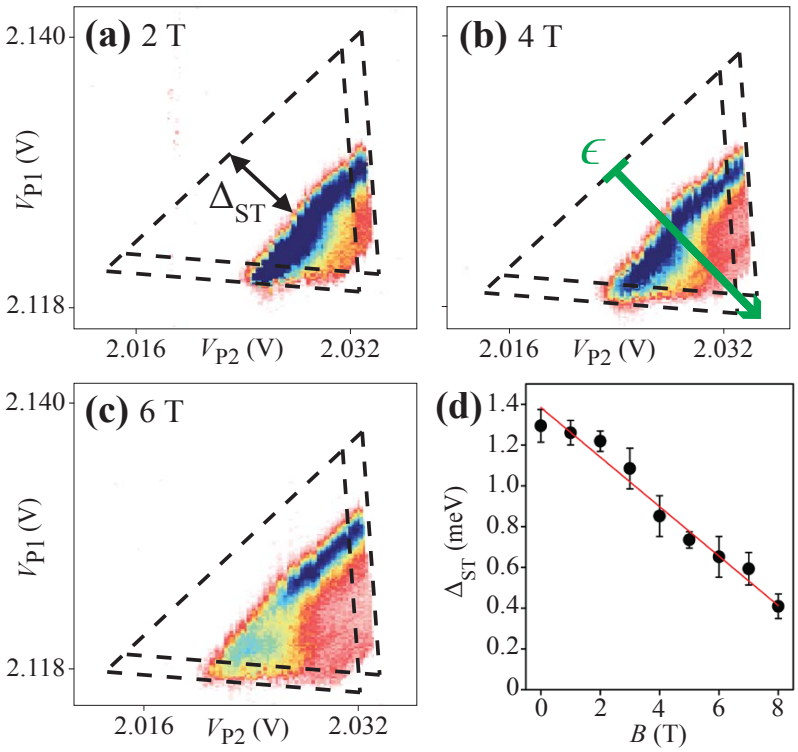

Figure 5.4: **Singlet-triplet splitting**. (a)−(c) DC measurements of the triangle pair analysed in Fig. 5.3, at $V_{SD} = +2.5$ mV, for different in-plane magnetic fields, B (scale bar same as Fig. 5.3(b)). The singlet−triplet splitting, Δ_{ST}, is defined by the triplet and singlet state of (0,2) as depicted in (a). As the magnetic field increases, Δ_{ST} decreases along the detuning axis of the triangle [labeled ϵ in (b)]. (d) The energy spacing Δ_{ST} as a function of in-plane magnetic field B. Δ_{ST} decreases at a rate $\sim$0.12 meV/T and is expected to approach zero at 11.3 T. From the linear fit (red line) through Δ_{ST}, the g-factor is 2.1 $\pm$ 0.2.

contrast with our observations. Therefore, such a state must lie above the triplet state we observe in Fig. 5.4. The ability of our structures to generate such a large valley-orbit splitting removes a major concern on the realizability of singlet-triplet qubits in a multivalley material such as silicon.

Leakage current in blockade regime. If some mechanism exists to mix the singlet and triplet states or to induce transitions between them, then the spin blockade can be lifted, leading to a measurable leakage current [74]. As shown in the blue cross box in Figure 5.3, transitions from T(1,1) to S(1,1) can lift the blockade, allowing electrons to transit the double dot until the next triplet is loaded, resulting in a non-zero time-averaged leakage current. Fig. 5.5(a) shows the surface plot of the leakage current I_{SD} as a function of both detuning ϵ and magnetic field B, while Figs. 5.5(b) and 5.5(c) show line traces of I_{SD} as a function of B at zero detuning and I_{SD} as a function of ϵ at zero magnetic field, respectively. We find that the leakage current has a maximum at $B \approx 0$ and falls to zero at $|B| \sim 700$ mT.

5.3 Discussion

The suppression of leakage current by an applied magnetic field has been observed in GaAs double quantum dots (DQDs) [74] and attributed to the effect of hyperfine coupling between the electron spins and the surrounding bath of nuclear spins. In that case the width δB of $I_{\mathrm{SD}}(B)$ yields the average strength of the hyperfine field. For an unpolarized nuclear spin bath $\delta B \approx \delta B_{\mathrm{max}}/\sqrt{N}$, where δB_{max} is the hyperfine field assuming fully polarized nuclei and N is the number of nuclei overlapping with the electron wave function. For a typical GaAs dot overlapping with $\sim 10^6 - 10^7$ nuclei, $\delta B_{\mathrm{max}} \sim 6$ T $\Rightarrow \delta B \sim 2 - 6$ mT [74, 60, 90]. In natural silicon, however, the hyperfine interaction is much smaller than in GaAs, with $\delta B_{\mathrm{max}} \approx 1.9$ mT [5]. Therefore, hyperfine coupling can be ruled out as a mechanism for the leakage current here.

An alternative mechanism for a transition from triplet to singlet has been recently proposed, where the spin flip is caused by inelastic cotunneling [109]. The

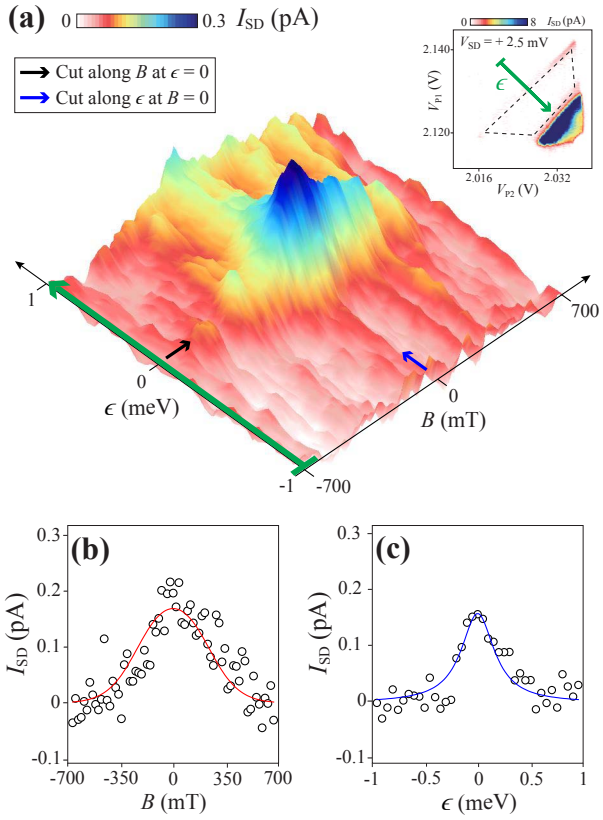

Figure 5.5: **Spin-flip cotunneling in Pauli spin blockade regime**. (a) A surface plot of leakage current through spin blockade as a function of energy detuning ϵ and magnetic field B, with gates settings as in Fig 5.3(b). (b) Cut along B at $\epsilon = 0$ energy detuning axis (black arrow) while (c) Cut along ϵ at $B = 0$ field (blue arrow). Fits of experimental data with spin-flip cotunneling relation give $\Gamma_D = 34$ μeV, $t = 0.5$ μeV and $T = 115$ mK.

spin-flip rates due to cotunneling from the spin-polarized triplet states, $T_{\pm}(1,1)$, are exponentially suppressed when the Zeeman energy is large compared to the thermal broadening of the electron states in the leads (i.e., for $g\mu_{\rm B}B > k_{\rm B}T$, where T is the electron temperature and B is the applied magnetic field). A rate-equation analysis accounting for the energy dependence of the spin-flip cotunneling rates [109] then gives a simple form in the limit of weak inter-dot tunneling t and weak cotunneling $W^0_{\rm cot}$ compared to the tunnel rates $\Gamma_{\rm S,D}$ between a dot and its nearby source or drain lead ($\sqrt{2}t < k_{\rm B}T$, $W^0_{\rm cot} \ll \Gamma_{\rm S,D}$) [22]:

$$I_{\rm SD}(B) = e\frac{4}{3}\frac{3W^0_{\rm cot}/2}{1+\frac{k_{\rm B}T}{2g\mu_{\rm B}B}\sinh\left(\frac{g\mu_{\rm B}B}{k_{\rm B}T}\right)}, \quad \epsilon = 0. \tag{5.1}$$

Here, the $B = 0$ spin-flip cotunneling rate (for $k_{\rm B}T > \sqrt{2}t$ and $|\epsilon| < |\Delta|, |e|V_{\rm SD}$) is:

$$W^0_{\rm cot} = \frac{k_{\rm B}T}{\pi\hbar}\left[\left(\frac{\hbar\Gamma_{\rm S}}{\Delta}\right)^2 + \left(\frac{\hbar\Gamma_{\rm D}}{\Delta - 2U' - 2|e|V_{SD}}\right)^2\right] \tag{5.2}$$

with mutual (inter-dot) charging energy U' and $\Delta = \alpha_1\delta V_{\rm P1} + \alpha_2\delta V_{\rm P2}$ for plunger gate voltages $\delta V_{\rm P1,P2}$ measured from the effective $(0,1)-(1,1)-(0,2)$ triple point (lower-left corner of the bias triangle in Fig. 5.3(b)). Eq. (5.2) accounts for virtual transitions between effective $(1,1)$ and $(0,1)$ (first term) as well as effective $(1,1)$ and $(1,2)$ charge states (second term).

In the present case, $\Delta \simeq |e|V_{\rm SD} \gg U'$. The higher current level in the upper right corner of Fig. 5.3(b) further suggests $\Gamma_{\rm D} \gg \Gamma_{\rm S}$, giving (for this particular experiment):

$$W^0_{\rm cot} \simeq \frac{k_{\rm B}T}{\pi\hbar}\left(\frac{\hbar\Gamma_{\rm D}}{|e|V_{\rm SD}}\right)^2. \tag{5.3}$$

Using the above expression for $W^0_{\rm cot}$, we then use Eq. (5.1) to fit to the $I_{\rm SD}(B)$ data in Fig. 5.5(b), giving us $\Gamma_{\rm D} = 34$ μeV for the tunneling rate and $T = 115$ mK for the electron temperature.

The $B = 0$ spin-flip cotunneling rate $W^0_{\rm cot}$ is energy-independent in the limit $\sqrt{2}t < k_{\mathbf{B}}T$. However, the leakage current does acquire a dependence on the energy

detuning, $\epsilon = \alpha_1 V_{\rm P1} - \alpha_2 V_{\rm P2}$, when the escape rate from the double-dot due to resonant tunneling is suppressed below the spin-flip cotunneling rate. This leads to a Lorentzian dependence of the current on detuning ϵ with a t-dependent width $\delta\epsilon$:

$$I_{\rm SD}(\epsilon) = e\frac{4}{3}\frac{W^0_{\rm cot}}{1+(\epsilon/\delta\epsilon)^2}, \quad B = 0, \tag{5.4}$$

$$\delta\epsilon = \left(\frac{3\Gamma_D t^2}{W^0_{\rm cot}}\right)^{1/2}. \tag{5.5}$$

Eq. (5.4) is valid in the same limit ($\sqrt{2}t < k_{\rm B}T$, $W^0_{\rm cot} \ll \Gamma_{\rm S,D}$) as Eq. ((5.1)). In the strong-tunneling limit, $\sqrt{2}t > k_{\rm B}T$, the theory predicts that $I(\epsilon)$ should show a strong resonant-tunneling peak of width $\sim t$, followed by a slowly-varying Lorentzian background described by Eq. ((5.4)) at large ϵ. The absence of a strong resonant-tunneling peak in the data of Fig. 5.5(c) confirms that the device is operating in the regime $\sqrt{2}t < k_{\rm B}T$, justifying our use of Eqs. (5.1) and (5.4) to analyse the data.

A nonlinear fit to the $I_{\rm SD}(\epsilon)$ data in Figs. 5.5(c) using Eq. (5.4) yields $t = 0.5$ μeV for the inter-dot tunneling rate, using our previously determined values $\Gamma_{\rm D} = 34$ μeV and $T = 115$ mK. These parameter values are well within the experimentally expected range. The small value of t indicates weak inter-dot tunnel coupling, consistent with the results shown in Fig. 5.3(b). We conclude that the spin-flip cotunneling mechanism provides a fully consistent explanation of the observed leakage current in the spin blockade regime. The mechanism could be applied to reanalyse previous experiments in group IV semiconductors [18] where the nature of the leakage current was not fully understood.

In conclusion, we have presented a lithographically-defined double quantum dot in intrinsic silicon showing excellent charge stability and low disorder. The multigate architecture provides independent control of electron number in each dot as well as a tunable tunnel coupling. We observed Pauli spin blockade in an *effective* two-electron system from which we extracted the singlet−triplet splitting. The leakage current in the spin blockade regime is well explained by a spin-flip cotun-

neling mechanism, which could be of widespread importance in group-IV materials with weak hyperfine coupling. The results obtained here provide a pathway towards investigation of spin blockade in silicon double quantum dots with *true* (1,1) and (2,0) electron states. Towards this end, we are planning future experiments incorporating a charge sensor to monitor the last few electrons [124]. We anticipate that such an architecture will provide excellent prospects for realizing singlet−triplet qubits in silicon [25]. It should be noted that my contribution was to the data analysis and understanding of the physics. The whole fabrication and measurement process have been performed at Dzurek's group the University of South Wales.

5.4 Acknowledgements

The authors thank D. Barber and R. P. Starrett for their technical support and acknowledge the infrastructure support provided by the Australian National Fabrication Facility. This work was funded by the Australian Research Council, the Australian Government, and by the U. S. National Security Agency and U.S. Army Research Office (under Contract No. W911NF-08-1-0527). W.A.C acknowledges the funding from the CIFAR JFA. F.Q. acknowledges funding from NSERC, WIN and QuantumWorks.

5.5 Author Contributions

N.S.L. fabricated the devices. N.S.L., W.H.L and C.H.Y designed and performed the experiments. W.A.C and F.Q. modelled the spin-flip cotunneling rate. N.S.L., F.A.Z., W.A.C, F.Q., A.M. and A.S.D. wrote the manuscript. A.S.D planned the project. All authors discussed the results and commented on the manuscript at all stages.

Chapter 6

Probing spin relaxation in a double quantum dot using frequency-dependent shot noise

6.1 Outline

We formulate a theory of frequency-dependent shot noise of a current through a double quantum dot in Pauli spin blockade regime. We use the general full counting statistics method to relate the average current and the shot noise at various time scales. Finally, we provide a general analytical equation for the frequency dependent Fano factor which can be used to determine both relaxation and dephasing.

6.2 Introduction

Understanding microscopic spin-relaxation processes in a double quantum dot is important for potential applications in the electron-spin-based quantum information processing [85] and spintronics (e.g., spin valves and spin diodes) [136], as well as molecular transport.[87] Complete understanding of the limits on spin lifetimes in quantum dots would provide a physical picture of underlying interactions and point to methods of suppressing unwanted decoherence and relaxation.

It is possible, in principle, to determine a single relaxation rate directly from the stationary current or zero-frequency noise of current passing through the quantum dot. However, to characterize multiple relaxation processes that occur simultaneously, it is useful to measure the transient current or the frequency-dependent noise to properly disentangle the relevant decay times.

Pulsed-gate techniques that measure spin relaxation via transport in single quantum dots are typically limited to measuring relaxation processes in a sufficiently large magnetic field[56, 103], as they require that the relevant levels are Zeeman split by more than the thermal broadening in the leads. The dominant spin-relaxation mechanism in most quantum dots (involving spin-orbit interaction and phonon emission) [66, 40, 67, 50] is strongly suppressed at small magnetic field ($1/T_1 \propto B^5$) (see, e.g., Table 1 of Ref. [21]). Thus, to determine the relaxation rates in these systems at low magnetic fields ($B \lesssim 1\,\mathrm{T}$) and typically achievable cryogenic temperatures, it is necessary to use a probe that is immune to thermal smearing in the leads. Such a probe is provided by the Pauli spin blockade of transport through a double quantum dot, which relies on spin-selection rules rather than energy conservation[98, 60, 138].

In this chapter, we apply a master equation approach to study shot noise. We compute ratio of the noise to current, the so called Fano factor [12], generalizing the method of ref. [76] to include spin and higher-order tunneling. We formulate a theory of the frequency-dependent current noise through a double quantum dot in the Pauli spin blockade regime including the effects of multiple relaxation processes. This theory gives a one-to-one correspondence between the form of the frequency-dependent Fano factor and the relevant relaxation rates and can therefore be used to determine these rates through a measurement of the current noise.

6.3 Double quantum dot in the Pauli spin blockade regime

The Pauli spin blockade [98, 74] (PSB) refers to the blockade of current based on the Pauli exclusion principle. PSB is crucial for the initialization and read-out of spins in quantum dots, [102] where the blocking of current through a double quantum dot (DQD) is conditional on the microscopic spin state of the electrons. The blockade can be lifted by any spin-flip mechanism. In quantum dots such spin-flip processes can be mediated by hyperfine interaction[60], spin-orbit interaction [105], or higher-order dot-lead tunneling (cotunneling) processes[79]. The blockade may also be partially lifted through relaxation processes mediated by a local spin dephasing process due to an inhomogeneous magnetic field [109, 79].

In this chapter we work in a regime where the three charge states $(0,1)$, $(1,1)$, $(0,2)$ can be accessed through energy-conserving transitions. Here, (n_L, n_R) indicates $n_{L(R)}$ electrons in the lowest orbital of the left(right) dot. We assume source and drain leads coupled to the left and right dot, respectively[53]. Including spin, seven states are involved in transport. There are two single-electron states ($|\uparrow\rangle = |(0,\uparrow)\rangle$ and $|\downarrow\rangle = |(0,\downarrow)\rangle$, corresponding to a spin-up and spin-down electron in the right dot, respectively), three spin-triplet states ($|T_+\rangle = |(\uparrow,\uparrow)\rangle$, $|T_-\rangle = |(\downarrow,\downarrow)\rangle$ and $|T_0\rangle = \left(|(\uparrow,\downarrow)\rangle + |(\downarrow,\uparrow)\rangle\right)/\sqrt{2}$). Additionally, there are two hybridized spin-singlet states $|S_\pm\rangle$, which describe linear combinations of $(1,1)$- and $(0,2)$-singlets due to an interdot tunnel coupling [109]. The exchange interaction due to an inter-dot tunneling lifts the degeneracy of singlet and triplet states and we assume an in-plane magnetic field induces a Zeeman splitting, so the energies corresponding to these seven states are all different (see Fig. 6.1). When the double dot is in a one-electron state, an electron may enter from the source lead, inducing a transition to one of the two-electron states. If the double dot ends up in one of the hybridized singlets, an electron may rapidly tunnel to the drain, contributing to the flow of current. However, if the double dot is in a spin-triplet state, tunneling transport is blocked until this triplet state undergoes a transition to a singlet. This is an example of

Pauli spin blockade.

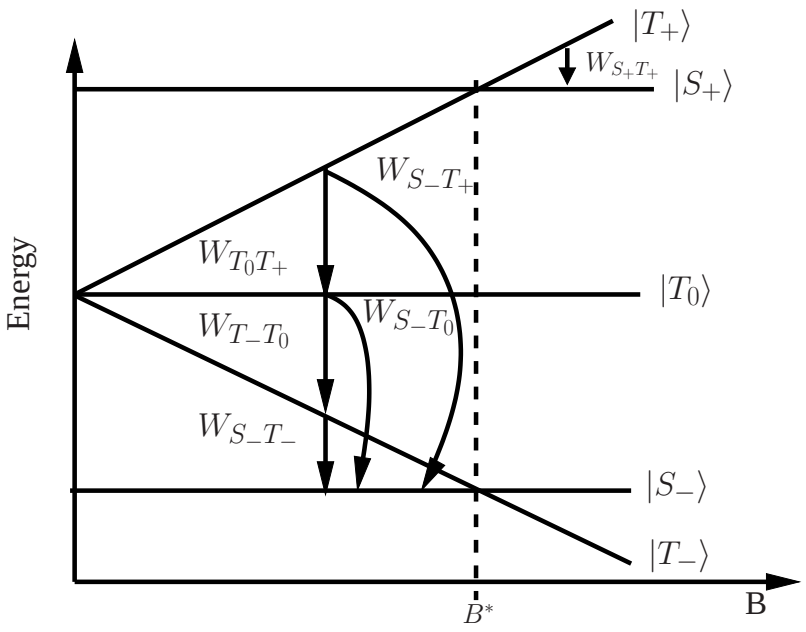

Figure 6.1: Double quantum-dot energy levels as a function of magnetic field B. Downward-pointing arrows represent the relaxation channel for each state. At B^*, the lowest-energy spin-polarized triplet becomes degenerate with the lowest-energy singlet, i.e., for a positive electron g-factor, $g > 0$, $E_{T_-}(B^*) = E_{S_-}$ where E_α is the energy of state $|\alpha\rangle$. At B^* the relaxation rate from $|T_-\rangle$ to $|S_-\rangle$ vanishes since $W_{S_-T_-}$ is assumed to be proportional to $|E_{T_-} - E_{S_-}|^\eta$ with $\eta > 0$. This is the case, e.g., for relaxation due to hyperfine interactions and phonon emission ($\eta = 3$),[40] spin-orbit interactions and phonon emission ($\eta = 5$),[67] or low-temperature cotunneling ($\eta = 1$).[109]

For this study, we consider a double quantum dot influenced by potentially several spin relaxation rates, as depicted in Fig. 6.1 (we assume excitation processes are weak compared to relaxation and can therefore be neglected). As will be shown, the frequency-dependent current noise, Eq. (6.1) below, typically features several steps with heights and widths that depend on these relaxation rates (See Fig. 6.2). The remainder of this chapter will be concerned with calculating the current noise and relating it to double-dot spin relaxation processes.

The noise spectrum $S_I(\omega)$ is given by the Fourier transform of the autocorrela-

tion function for the fluctuation in the source current $\delta I(t) = I(t) - \langle I \rangle$,

$$S_I(\omega) = \frac{1}{2}\int_{-\infty}^{\infty} \langle \{\delta I(\tau), \delta I(0)\} \rangle \, e^{-i\omega\tau} \mathrm{d}\tau. \tag{6.1}$$

Here, $\{,\}$ is an anticommutator and $\langle \cdots \rangle$ denotes an average over the joint quantum state of double dot and left and right leads. In the large-bias and weak-coupling limit ($\Delta\mu \gg \Delta E \gg \Gamma, kT$, where $\Delta\mu$ is the bias, ΔE is the typical double-dot energy level spacing, Γ is the dot-lead tunneling rate [throughout this thesis we set $\hbar = 1$] and T is the lead temperature with Boltzmann's constant k), we apply the Born approximation (weak coupling to the source and drain leads), as well as the Markov approximation (short dot-lead correlation time compared to tunneling time)[37]. In addition, we assume a short phase-coherence time for superpositions of isolated double-dot eigenstates. In this regime the average of the current operator I can be expressed as[37]

$$\langle I \rangle \approx \langle \mathcal{I} \rangle = \sum_{\alpha,\beta} \mathcal{I}_{\alpha\beta} \bar{\rho}_\beta, \tag{6.2}$$

where $\mathcal{I}_{\alpha\beta} = -|e| \sum_{j=\pm 1} j \delta_{n_\alpha + j, n_\beta} W^s_{\alpha\beta}$ gives the matrix elements of the current superoperator, $\mathcal{I}$, in the sequential-tunneling regime, in which electrons tunnel one by one. n_α gives the number of electrons in the double dot in state $|\alpha\rangle$. $W^s_{\alpha\beta}$ is the transition rate from state $|\beta\rangle$ to $|\alpha\rangle$ allowing the transfer of one electron to the double dot from the source lead when $\Delta\mu \gg kT$. The current superoperator, $\mathcal{I}$, acts on the reduced double-dot density matrix, with diagonal element ρ_α, where α runs over all seven relevant one- and two-electron states ($\alpha, \beta \in \{\uparrow, \downarrow, S_\pm, T_\pm, T_0\}$). In Eq. (6.2), $\bar{\rho}_\alpha$ is the stationary solution ($\dot{\bar{\rho}}_\alpha = 0$) of the Pauli master equation,

$$\dot{\rho}_\alpha(t) = \sum_\beta \mathcal{M}_{\alpha\beta} \rho_\beta(t), \tag{6.3}$$

where the rate matrix is $\mathcal{M}_{\alpha\beta} = -\delta_{\alpha\beta} W_\alpha + W_{\alpha\beta}$, $W_{\alpha\beta}$ is the transition rate from $|\beta\rangle$ to $|\alpha\rangle$, and $W_\alpha = \sum_\gamma W_{\gamma\alpha}$ is the total decay rate out of state $|\alpha\rangle$. For notational

convenience we use $W_x \equiv W_{T_x}$, with $x = \{0, \pm\}$. The stationary solution, $\bar{\rho}$, is the right eigenvector of the rate matrix, $\mathcal{M}$, with eigenvalue equal to zero.

To make analytical progress, we reduce the total number of coupled equations in the Pauli master equation, Eq. (6.3), by making physically realistic assumptions about spin-independent tunneling rates. We rewrite the occupation probabilities of the two states, $|\uparrow\rangle$ and $|\downarrow\rangle$, through a change of variables, $\rho_g(t) \equiv \rho_g^+(t) = \rho_\uparrow(t) + \rho_\downarrow(t)$, and $\rho_g^-(t) = \rho_\uparrow(t) - \rho_\downarrow(t)$. As shown in appendix C, if $W_g \equiv \frac{1}{2}\sum_\alpha (W_{\alpha\uparrow} + W_{\alpha\downarrow}) \gg \frac{1}{2}\left|\sum_\alpha (W_{\alpha\uparrow} - W_{\alpha\downarrow})\right|$ and $W_g \gg \left|\sum_\alpha (W_{\uparrow\alpha} - W_{\downarrow\alpha})\right|$, then ρ_g^- decouples from the rest of the original Pauli master equation, with negligible corrections. Assuming spin-independent tunneling from the source to the double dot, as well as the high-bias regime, these conditions are satisfied. We define transition rates associated with the ground-state doublet population, ρ_g, by $W_{g\alpha} = (W_{\uparrow\alpha} + W_{\downarrow\alpha})$ and $W_{\alpha g} = \frac{1}{2}(W_{\alpha\uparrow} + W_{\alpha\downarrow})$. The singlets, $|S_\pm\rangle$, are directly coupled to the drain in the sequential tunneling regime, and we assume this coupling is large compared to the double-dot spin relaxation rates, i.e., $W_{T_x S_\pm} \ll W_{g S_\pm}$, where $x \in \{\pm, 0\}$. Thus, we neglect transitions from singlets, $|S_\pm\rangle$, to the triplets, $|T_{\pm,0}\rangle$. Focusing on the resonant tunnelling regime [1], we have $W_S = \frac{1}{2}\left(W_{gS_+} + W_{gS_-}\right) \gg \frac{1}{2}\left|W_{gS_+} - W_{gS_-}\right|$ and $W_S \gg \left|\sum_\alpha \left(W_{S_+\alpha} - W_{S_-\alpha}\right)\right|$, which enables us to decouple $\rho_S^-(t) = \rho_{S_+}(t) - \rho_{S_-}(t)$ from the original Pauli master equation. Thus, we define a singlet-state doublet population, $\rho_S(t) = \rho_{S_+}(t) + \rho_{S_-}(t)$ with corresponding rates $W_{S\alpha} = W_{S_+\alpha} + W_{S_-\alpha}$ and $W_{\alpha S} = \frac{1}{2}\left(W_{\alpha S_+} + W_{\alpha S_-}\right)$, by direct analogy with the new variable $\rho_g(t)$. We assume a pure magnetic dipole coupling induces spin-flips, so that the transition rate connecting the two spin-polarized triplets vanishes, $W_{T_+T_-} = 0$ (see Fig. 1), and the remaining spin-triplet transitions depend only on the relative energy of the initial and final states (due to, e.g., the energy-dependent density of states of an environment). In the absence of a zero-field splitting, we then find that the nonzero triplet rates are equal ($W_{TT} = W_{T_0T_+} = W_{T_-T_0}$). Assuming a spin-independent tunnelling rate from source to the double quantum dot gives

[1] With interdot tunnel coupling t and energy detuning ϵ separating the (1,1) and (0,2) charge states, the resonant-tunnelling regime corresponds to $\epsilon \lesssim t$.

$W_{Sg} = W_{T_0 g} = W_{T_\pm g}$.

To proceed with the frequency-dependent noise calculation, we work from the Pauli master equation, Eq. (6.3), where $\rho = \left(\rho_{T_+}, \rho_{T_0}, \rho_{T_-}, \rho_S, \rho_g\right)^T$ and the rate matrix $\mathcal{M}$ is as follows,

$$\mathcal{M} = \begin{pmatrix} -W_+ & 0 & 0 & 0 & W_g/4 \\ W_{TT} & -W_0 & 0 & 0 & W_g/4 \\ 0 & W_{TT} & -W_- & 0 & W_g/4 \\ W_{ST_+} & W_{ST_0} & W_- & -W_S & W_g/4 \\ 0 & W_{gT_0} & 0 & W_S & -W_g \end{pmatrix}. \tag{6.4}$$

Here, W_{gT_0} is the rate for a transition from T_0 to either one-electron state, $|\uparrow\rangle, |\downarrow\rangle$, which can be assisted by a local dephasing mechanism or a gradient in the magnetic field [109]. To evaluate the frequency-dependent noise in Eq. (6.1), we first find the superoperator corresponding to the two-time current correlation function within the Born-Markov approximation. The autocorrelation function for the current $\langle I(\tau)I(0)\rangle$ has two parts: the first part arises due to interactions in the underlying system, and the second contributes to the noise due to the discreteness of the electron charge and gives rise to white noise, the so-called Schottky term, [58, 76, 37]

$$\frac{1}{2}\langle\{\delta I(\tau), \delta I(0)\}\rangle \approx \langle \mathcal{I}\mathcal{R}(\tau)\mathcal{I}\rangle + S_P\delta(\tau) - \langle I\rangle^2. \tag{6.5}$$

where $\langle \mathcal{I}\mathcal{R}(\tau)\mathcal{I}\rangle$ is defined through Eq. (6.2). Here, $S_P = e\langle I\rangle$ is the Poissonian (Schottky) noise. The matrix $\mathcal{R}(\tau) = e^{\mathcal{M}|\tau|}$ generates the time evolution of $\rho_\alpha(\tau)$ from Eq. (6.3). The symmetry in time, $|\tau|$, occurs because we calculate the symmetrized (classical) noise in the stationary regime, see Eq. (6.1). By Fourier transforming Eq. (6.5), and decomposing the resolvent, $\mathcal{R}(\omega)$ [Fourier transform of $\mathcal{R}(\tau)$, i. e., $\mathcal{R}(\omega) = \int_{-\infty}^{\infty} \mathrm{d}\tau \mathrm{e}^{-\mathrm{i}\omega\tau}\mathcal{R}(\tau)$], into the eigenbasis of $\mathcal{M}$, the frequency-dependent Fano factor is expressed in terms of a sum over Lorentzians[34]

$$F(\omega) \;=\; S_I(\omega)/S_P = 1 + \sum_{j=1}^{4} \Delta F_j \frac{\lambda_j^2}{\omega^2 + \lambda_j^2}. \tag{6.6}$$

Here, $\Delta F_j = \frac{2}{\lambda_j \langle I \rangle} \langle \mathcal{I}\mathcal{E}_j\mathcal{I} \rangle$ for $j \geq 1$. The eigenvalues of $\mathcal{M}$ are denoted $\lambda = -\{\lambda_0, \lambda_1, \cdots, \lambda_4\}$ with $\lambda_{j+1} > \lambda_j$, and where $\lambda_0 = 0$ is the the zero eigenvalue of $\mathcal{M}$ corresponding to the stationary solution of Eq. (6.3). $\mathcal{E}_j$ is the projector onto the eigenvector corresponding to eigenvalue λ_j. A set of orthonormal projectors $\{\mathcal{E}_j = |\lambda_j)(\lambda_j|\}$ can be constructed from the right and left eigenvectors ($|\lambda_j)$ and $(\lambda_j|$, respectively). Note that since $\mathcal{M}$ is not Hermitian, the left and right eigenvectors are not conjugates. We further note that the contribution from the zero eigenvalue of $\mathcal{M}$ ($\lambda_0 = 0$) in the spectral decomposition of $\mathcal{R}(\omega)$ cancels the term proportional to $\langle I \rangle^2$ in Eq. (6.5). [29]

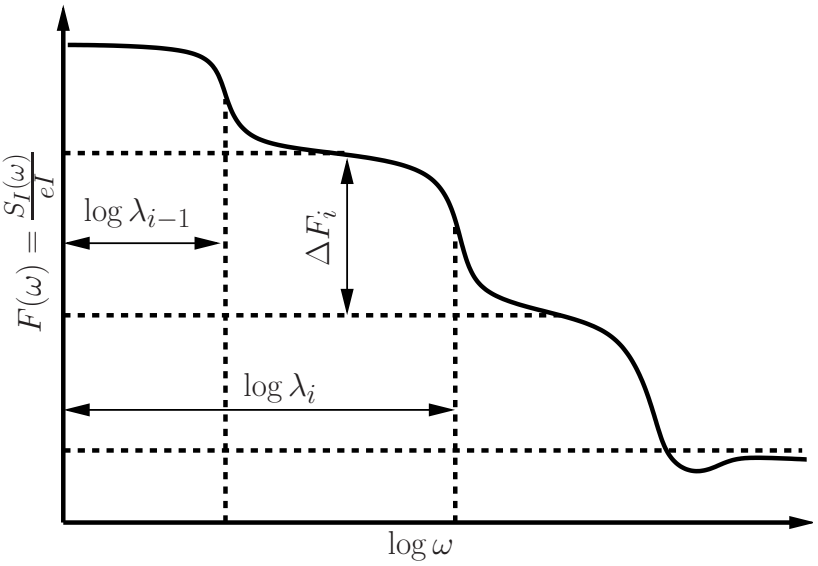

Figure 6.2: For well-separated eigenvalues of the rate matrix $\mathcal{M}$ ($\lambda_{i-1} \ll \lambda_i$) the Fano factor has several plateaus on a linear-log plot. The height of each step between plateau is determined by F_i [defined in Eq. (6.17)] and the plateaus width is set by $\log \lambda_i$.

Although it is always possible to evaluate $F(\omega)$ from eq. (6.6) by numerically diagonalizing the rate matrix to obtain the eigenvalues and right/left eigenvectors, a closed-form analytical expression is often difficult to obtain. In the remainder of this chapter, we focus on deriving simple analytical expressions for the Lorentzian prefactors ΔF_j and the eigenvalues λ_j for a double quantum dot without evaluating

the eigenvectors explicitly.

We now assume spin-flip rates that vanish near a degeneracy at applied magnetic field $B = B^*$ (see caption of fig. 6.1 for examples). In this case, for a magnetic field B close to B^*, we have $W_- \ll W_+, W_0$. Furthermore, we assume $W_+, W_0 \ll W_S, W_g$. In this regime, we find the eigenvalues of $\mathcal{M}$ by expanding the characteristic equation for the rate matrix in Eq. (6.4), with small corrections of order $\mathcal{O}\left(\frac{W_x}{W_g}\right)$ and $\mathcal{O}\left(\frac{W_x}{W_S}\right)$ ($x \in \{\pm, 0\}$), giving the following approximation in the limit of vanishing W_{T_-}:

$$\lambda \approx -\left\{0, \frac{1}{3}\left(W \pm \sqrt{W^2 + 3W_+\left(-W + W_+\right) - 3W_{\mathrm{TT}}^2}\right), \right. \\ \left. \frac{1}{2}\left(\Sigma \pm \sqrt{\Sigma^2 - 3W_S W_g}\right)\right\}, \quad (6.7)$$

where $W = W_{TT} + W_0 + W_+$, and $\Sigma = W_g + W_S$. Σ^{-1} is the effective transit time for an electron to pass from the left lead to the right lead, when no triplet state is occupied. Any strong local dephasing mechanism will generically lead to $W_0 \gg W_+$, based on which Eq. (6.7) can be further approximated, giving

$$\lambda \approx -\left\{0, \frac{W_+}{2}, \frac{2W_0}{3}, \frac{3W_S W_g}{4\Sigma}, \Sigma - \frac{3W_S W_g}{4\Sigma}\right\}. \quad (6.8)$$

Each distinct eigenvalue λ_j is associated with a frequency (or time) scale at which a blocked state begins to contribute to transport. This leads to a sequence of plateaus in the frequency-dependent Fano factor $F(\omega)$ (Fig. 6.2). In the next section we explain how the Fano factor is related to the charge transferred during bursts of transient current in order to approximate the Lorentzian prefactors ΔF_j, which set the step heights in Fig. 2.

6.4 Dynamical channel blockade and electron bunching

In this section, we use the method of full counting statistics [81, 9] to relate the Fano factor to the first moment of charge transported through the quantum dot. Although the technique allows a direct extension to higher-order cumulants, it is used here merely as a tool to calculate the current and the noise. These results are important for a general understanding of the frequency-dependent noise calculation presented in the remainder of this chapter.

The Cumulant Generating Function (CGF), $S(\chi)$, is defined through [81]

$$e^{S(\chi)} = \sum_N e^{iN\chi} P_N, \tag{6.9}$$

where P_N is the probability that exactly N electrons are transferred through the double dot during an experiment of duration t_0, and χ is the counting field, an auxiliary variable. From the cumulant generating function, the k^{th} cumulant is found through

$$C_k = (-i)^k \lim_{\chi\to 0} \frac{d^k S(\chi)}{d\chi^k}, \tag{6.10}$$

where $C_1 = \bar{N}$, $C_2 = \overline{(N-\bar{N})^2}$, and $\overline{N^k} = \sum_{N=0}^{\infty} N^k P_N$ for $k = 1, 2, ...$ The stationary current through the double dot $\langle I\rangle$ and zero-frequency noise $S_I(0)$ are related to the first and second cumulant through $\langle I\rangle = \lim_{t_0\to\infty} eC_1/t_0$ and $S_I(0) = \lim_{t_0\to\infty} e^2C_2/t_0$, respectively.[2]

Here, we aim to find the CGF, $S(\chi)$, in the dynamical channel blockade regime[9],

[2]The second cumulant of the transported electron number C_2 is related to the current noise by making the identification $C_2 = \overline{(\delta N(t_0))^2} = \left\langle (\delta N(t_0))^2 \right\rangle$, where $\delta N(t) = N(t) - \langle N(t)\rangle$. With $\delta Q(t_0) = e\delta N(t_0) = \int_0^{t_0} dt \delta I(t)$, we have $C_2 = e^{-2}\int_0^{t_0} dt \int_0^{t_0} dt' \langle \delta I(t)\delta I(t')\rangle$. Using the fact that $\langle \delta I(t)\delta I(0)\rangle = \langle \delta I(t+t')\delta I(t')\rangle$ (i.e., $\delta I(t)$ is a stationary random process) gives $e^2C_2 = t_0 \int_{-t_0}^{t_0} dt \langle \delta I(t)\delta I(0)\rangle$. For $t_0 \gg \tau_c$, where $\tau_c \sim 1/\gamma$ is the correlation time of $\langle \delta I(t)\delta I(0)\rangle$, and assuming $[\delta I(t), \delta I(t')] = 0$ (the classical-noise limit), we find $e^2C_2/t_0 \simeq 2^{-1}\int_{-\infty}^{\infty} \langle \{\delta I(t), \delta I(0)\}\rangle = S_I(\omega = 0)$, using the definition given in Eq. (6.1).

where one or some of states in the double dot have small escape rate compared to other states. For a double quantum dot in the Pauli spin blockade regime, we consider the case where there is a hierarchy of spin relaxation rates [such a regime has already been assumed in deriving Eq. (6.8)]. We use this hierarchy to approximate the cumulant generating function, $S(\chi)$. To illustrate the idea, let us first consider a simplified model in which escape from the blockaded double quantum dot is associated with only two rates, one fast (Γ) and the other slow ($\gamma \ll \Gamma$). The fast rate Γ represents the typical timescale for a spin singlet to be converted to a single-electron state allowing an electron to tunnel to the drain, while the slow rate γ describes a slow triplet-to-singlet relaxation process. As shown in Fig. 6.3, current through the double dot is characterized by bursts of duration $\sim 1/\Gamma$, in which several electrons may pass through the double dot, followed by a long pause of zero current for a time $\sim 1/\gamma$, when the double dot remains in a blocked (spin triplet) configuration.

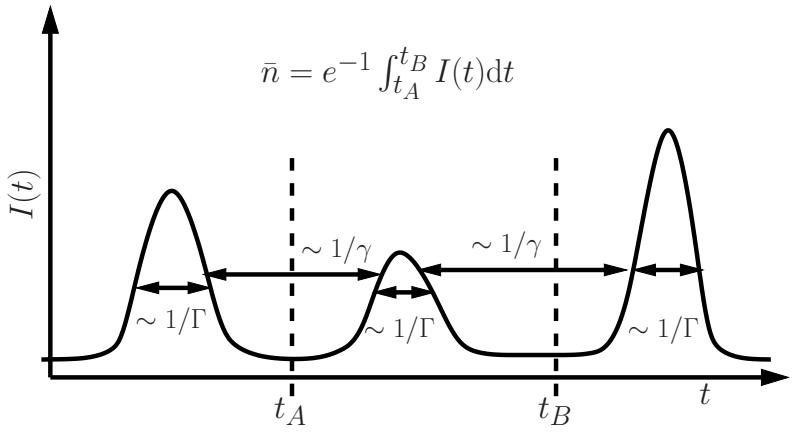

Figure 6.3: Schematic illustration of the transient current. Transient current is a sequence of current bursts with duration Γ^{-1} and separation γ^{-1}. We characterize each burst with the total number of electrons that have passed through the system, electron bunching, n. Here $|t_B - t_A| \sim \gamma^{-1}$.

The current is measured for a long time t_0 such that $\gamma t_0 \gg 1$. Since $\gamma \ll \Gamma$, the bursts of current can be taken to be independent and the experiment averages over many individual bursts. In this case, the CGF is given by the weighted sum of CGFs for many independent Poissonian processes [9], $S(\chi) = \sum_n f_n S_n$, each of which

carries an elementary charge ne (where $S_n(\chi) = e^{in\chi} - 1$) with an average frequency f_n. The probability that the double dot is in a blocked configuration after a single electron is transferred to the double dot from the source is P_B. The probability that exactly n electrons are transferred between blocking events is $(1 - P_B)^{n-1} P_B$, which gives $f_n = \gamma t_0 (1 - P_B)^{n-1} P_B$, where γt_0 is the total number of current bursts during time t_0. Thus,

$$S(\chi) = \gamma t_0 \sum_{n=1}^{\infty} P_B (1 - P_B)^{n-1} (e^{in\chi} - 1) \tag{6.11}$$

$$= \gamma t_0 \frac{e^{i\chi} - 1}{1 - e^{i\chi}(1 - P_B)}. \tag{6.12}$$

Eq. (6.12) has been previously derived in Ref. [9] for the special case of a three-level quantum dot with a single blocked state, leading to $P_B = 1/2$. The average number of electrons transferred from the source to the double dot in each current burst is

$$\bar{n} = \sum_{n=1}^{\infty} n P_B (1 - P_B)^{n-1} = \frac{1}{P_B}. \tag{6.13}$$

Inserting Eq. (6.12) into Eq. (6.10) gives the first and second cumulants as well as their ratio (the Fano factor F):

$$C_1 = \frac{\gamma t_0}{P_B} = \gamma t_0 \bar{n}, \tag{6.14}$$

$$C_2 = C_1 (2\bar{n} - 1), \tag{6.15}$$

$$F = \frac{C_2}{C_1} = 2\bar{n} - 1. \tag{6.16}$$

For any $P_B \neq 1$, Eq. (6.11) describes a non-Poissonian process. Consequently, the Fano factor does not have a simple interpretation in terms of the ratio of an effective charge to the electron charge, i.e. $F \neq e^*/e$ with $e^* = \bar{n}e$. However, a simple linear relationship still exists between the effective charge and the Fano factor as given by Eq. (6.16). It is interesting to note that F is fully determined by the blocking probability P_B regardless of the physical origin of the blockade;

i.e., different physical systems have the same Fano factor whenever they have the same blocking probability (the same ratio of blocked to unblocked states). For example, $F = 3$ (corresponding to $P_B = 1/2$) is predicted and measured in many systems with dynamical-channel blockade [32, 125, 126, 14] and the above argument explains why $F = 3$ is ubiquitous (this value of the Fano factor is found whenever the number of blocked and unblocked states is equal).

One interesting consequence of Eq. (6.13) is that the effective charge $e^* = \bar{n}e$ has a universal fractional value whenever the blocking probability P_B is fractional. For example, in the Pauli spin blockade regime of transport through a double quantum dot and in the absence of spin relaxation or dephasing processes, three of four two-electron spin states are blocked, giving $P_B = 3/4$ (triplets are blocked, while singlets conduct current). This results in $n = 4/3$,[109] leading to a universal fractional Fano factor $F = 5/3$ based on Eq. (6.16). This value of $F = 5/3$ for the spin blockade has been found previously.[119] A fractional Fano factor of $F = 5/3$ has also been cited as evidence of many-body correlations in the backscattering from a Kondo impurity.[121, 140, 28] However, based on the above analysis, it is clear that the same ratio occurs in a simple theory of uncorrelated tunneling processes through a system that only has strong two-body correlations.

6.5 Analytical Fano factor

There may be several decay rates associated with transitions between different double-quantum-dot levels. For well-separated decay rates, and consequently eigenvalues, $\lambda_i \ll \lambda_{i+1}$, from Eq. (6.6) we find,

$$F_{i+1} \approx 1 + \sum_{j=i+1}^{4} \Delta F_j, \qquad i = 0, \cdots, 3 \tag{6.17}$$

where $F_{i+1} \equiv F(\lambda_i \ll \omega \ll \lambda_{i+1})$ and we have neglected terms of order of $\mathcal{O}\left(\frac{\omega^2}{\lambda_{i+1}^2}\right)$ and $\mathcal{O}\left(\frac{\lambda_i^2}{\omega^2}\right)$. From Eq. (6.17) we find a direct relationship between the Lorentzian

prefactors, ΔF_j, and Fano factor step height as

$$\Delta F_j = F_j - F_{j+1}. \tag{6.18}$$

As shown in the previous section (Sec. III), the value of the Fano factor can be determined from the average number of electrons transferred, and consequently from the blocking probability. Since, we are interested in the frequency-dependent behaviour of the Fano factor we need to study the time-dependent blocking probability. We use an n-resolved master equation [141, 108] to provide a mathematical definition for the blocking probability. In the n-resolved master equation approach the population density after nth electron transfer (nth jump), $\rho^n(t)$, is given by,

$$\dot{\rho}^n(t) \;=\; \mathcal{M}_0\rho^n(t) + \mathcal{J}\rho^{n-1}(t) \tag{6.19}$$

where $\mathcal{J}_{\alpha\beta} = \delta_{g\beta}W^s_{\alpha g}$ is the source jump superoperator and $\mathcal{M}_0 = \mathcal{M} - \mathcal{J}$. Within this formalism the blocking probability, the probability that the double dot is in a blocked configuration after a single electron is transferred, is given by: $P_B(t) = \mathrm{Tr}[\rho^1(t)]$ where the Tr gives the sum of the vector elements. Solving for $\rho^1(t)$ from Eq. (6.19) gives,

$$P_B(t) \;\equiv\; \mathrm{Tr}\left[e^{\mathcal{M}_0 t}\int_0^t \mathrm{d}\sigma e^{-\mathcal{M}_0\sigma}\mathcal{J}e^{\mathcal{M}_0\sigma}\rho(0)\right]. \tag{6.20}$$

Here, $\mathcal{R}_0(t) = e^{\mathcal{M}_0 t}$ is the "free" time translation superoperator of occupation probabilities with no transfer of electron from the source. Using Eq. (6.13) and Eq. (6.16), the Lorentzian prefactors in terms of blocking probabilities are found to be

$$\Delta F_j \;=\; 2\left[P_B^{-1}(t_j) - P_B^{-1}(t_{j+1})\right], \tag{6.21}$$

where we set $t_i^{-1} \simeq (\lambda_i\lambda_{i+1})^{1/2}$, the geometric mean of λ_i and λ_{i+1}. Hence, in order to find a closed form expression for the Lorentzian prefactors, ΔF_i, we need to approximate blocking probabilities, $P_B(t_i)$.

To evaluate the blocking probability, $P_B(t_i)$, from eq. 6.20, we assume that W_g is the largest rate in the system ($W_g \gg W_\alpha$ where $\alpha \neq g$) and we start from the one-electron subspace at time zero, i.e., $\rho_\alpha(0) = \delta_{\alpha g}$. Then, the blocking probability for $t \gg W_g^{-1}$ is found through, ($\alpha \neq g$)

$$P_B(t) = \mathrm{Tr}\left(e^{\mathcal{M}_0 t}\mathcal{J}\rho(0)/W_g\right) + \mathcal{O}\left(\frac{W_\alpha}{W_g}\right), \tag{6.22}$$

since $\rho(0)$ is the eigenvector of $\mathcal{M}_0$ with eigenvalue $-W_g$ which gives: $\mathcal{R}_0(t')\rho(0) = e^{-W_g t'}\rho(0)$. To further investigate properties of $P_B(t)$, it is convenient to work with the Laplace transform of $P_B(t)$, i.e., $\tilde{P}_B(s) = \int_0^\infty e^{-st}P_B(t)\mathrm{d}t$. Using Eq. (6.22), the Laplace transform of $P_B(t)$ is given by

$$\tilde{P}_B(s) \;=\; \mathrm{Tr}\left[(s - \mathcal{M}_0)^{-1}\,\mathcal{J}\rho(0)/W_g\right] \tag{6.23}$$

Decomposing $\mathcal{M}_0$ into diagonal, $-\mathcal{D}$, and off-diagonal, $\mathcal{T}$, parts as: $\mathcal{M}_0 = -\mathcal{D}+\mathcal{T}$. Thus we rewrite Eq. (6.23) as,

$$\tilde{P}_B(s) \;=\; \mathrm{Tr}\left[(1 - \mathcal{P}(s))^{-1}\mathcal{D}^{-1}(s)\mathcal{J}\rho(0)/W_g\right] \tag{6.24}$$

where $\mathcal{P}(s) = \mathcal{T}\mathcal{D}^{-1}(s)$ and $\mathcal{D}(s) = \mathcal{D} + s$. Since $\mathcal{D}(s)$ is a non-singular diagonal matrix, its inverse is simply the inverse of its diagonal element.

Now we want relate $\tilde{P}_B(s)$ and $P_B(t)$ directly without inverting the Laplace transform. First note that, we have $P_B(0) = \lim_{s\to\infty} s\tilde{P}_B(s)$ and $P_B(\infty) = \lim_{s\to 0} s\tilde{P}_B(s)$, respectively. Since $P_B(t)$ can be written as superposition of exponentially decay function, i.e., $P_B(t) = \sum_j c_j e^{-\lambda_j t}$. Hence, the Laplace transform can simply be found as $\tilde{P}_B(s) = \sum_j \frac{c_j}{\lambda_j + s}$. For well-separated eigenvalues $\lambda_j \ll \lambda_{j+1}$, we find,

$$\lim_{t\to t_i} P_B(t) = \lim_{s\to s_i} s\tilde{P}_B(s) + \mathcal{O}\left(\sqrt{\lambda_i \lambda_{i+1}^{-1}}\right), \tag{6.25}$$

where $s_i \simeq t_i^{-1} \simeq \sqrt{\lambda_i\lambda_{i+1}}$. In the logarithmic plot, (see Fig .6.2), $\log(s_i)$ is the arithmetic mean of $\log(\lambda_i)$ and $\log(\lambda_{i+1})$. It only remains to take the limit of $s\tilde{P}_B(s)$

when $s \to s_i$ as following,

$$P_B(t_i) \approx s_i \tilde{P}_B(s_i) \tag{6.26}$$

$$= \mathrm{Tr}\left[(1-\mathcal{P}(s_i))^{-1} s_i \mathcal{D}^{-1}(s_i) \mathcal{J}\rho(0)/W_g\right] \tag{6.27}$$

where $s_i \simeq t_i^{-1}$ and we have dropped terms of the order $\sqrt{\lambda_i \lambda_{i+1}^{-1}}$. Approximating $\mathcal{P}_{\alpha\beta}(s_i) = \frac{W_{\beta\alpha}}{s_i + W_\alpha} \approx \mathcal{P}_{\alpha\beta}(0)\theta(W_\alpha - s_i)$ and $s_i \mathcal{D}^{-1}_{\alpha\beta}(s_i) = \frac{s_i}{s_i + W_\alpha}\delta_{\alpha\beta} \approx \delta_{\alpha\beta}\theta(s_i - W_\beta)$ in eq. 6.26, give,

$$P_B(t_i) \approx \mathrm{Tr}\left[(1-\mathcal{P}(s_i))^{-1} u(s_i)\right] \tag{6.28}$$

where $u(s_i) = s_i \mathcal{D}^{-1}(s_i)\mathcal{J}\rho(0)/W_g$ which for well separated decay rates is approximated by $u_\alpha(s_i) \approx \frac{W_{\alpha g}}{W_g}\theta(s_i - W_\alpha)$.

For a double quantum dot, $\gamma \sim W_- \ll W_+ \ll W_0 \ll \lambda_3 \sim \lambda_4 \sim \Gamma$ is used. For a long time scale, $W_+^{-1} \ll t_1 \ll W_-^{-1}$, the two-electron ground state T_- is the only blocked state at the long time, and the result is $P_B(t_1) = \frac{1}{4}(1 + p + pq)$, where the branching ratios are introduced:

$$p = P_{T_- T_0} = W_{TT}/W_0, \tag{6.29}$$

$$q = P_{T_0 T_+} = W_{TT}/W_+. \tag{6.30}$$

For $W_0^{-1} \ll t_2 \ll W_+^{-1}$, both $T_\pm$ states are blocked, which leads to $P_B(t_2) = \frac{1}{4}(2 + p)$. For $\Gamma^{-1} \ll t_3 \ll W_0^{-1}$, all three triplets are blocked, but singlets still contribute resulting in $P_B(t_3) = \frac{3}{4}$ and finally, for very short times $t \ll \Gamma^{-1}$, all the states are blocked, i.e., $P_B(0) = 1$. Although noise in the Pauli spin blockade regime is super-Poissonian, as shown below the presence of sub-Poissonian noise ($F(\omega) < 1$) is inevitable at some higher frequency scale. Noting that $\Delta F_j = \frac{2}{\lambda_j \langle I\rangle}\langle \mathcal{I}\mathcal{E}_j\mathcal{I}\rangle$ and $\sum_{j=0}^{4}\mathcal{E}_j = 1$ we find that,

$$\sum_{j=1}^{4} \lambda_j \Delta F_j \approx -2e^{-1}\langle I\rangle \tag{6.31}$$

where we have neglected the contribution of double electron transfer, i.e., $\langle \mathcal{I}^2 \rangle = 0$. Since, the stationary current is proportional to the smallest rate in the system, here, $\langle I \rangle \propto W_-$. Thus, for the case where $W_- \to 0$ and using the fact that the Fano factor step height at very large frequencies (short time scale) is unity, $F(\omega \gtrsim \lambda_4) = 1$, (we can see this by setting $\omega \gtrsim \lambda_4$ in Eq. (6.17)) we find $\sum_{j=1}^{4} \lambda_j \Delta F_j = \sum_{j=1}^{4} (F_j - 1)\, \Delta\lambda_j \approx 0$ where $\Delta\lambda_j = \lambda_j - \lambda_{j-1}$. The above equation, Eq. 6.31, implies that if some of the Fano factor step heights, F_j, are larger than one (super-Poissonian) then some other have to be less than one (sub-Poissonian). Note that, in our formalism we can not associate a blocking probability to the sub-Poissonian Fano factor, $F < 1$. However, we use the following sum rule in Eq. (6.31), to approximate the step height of the Fano factor at sub-Poissonian regime.

Combining all of the above information the frequency-dependent Fano factor is determined to

$$F(\omega) = 1 + \frac{4W_+^2}{4\omega^2 + W_+^2} + \frac{16W_0^2}{3\,(9\omega^2 + 4W_0^2)} + \frac{2}{3}\left(\frac{\lambda_3^2}{\omega^2 + \lambda_3^2} - \frac{\lambda_4\lambda_3}{\omega^2 + \lambda_4^2}\right) + \mathcal{O}(p,q), \tag{6.32}$$

where $\lambda_3 = \frac{3W_S W_g}{8\Sigma}$ and $\lambda_4 = 2\Sigma - \frac{3W_S W_g}{8\Sigma}$. For $\omega \ll \lambda_3$, only the super-Poissonian part appears where we can simplify the Fano factor further to,

$$F(\omega) \;=\; \frac{5}{3} + \frac{4W_+^2}{4\omega^2 + W_+^2} + \frac{16W_0^2}{3\,(9\omega^2 + 4W_0^2)} + \mathcal{O}\left(\frac{\lambda_3}{\lambda_4}\right). \tag{6.33}$$

The comparison between the above analytical result from Eq. (6.32) and the numerical result given directly from the numerical calculation of Eq. (6.6) is plotted in Fig. (6.4), where we assume cotunneling as a source of spin-flip relaxation. As it was shown [109] the cotunneling relaxation depends linearly on the magnetic field ($W_{\rm cot} \propto B$) which implies $W_{ST_0} = W_{TT}$ at B^* where T_- and S is degenerate. Furthermore, since at B^* Zeeman splitting of T_+ is twice the T_0 ($|E_{T_+} - E_S| = 2|E_{T_0} - E_S|$), then $W_{ST_+} = 2W_{ST_0} = 2W_{TT}$.

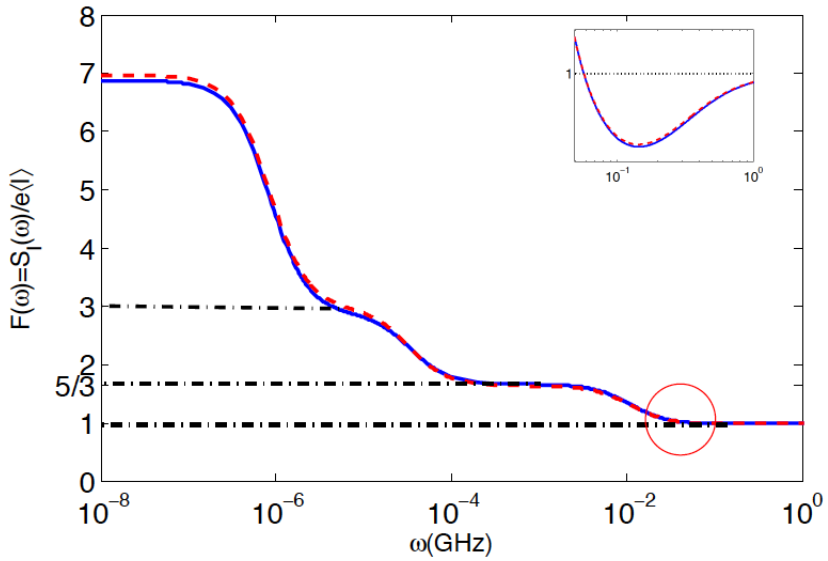

Figure 6.4: We assume strong local dephasing mechanism which gives $W_{gT_0} = 100W_{TT}$, and also we assume $W_g \simeq 10W_S = 10^4 W_{TT}$. For $W_{TT} \sim 10^{-8} - 10^{-3}\mu eV$ we can tune $W_g \sim 10^{-4} - 10\mu eV$ which is experimentally accessible. At these values we have plotted both (exact) numerical plot (solid curve) and analytical plot (dashed curve) in Eq. (6.32). In this case $p \approx 0$ and $q \approx \frac{1}{2}$ which result in $F_1 \approx 7$, $F_2 = 3$ and $F_1 = \frac{5}{3}$ which are the values of plateau exhibited by horizontal dashed lines. Inset: the sup-Poissonian dip which appears in the circled area is shown in the inset.

As shown in Fig. 6.4, we find an excellent agreement between our analytical result, Eq. (6.32), and numerical solution.

6.6 Conclusions

Conventional pulsed-gate techniques for measuring spin relaxation in a quantum dot operate only at large energy splitting, where the electron Zeeman energy exceeds the thermal broadening ($\sim k_B T$) of Fermi-liquid leads. An alternative is to measure a transient effective charge e^*, or equivalently, the zero-frequency noise in the Pauli spin blockade regime [109], where spin-selection rules, rather than energy conservation, provide the mechanism for initialization and readout. This method allows for the characterization of certain aspects of the decay process. However, multi-level systems (such as double quantum dots) often exhibit several decay rates due to distinct physical mechanisms.

In this work, we formulate a theory of the frequency-dependent current noise through a double quantum dot in the Pauli spin blockade regime, including the effects of multiple relaxation processes. This theory provides a one-to-one correspondence between the form of the frequency-dependent Fano factor and the relevant relaxation rates and can therefore be used to determine these rates through a measurement of the current noise.

For future work we want to include off-diagonal terms in Master equation, in order to measure T_2 in double quantum dot similar to the case described in Engel et al [35, 36]. Furthermore, we can calculate higher-order cumulants to increase the number of independent rates that can be extracted in experiment.

Chapter 7

Summary and Outlook

The main theme of this thesis is to study the electron transport through double quantum dots coupled to normal leads, in the so-called spin-blockade regime. Here, the current is blocked due to the absence of transitions between singlet and triplet states within the quantum dots. A small leakage current will flow if the singlet and triplet states are mixed. This spin mixing occurs due to several possible spin-flip processes. In the first two chapters, we provide the necessary background information about double quantum dots. We also briefly review the spin mixing due to phonon-induced hyperfine and spin-orbit interaction.

In chapter 3, we consider the effect of natural dot-lead higher order tunneling (cotunneling) on transport in the spin-blockade regime. This interaction is an intrinsic property of these systems. Despite the fact that this interaction is rather weak, it can, as shown in this thesis, strongly influence the dynamics of electron spins in quantum dots. In this chapter, a theory of spin-flip cotunneling process is developed and its basic properties of stationary and transient leakage current in the Pauli spin blockade regime in double quantum dot is presented.

The general magnetic and detuning dependent stationary leakage current due to (any) spin-flip processes at finite magnetic fields are studied in chapter 4. First we have presented a general theory of the stationary current in an intuitive way. In the presence of an additional local dephasing process or nonuniform magnetic field, we obtain a simple analytical expression for the leakage current giving the full

dependence on the applied magnetic field and the energy detuning. Our findings are important for understanding the nature of the leakage, especially in systems where other spin-flip mechanisms are absent.

The subject of chapter 5 is to study the observed leakage current in a silicon double dot in Pauli spin blockade regime. In group III-V semiconductors such as GaAs, nuclear spins are always present and produce strong decoherence of the electron spin degree of freedom. Group-IV semiconductors such as silicon, silicon-germanium and carbon can be isotopically purified, leaving only spinless isotopes. The weak spin-orbit coupling and the absence of piezoelectric electron-phonon coupling allow for extremely long spin relaxation times. We have shown that the leakage current in spin blockade has a peculiar magnetic field dependence, unrelated to electron-nuclear effects and consistent with the effect of spin-flip cotunneling processes.

In the last chapter, I present the theory of frequency-dependent shot noise of a double quantum dot in the Pauli spin blockade regime, including the effects of multiple relaxation processes. Understanding the microscopic spin-relaxation processes in the double quantum dot is important for future spin-based quantum devices. A complete theoretical picture of the limits on the spin lifetimes in quantum dots is still missing. In this chapter, we apply a quantum master equation approach to study current autocorrelation in a double quantum dot, where we compute noise to current ratio, the so-called Fano factor. This theory gives a one-to-one correspondence between the form of the frequency-dependent Fano factor and the relevant relaxation rates and can therefore be used to determine these rates through a measurement of the current autocorrelation.

The results in this thesis point toward several directions for later studies. In future, I aim to study recently observed anomalies in dynamical nuclear polarizations in double quantum dots utilizing our calculations of spin-flip cotunneling. Interesting phenomena such as hysteresis, switching and long period oscillatory behaviour of electric current were observed in Pauli-spin blockade regime in lateral double quantum dots [99, 8, 115, 114]. Strong evidences were presented, linking

the observed phenomena to the collective behaviour of the nuclear spins in the lattice. Recent studies [8, 115] have shown that nuclear spin polarization in double quantum dots requires an additional mechanism of spin-flip, independent of electron-nuclear hyperfine interaction, to create a preferred polarization direction. So far, this mechanism was only taken into account phenomenologically and may not be able to predict qualitative behavior on the external fields.

There is also more work to be done to exploit applications of spin-orbit interaction in low dimensional systems. Recently, spin-orbit coupling in correlated electron materials has provided an exciting opportunity in creating a new class of electronic states. Several new collective states of matter have been proposed in this context, including novel spin-orbital ordered states, spin liquid, and various topological phases [63, 72, 16, 17, 10]. Additionally, spin-orbit interaction is proven to be useful in implementing holonomic quantum gates in quantum dots [49].

Appendix A

Auxiliary materials for Chapter 3

A.1 Identifying spin decay

In this supplement we show how to extract the magnetic-field dependence of microscopic relaxation processes at low field from the observed number of electrons that pass through the double dot between blocking events in the Pauli spin blockade regime. This measurement can be used to distinguish between spin-orbit, hyperfine-, and cotunneling-mediated spin relaxation mechanisms at low magnetic field, where other methods for single-spin detection fail[33].

We recall the definitions for the branching ratios p and q (given before Eq. (9) of the main text),

$$p = \frac{W_{T_0\to T_-}}{W_{T_0\to T_-} + W_{T_0\to S_-} + \sum_\sigma W_{T_0\to\sigma}}, \tag{A.1}$$

$$q = \frac{W_{T_+\to T_0}}{W_{T_+\to T_0} + W_{T_+\to S_+} + W_{T_+\to S_-}}. \tag{A.2}$$

These expressions can be simplified under certain experimental conditions. In particular, we consider the case when there is no magnetic field gradient present, $\delta b = 0$, and a sufficiently weak Zeeman splitting, so that transition rates from triplets to triplets (split by the Zeeman energy) are smaller than those from triplets to singlets (split by exchange) ($W_{T_m\to T_{m'}} \ll W_{T_m\to S_\pm}$). With $\delta b = 0$, the field-assisted

sequential-tunneling rates vanish:

$$W_{T_0 \to \sigma} = 0, \tag{A.3}$$

and for a generic spin-flip Hamiltonian [1],

$$W_{T_+ \to T_0} = W_{T_0 \to T_-} = W_{TT}. \tag{A.4}$$

The rate $W_{T_0 \to S_-}$ is independent of Zeeman splitting, $b = g\mu B$, since the $T_0 - S_-$ splitting is independent of the global field. In contrast, $W_{TT} \propto b^\eta$ for small magnetic field, depending on the spin-flip mechanism (as we have shown in the main text, $\eta = 1$ for cotunneling-mediated spin-flips at low temperature, and previous work has shown $\eta = 5$ for spin-orbit-mediated spin flips with phonon emission [67], and $\eta = 3$ for hyperfine-mediated spin flips with phonon emission [39]). For sufficiently small Zeeman splitting b, the triplets become degenerate resulting in vanishing rates, allowing us to approximate

$$\frac{W_{TT}}{W_{T_+ \to S_\pm}} \quad , \quad \frac{W_{TT}}{W_{T_0 \to S_-}} \ll 1 \tag{A.5}$$

$$\Rightarrow p \approx \frac{W_{TT}}{W_{T_0 \to S_-}} \ll 1 \tag{A.6}$$

$$\Rightarrow q \approx \frac{W_{TT}}{\sum_{\alpha=\pm} W_{T_+ \to S_\alpha}} \ll 1 \tag{A.7}$$

In this regime, we approximate m by its leading-order form in the small ratio $W_{TT}/W_{S_\pm}$:

$$m = \frac{3 - p - pq}{1 + p + pq} = 3 - 2p + O(p^2) + O(pq), \tag{A.8}$$

$$m = 3 - 2\frac{W_{TT}}{W_{T_0 \to S_-}} + O\left(\left(\frac{W_{TT}}{W_{T \to S}}\right)^2\right). \tag{A.9}$$

[1] We calculate golden-rule spin-flip rates assuming a perturbation of the form $V_{sf} = \sum_l S_l^+ \Sigma_l + \Sigma_l^\dagger S_l^-$, where $S_l^\pm$ is a raising/lowering operator for the spin on dot l and Σ_l is a general (local) environment operator.

Thus, by measuring $m(b) \cong 3 - \gamma b^{\eta}$, it is possible to extract the relevant spin-flip mechanism: η = 5,3, or 1 for spin-orbit interaction with phonon emission [67], hyperfine interaction with phonon emission [39], or cotunneling, respectively.

A.2 Processes leading to dot excitation

In our analysis we have neglected processes that can lead to excitation of the double dot at finite bias (see, e.g., Fig. A.1(b) for an example). These processes can lead to nonvanishing stationary populations of excited dot states, which would correspond to "initialization errors" in the scheme we have proposed. However, we find that the leading excitation processes are suppressed by the small parameter

$$\frac{W^{b}_{\alpha\beta}}{W^{a}_{\alpha\beta}} \propto \left(\frac{\Delta}{U}\right)^{2} \ll 1, \tag{A.10}$$

where U is the energy cost for double occupancy of one of the dots. Specifically, we have neglected virtual transitions to $(1,0)$-charge states. Here, $W^{a(b)}_{\alpha\beta}$ is the transition rate from $|\alpha\rangle$ to $|\beta\rangle$ due to process $a(b)$ in Fig A.1. The purity of the initial state will be reduced by a correction of the order $\left(\frac{\Delta}{U}\right)^{2}$ which is negligible in our chosen regime.

A.3 Detuning and field dependence of current

In Fig. A.2, we show a density plot of the stationary current as a function of magnetic field and detuning for typical experimental parameters. The current shows a suppression at $B = 0$ corresponding to the zero-field dip in Fig. 2 of the main text. Solid white lines are drawn to indicate when the lowest-energy triplet state becomes the ground state (i.e., when $|g\mu_B B| > |E_{S_-}|$). Fig. 2 of the main text corresponds to a cut along $\epsilon = 0$ of Fig. A.2, indicated here with a white dashed line.

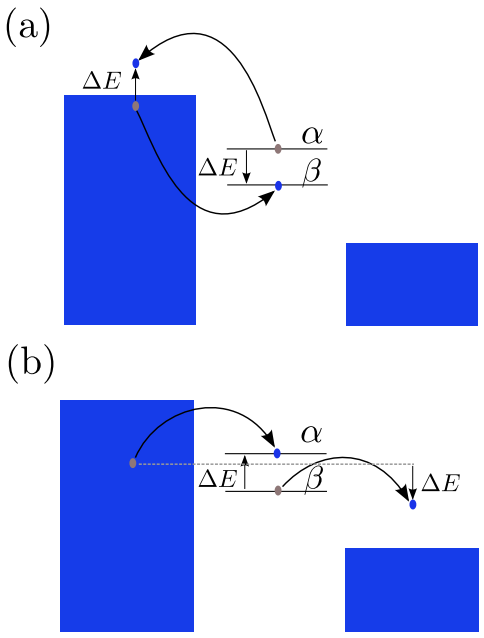

Figure A.1: $|\alpha\rangle$ and $|\beta\rangle$ are double dot energy eigenstates and $\Delta E = E_\alpha - E_\beta > 0$. a) Available cotunneling processes b) Neglected cotunneling processes

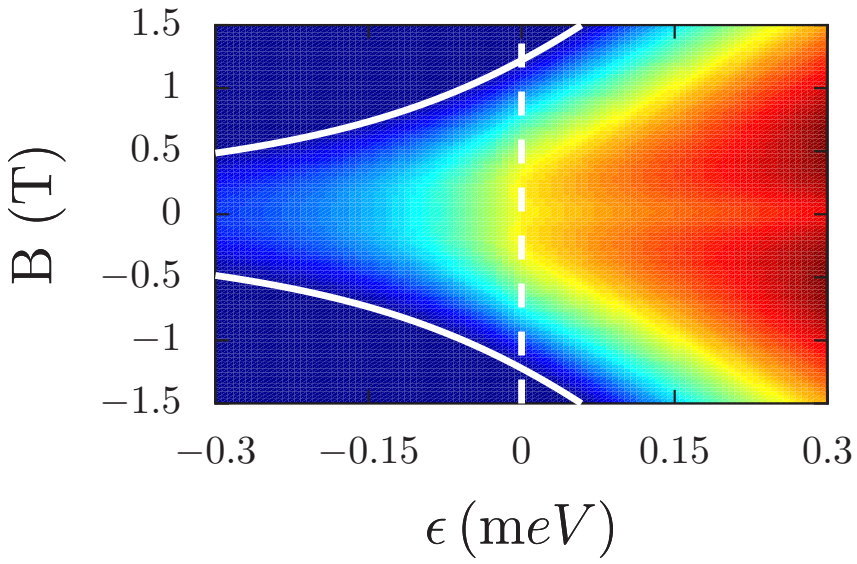

Figure A.2: Magnetic field and detuning dependence of leakage current in the spin-blockade regime. We have taken $T = 40\,\mathrm{mK}$, $\mu_L = \mu_R = 10\,\mu eV$, $t = 100\,\mu eV$, $\Delta = 1\,\mathrm{m}eV$, $\delta B = 200\,\mathrm{mT}$, and $g = 2.0$. A density plot shows a suppression in the current at $B = 0$ and a sharp cutoff when $|g\mu_B B| > |E_{S_-}|$ (solid white lines). The current runs from $I = 0$ (dark blue) to $I = 1.7\,\mathrm{pA}$ (dark red).

Appendix B

Hamiltonian and eigenstates

In this appendix we set the precise definition for the Hamiltonian and isolated double-dot eigenstates. The starting point is a standard tunneling Hamiltonian for a double quantum dot coupled to leads

$$H = H_{\rm dd} + \sum_l H_l + \sum_l H_{\rm dl}, \tag{B.1}$$

where $H_{\rm dd}$ is the Hamiltonian of the double dot, H_l describes Fermi liquid lead l, and $H_{\rm dl}$ gives the tunnel coupling between lead l and dot l, with $l = L(R)$ for the left (right) dot/lead, respectively:

$$\begin{aligned} H_{\rm dd} &= H_C + H_T + H_Z, & \text{(B.2)} \\ H_l &= \sum_{k\sigma} \epsilon_{lk\sigma} c^\dagger_{lk\sigma} c_{lk\sigma}, & \text{(B.3)} \\ H_{\rm dl} &= \sum_{k\sigma} \left(t_l c^\dagger_{lk\sigma} d_{l\sigma} + \text{h.c.} \right). & \text{(B.4)} \end{aligned}$$

Here, $c_{lk\sigma}$ annihilates an electron in lead l, orbital state k with spin σ having energy $\epsilon_{lk\sigma}$. The operator $d_{l\sigma}$ annihilates an electron in dot orbital l with spin σ. The Coulomb interaction $H_{\rm C}$, inter-dot tunneling Hamiltonian $H_{\rm T}$ and Zeeman

term $H_{\rm Z}$ are

$$H_C = \sum_l \left[\frac{U}{2} n_l(n_l - 1) - V_l n_l\right] + U' n_L n_R, \tag{B.5}$$

$$H_T = -t \sum_\sigma \left(d^\dagger_{L\sigma} d_{R\sigma} + \text{h.c.}\right), \tag{B.6}$$

$$H_Z = \frac{B}{2} \sum_l (n_{l\uparrow} - n_{l\downarrow}), \tag{B.7}$$

with number operator defined in the usual way, $n_l = \sum_\sigma n_{l\sigma}$; $n_{l\sigma} = d^\dagger_{l\sigma} d_{l\sigma}$. In the above expressions, U and U' describe the on-site and nearest-neighbor charging energies, respectively, in a constant-interaction model, V_l gives the local electrostatic potential for dot orbital l, t is the inter-dot tunnel coupling, and B is the applied magnetic field (assumed here to be in-plane so that orbital effects are negligible).

It is convenient to define new energy variables

$$\epsilon = V_R - V_L - U + U', \tag{B.8}$$

$$\Delta = V_R + V_L - U - U', \tag{B.9}$$

where physically, the energy detuning ϵ gives the relative energy difference between $(1,1)$ and $(0,2)$ charge configurations and Δ describes the absolute 'depth' of the $(1,1)$ charge configuration. Diagonalizing $H_{\rm dd}$ in the space of $(1,1)$, $(0,1)$ and $(0,2)$ charge configurations gives the eigenenergies, assuming a real positive tunnel coupling, $t > 0$ (and defining $E_0(\Delta) = -U - \Delta$):

$$E_\sigma = -E_0(\Delta) - \frac{1}{2}(\epsilon - \Delta) + \sigma B/2, \tag{B.10}$$

$$E_{T_\pm} = -E_0(\Delta) \pm B, \tag{B.11}$$

$$E_{T_0} = -E_0(\Delta), \tag{B.12}$$

$$E_{S_\pm} = -E_0(\Delta) - \frac{1}{2}\left(\epsilon \mp \sqrt{\epsilon^2 + 8t^2}\right). \tag{B.13}$$

The associated eigenstates are

$$|\sigma\rangle = d^\dagger_{R\sigma}|0\rangle\,, \tag{B.14}$$

$$|T_+\rangle = d^\dagger_{L\uparrow}d^\dagger_{R\uparrow}|0\rangle\,, \tag{B.15}$$

$$|T_-\rangle = d^\dagger_{L\downarrow}d^\dagger_{R\downarrow}|0\rangle\,, \tag{B.16}$$

$$|T_0\rangle = \frac{1}{\sqrt{2}}\left(d^\dagger_{L\uparrow}d^\dagger_{R\downarrow} + d^\dagger_{L\downarrow}d^\dagger_{R\uparrow}\right)|0\rangle\,, \tag{B.17}$$

$$|S_\pm\rangle = \sqrt{C_\pm}\,|S(1,1)\rangle \mp \sqrt{C_\mp}\,|S(0,2)\rangle\,. \tag{B.18}$$

where the hybridization of the $|S(1,1)\rangle$ and $|S(0,2)\rangle$ singlet states in $|S_\pm\rangle$ is controlled by the parameters

$$C_\pm = \frac{\sqrt{\epsilon^2+8t^2}\pm\epsilon}{2\sqrt{\epsilon^2+8t^2}}. \tag{B.19}$$

The singlets are defined more precisely in terms of creation and annihilation operators by

$$|S(1,1)\rangle = \frac{1}{\sqrt{2}}\left(d^\dagger_{L\uparrow}d^\dagger_{R\downarrow} - d^\dagger_{L\downarrow}d^\dagger_{R\uparrow}\right)|0\rangle\,, \tag{B.20}$$

$$|S(0,2)\rangle = d^\dagger_{R\uparrow}d^\dagger_{R\downarrow}|0\rangle\,. \tag{B.21}$$

Appendix C

State reduction criteria

In this appendix we show how to reduce the total number of equations from the Pauli master equation, when the decay rates for two states are of the same order. Consider two different states, say $|\uparrow\rangle$ and $|\downarrow\rangle$ with the following equations of motion,

$$\dot{\rho}_{\uparrow}(t) = -W_{\uparrow}\rho_{\uparrow}(t) + \sum_{\alpha} W_{\uparrow\alpha}\rho_{\alpha}(t), \tag{C.1}$$

$$\dot{\rho}_{\downarrow}(t) = -W_{\downarrow}\rho_{\downarrow}(t) + \sum_{\alpha} W_{\downarrow\alpha}\rho_{\alpha}(t), \tag{C.2}$$

where $W_{\sigma} = \sum_{\alpha} W_{\alpha\sigma}$ for $\sigma = \uparrow, \downarrow$. Now, writing the above equations in terms of $\rho_g^{\pm}(t)$,

$$\rho_g^{\pm}(t) \;\; = \;\; \rho_{\uparrow}(t) \pm \rho_{\downarrow}(t), \tag{C.3}$$

we can rewrite the sum and difference of Eqs. (C.1,C.2) as

$$\dot{\rho}_g^{+}(t) = -\rho_g^{+}(t)W_g^{+} + \rho_g^{-}(t)W_g^{-} + \sum_{\alpha} W_{g\alpha}^{+}\rho_{\alpha}(t), \tag{C.4}$$

$$\dot{\rho}_g^{-}(t) = -\rho_g^{-}(t)W_g^{+} + \rho_g^{+}(t)W_g^{-} + \sum_{\alpha} W_{g\alpha}^{-}\rho_{\alpha}(t). \tag{C.5}$$

Here, $W_g^{\pm} = \frac{1}{2}\sum_{\alpha}(W_{\alpha\uparrow} \pm W_{\alpha\downarrow})$ and $W_{g\alpha}^{\pm} = (W_{\uparrow\alpha} \pm W_{\downarrow\alpha})$. Assuming $\rho_{\uparrow}(0) = \rho_{\downarrow}(0) = \frac{1}{2}$, i.e., $\rho_g^{-}(0) = 0$, integrating Eq. (C.5), and using the mean-value theorem,

we find,

$$\rho_g^-(t) = \rho_g^+(\tau)\frac{W_g^-}{W_g^+}\left(1 - e^{-W_g^+ t}\right) + \\ + \sum_\alpha \rho_\alpha(\tau_\alpha)\frac{W_{g\alpha}^-}{W_g^+}\left(1 - e^{-W_g^+ t}\right) \tag{C.6}$$

where $\tau, \tau_\alpha \in [0, t]$. Noting that $\rho_g^+(\tau), \rho_\alpha(\tau_\alpha) \leq 1$ and $\left(1 - e^{-W_g^+ t}\right) \leq 1$, we can bound the value of ρ_g^- in Eq. (C.4) as

$$\rho_g^-(t) \leq \frac{W_g^- + \sum_\alpha W_{g\alpha}^-}{W_g^+}. \tag{C.7}$$

Now, if we have,

$$\left|\frac{W_g^-}{W_g^+}\right| + \left|\frac{\sum_\alpha W_{g\alpha}^-}{W_g^+}\right| \ll 1, \tag{C.8}$$

we can safely neglect $\rho_g^-(t)$ from the original Pauli master equation. In the text we neglect all the W^- contributions and use the following notation: $W_g \equiv W_g^+$, $W_{g\alpha} \equiv W_{g\alpha}^+ = (W_{\uparrow\alpha} + W_{\downarrow\alpha})$ and $W_{\alpha g} \equiv W_{\alpha g}^+ = \frac{1}{2}(W_{\alpha\uparrow} + W_{\alpha\downarrow})$.

References

[1] Veniamin A. Abalmassov and Florian Marquardt. Electron-nuclei spin relaxation through phonon-assisted hyperfine interaction in a quantum dot. *Phys. Rev. B*, 70:075313, Aug 2004. 3

[2] S. Amasha, I. J. Gelfand, M. A. Kastner, and A. Kogan. Kondo temperature dependence of the kondo splitting in a single-electron transistor. *Phys. Rev. B*, 72:045308, Jul 2005. 2

[3] S. Amasha and Massachusetts Institute of Technology. Dept. of Physics. *Electron Tunneling and Spin Relaxation in a Lateral Quantum Dot*. Massachusetts Institute of Technology, Department of Physics, 2008. 7, 17

[4] R. C. Ashoori. Electrons in artificial atoms. *Nature*, 379(6564):413–419, 02 1996. 1

[5] Lucy V. C. Assali, Helena M. Petrilli, Rodrigo B. Capaz, Belita Koiller, Xuedong Hu, and S. Das Sarma. Hyperfine interactions in silicon quantum dots. *Phys. Rev. B*, 83:165301, Apr 2011. 63

[6] Guy Austing, Chris Payette, Guolin Yu, and James Gupta. Hyperfine-coupling-programming of current through coupled quantum dots with multiple-sweep bias voltage waveforms. *Japanese Journal of Applied Physics*, 48(4):04C143, 2009. 19

[7] C. Barthel, J. Medford, C. M. Marcus, M. P. Hanson, and A. C. Gossard.

Interlaced dynamical decoupling and coherent operation of a singlet-triplet qubit. *Phys. Rev. Lett.*, 105:266808, Dec 2010. 55

[8] J. Baugh, Y. Kitamura, K. Ono, and S. Tarucha. Large nuclear overhauser fields detected in vertically coupled double quantum dots. *Phys. Rev. Lett*, 99(9):96804, 2007. 16, 19, 30, 88, 89

[9] W. Belzig. Full counting statistics of super-Poissonian shot noise in multilevel quantum dots. *Phys. Rev. B*, 71(16):161301, 2005. 77, 78, 79

[10] W. Beugeling, N. Goldman, and C. Morais Smith. Topological phases in a two-dimensional lattice: Magnetic field versus spin-orbit coupling. *Phys. Rev. B*, 86:075118, Aug 2012. 89

[11] MJ Biercuk, S. Garaj, N. Mason, JM Chow, and CM Marcus. Gate-defined quantum dots on carbon nanotubes. *Nano letters*, 5(7):1267–1271, 2005. 1

[12] Y. M. Blanter and M. Büttiker. Shot noise in mesoscopic conductors. *Physics Reports*, 336:1–166, September 2000. 69

[13] Hendrik Bluhm, Sandra Foletti, Izhar Neder, Mark Rudner, Diana Mahalu, Vladimir Umansky, and Amir Yacoby. Dephasing time of gaas electron-spin qubits coupled to a nuclear bath exceeding 200[thinsp][mu]s. *Nat Phys*, 7(2):109–113, 02 2011. 55

[14] L. Bogani and W. Wernsdorfer. Molecular spintronics using single-molecule magnets. *Nature Materials*, 7:179–186, March 2008. 80

[15] M. R. Buitelaar, J. Fransson, A. L. Cantone, C. G. Smith, D. Anderson, G. A. C. Jones, A. Ardavan, A. N. Khlobystov, A. A. R. Watt, K. Porfyrakis, et al. Pauli spin blockade in carbon nanotube double quantum dots. *Phys. Rev. B*, 77(24):245439, 2008. 30

[16] Gang Chen and Leon Balents. Spin-orbit effects in $na_4ir_3o_8$: A hyper-kagome lattice antiferromagnet. *Phys. Rev. B*, 78:094403, Sep 2008. 89

[17] Gang Chen, Rodrigo Pereira, and Leon Balents. Exotic phases induced by strong spin-orbit coupling in ordered double perovskites. *Phys. Rev. B*, 82:174440, Nov 2010. 89

[18] H. O. H. Churchill, A. J. Bestwick, J. W. Harlow, F. Kuemmeth, D. Marcos, C. H. Stwertka, S. K. Watson, and C. M. Marcus. Electron–nuclear interaction in 13c nanotube double quantum dots. *Nature Physics*, 5(5):321–326, 2009. 3, 19, 24, 27, 30, 66

[19] H. O. H. Churchill, F. Kuemmeth, J. W. Harlow, A. J. Bestwick, E. I. Rashba, K. Flensberg, C. H. Stwertka, T. Taychatanapat, S. K. Watson, and C. M. Marcus. Relaxation and dephasing in a two-electron $^{13}\mathbf{C}$ nanotube double quantum dot. *Phys. Rev. Lett.*, 102:166802, Apr 2009. 19

[20] W. A. Coish and J. Baugh. Nuclear spins in nanostructures. *Physica Status Solidi B Basic Research*, 246:2203–2215, October 2009. 16

[21] W. A. Coish, V. N. Golovach, J. C. Egues, and D. Loss. Measurement, control, and decay of quantum-dot spins. *Physica Status Solidi (b)*, 243:3658, June 2006. 69

[22] W. A. Coish and F. Qassemi. Leakage-current line shapes from inelastic cotunneling in the Pauli spin blockade regime. *Phys. Rev. B*, 84(24):245407, December 2011. 3, 4, 65

[23] William A. Coish and Daniel Loss. *Quantum Computing with Spins in Solids*. John Wiley & Sons, Ltd, 2007. 10

[24] T. A. Costi. Kondo effect in a magnetic field and the magnetoresistivity of kondo alloys. *Phys. Rev. Lett.*, 85:1504–1507, Aug 2000. 2

[25] Dimitrie Culcer, Łukasz Cywiński, Qiuzi Li, Xuedong Hu, and S. Das Sarma. Realizing singlet-triplet qubits in multivalley si quantum dots. *Phys. Rev. B*, 80:205302, Nov 2009. 67

[26] Dimitrie Culcer, Łukasz Cywiński, Qiuzi Li, Xuedong Hu, and S. Das Sarma. Quantum dot spin qubits in silicon: Multivalley physics. *Phys. Rev. B*, 82:155312, Oct 2010. 57, 61

[27] J. Danon and Y. V. Nazarov. Pauli spin blockade in the presence of strong spin-orbit coupling. *Phys. Rev. B*, 80(4):041301, 2009. 30, 52

[28] T. Delattre, C. Feuillet-Palma, L. G. Herrmann, P. Morfin, J.-M. Berroir, G. Fève, B. Plaçais, D. C. Glattli, M.-S. Choi, C. Mora, and T. Kontos. Noisy Kondo impurities. *Nature Physics*, 5:208–212, March 2009. 80

[29] I. Djuric, B. Dong, and H. L. Cui. Theoretical investigations for shot noise in correlated resonant tunneling through a quantum coupled system. *Journal of Applied Physics*, 99(6):063710, March 2006. 75

[30] M. Dolev, M. Heiblum, V. Umansky, Ady Stern, and D. Mahalu. Observation of a quarter of an electron charge at the [ngr] = 5/2 quantum hall state. *Nature*, 452(7189):829–834, 04 2008. 27

[31] G. Dresselhaus. Spin-orbit coupling effects in zinc blende structures. *Phys. Rev.*, 100:580–586, Oct 1955. 14, 15

[32] F. Elste and C. Timm. Transport through anisotropic magnetic molecules with partially ferromagnetic leads: Spin-charge conversion and negative differential conductance. *Phys. Rev. B*, 73(23):235305, June 2006. 80

[33] J. M. Elzerman, R. Hanson, L. H. Willems van Beveren, B. Witkamp, L. M. K. Vandersypen, and L. P. Kouwenhoven. Single-shot read-out of an individual electron spin in a quantum dot. *Nature*, 430:431–435, July 2004. 2, 90

[34] C. Emary, D. Marcos, R. Aguado, and T. Brandes. Frequency-dependent counting statistics in interacting nanoscale conductors. *Phys. Rev. B*, 76:161404, Oct 2007. 74

[35] H.-A. Engel and D. Loss. Detection of Single Spin Decoherence in a Quantum Dot via Charge Currents. *Phys. Rev. Lett.*, 86:4648–4651, May 2001. 86

[36] H.-A. Engel and D. Loss. Single-spin dynamics and decoherence in a quantum dot via charge transport. *Phys. Rev. B*, 65(19):195321, May 2002. 86

[37] H.-A. Engel and D. Loss. Asymmetric Quantum Shot Noise in Quantum Dots. *Physical Review Letters*, 93(13):136602–+, September 2004. 72, 74

[38] Sigurdur I. Erlingsson, Oleg N. Jouravlev, and Yuli V. Nazarov. Coherent oscillations of current due to nuclear spins. *Phys. Rev. B*, 72:033301, Jul 2005. 19

[39] Sigurdur I. Erlingsson and Yuli V. Nazarov. Hyperfine-mediated transitions between a zeeman split doublet in gaas quantum dots: The role of the internal field. *Phys. Rev. B*, 66:155327, Oct 2002. 3, 91, 92

[40] Sigurdur I. Erlingsson, Yuli V. Nazarov, and Vladimir I. Fal'ko. Nucleus-mediated spin-flip transitions in gaas quantum dots. *Phys. Rev. B*, 64:195306, Oct 2001. 3, 69, 71

[41] L. Fedichkin and A. Fedorov. Error rate of a charge qubit coupled to an acoustic phonon reservoir. *Phys. Rev. A*, 69:032311, Mar 2004. 55

[42] Jan Fischer, Mircea Trif, W.A. Coish, and Daniel Loss. Spin interactions, relaxation and decoherence in quantum dots. *Solid State Communications*, 149:1443 – 1450, 2009. <ce:title>Fundamental Phenomena and Applications of Quantum Dots</ce:title>. 16

[43] S. Foletti, H. Bluhm, D. Mahalu, V. Umansky, and A. Yacoby. Universal quantum control of two-electron spin quantum bits using dynamic nuclear polarization. *Nature Physics*, 5:903–908, December 2009. 3, 16

[44] J. Fransson and M. Råsander. Pauli spin blockade in weakly coupled double quantum dots. *Phys. Rev. B*, 73:205333, May 2006. 19, 55

[45] T. Fujisawa, D. G. Austing, Y. Tokura, Y. Hirayama, and S. Tarucha. Allowed and forbidden transitions in artificial hydrogen and helium atoms. *Nature*, 419:278–281, 2002. 31

[46] T. Fujisawa, D. G. Austing, Y. Tokura, Y. Hirayama, and S. Tarucha. Electrical pulse measurement, inelastic relaxation, and non-equilibrium transport in a quantum dot. *Journal of Physics: Condensed Matter*, 15:R1395, 2003. 30, 31

[47] G. Giedke, J. M. Taylor, D. D'Alessandro, M. D. Lukin, and A. Imamoğlu. Quantum measurement of a mesoscopic spin ensemble. *Phys. Rev. A*, 74:032316, Sep 2006. 3

[48] D. Goldhaber-Gordon, J. Göres, M. A. Kastner, Hadas Shtrikman, D. Mahalu, and U. Meirav. From the kondo regime to the mixed-valence regime in a single-electron transistor. *Phys. Rev. Lett.*, 81:5225–5228, Dec 1998. 2

[49] V. N. Golovach, M. Borhani, and D. Loss. Holonomic quantum computation with electron spins in quantum dots. *Phys. Rev. A*, 81(2):022315, February 2010. 89

[50] Vitaly N. Golovach, Alexander Khaetskii, and Daniel Loss. Phonon-induced decay of the electron spin in quantum dots. *Phys. Rev. Lett.*, 93:016601, Jun 2004. 3, 15, 22, 69

[51] V.N. Golovach, A. Khaetskii, and D. Loss. Spin relaxation at the singlet-triplet crossing in a quantum dot. *Phys. Rev. B*, 77(4):045328, 2008. 3, 52

[52] M. R. Gräber, W. A. Coish, C. Hoffmann, M. Weiss, J. Furer, S. Oberholzer, D. Loss, and C. Schönenberger. Molecular states in carbon nanotube double quantum dots. *Phys. Rev. B*, 74:075427, Aug 2006. 24

[53] R. Hanson, L. P. Kouwenhoven, J. R. Petta, S. Tarucha, and L. M. K. Vandersypen. Spins in few-electron quantum dots. *Rev. Mod. Phys.*, 79:1217–1265, Oct 2007. 5, 8, 9, 11, 13, 55, 70

[54] R. Hanson, L. H. Willems van Beveren, I. T. Vink, J. M. Elzerman, W. J. M. Naber, F. H. L. Koppens, L. P. Kouwenhoven, and L. M. K. Vandersypen. Single-shot readout of electron spin states in a quantum dot using spin-dependent tunnel rates. *Phys. Rev. Lett.*, 94:196802, May 2005. 2

[55] R. Hanson, L. M. K. Vandersypen, L. H. Willems van Beveren, J. M. Elzerman, I. T. Vink, and L. P. Kouwenhoven. Semiconductor few-electron quantum dot operated as a bipolar spin filter. *Phys. Rev. B*, 70:241304, Dec 2004. 2

[56] R. Hanson, B. Witkamp, L. M. Vandersypen, L. H. van Beveren, J. M. Elzerman, and L. P. Kouwenhoven. Zeeman Energy and Spin Relaxation in a One-Electron Quantum Dot. *Phys. Rev. Lett.*, 91(19):196802, November 2003. 69

[57] H. B. Heersche, Z. De Groot, J. A. Folk, H. S. J. Van der Zant, C. Romeike, M. R. Wegewijs, L. Zobbi, D. Barreca, E. Tondello, and A. Cornia. Electron transport through single mn_ {12} molecular magnets. *Phys. Rev. Lett*, 96(20):206801, 2006. 29

[58] S. Hershfield, J. H. Davies, P. Hyldgaard, C. J. Stanton, and J. W. Wilkins. Zero-frequency current noise for the double-tunnel-junction Coulomb blockade. *Phys. Rev. B*, 47:1967–1979, January 1993. 74

[59] J. Iñarrea, G. Platero, and A. H. MacDonald. Electronic transport through a double quantum dot in the spin-blockade regime: Theoretical models. *Phys. Rev. B*, 76(8):085329, 2007. 19, 30

[60] A. C. Johnson, J. R. Petta, C. M. Marcus, M. P. Hanson, and A. C. Gossard. Singlet-triplet spin blockade and charge sensing in a few-electron double quantum dot. *Phys. Rev. B*, 72:165308, Oct 2005. 14, 55, 59, 60, 61, 63, 69, 70

[61] O. N. Jouravlev and Y. V. Nazarov. Electron transport in a double quantum dot governed by a nuclear magnetic field. *Phys. Rev. Lett*, 96(17):176804, 2006. 19, 30

[62] B. E. Kane. A silicon-based nuclear spin quantum computer. *Nature*, 393:133–137, May 1998. 2

[63] C. L. Kane and E. J. Mele. Quantum spin hall effect in graphene. *Phys. Rev. Lett.*, 95:226801, Nov 2005. 89

[64] M. I. Katsnelson, K. S. Novoselov, and A. K. Geim. Chiral tunnelling and the Klein paradox in graphene. *Nature Physics*, 2:620–625, September 2006. 1, 2

[65] Alexander V. Khaetskii, Daniel Loss, and Leonid Glazman. Electron spin decoherence in quantum dots due to interaction with nuclei. *Phys. Rev. Lett.*, 88:186802, Apr 2002. 3, 16

[66] Alexander V. Khaetskii and Yuli V. Nazarov. Spin relaxation in semiconductor quantum dots. *Phys. Rev. B*, 61:12639–12642, May 2000. 69

[67] Alexander V. Khaetskii and Yuli V. Nazarov. Spin-flip transitions between zeeman sublevels in semiconductor quantum dots. *Phys. Rev. B*, 64:125316, Sep 2001. 3, 69, 71, 91, 92

[68] D. Klauser, W. A. Coish, and Daniel Loss. Nuclear spin state narrowing via gate-controlled rabi oscillations in a double quantum dot. *Phys. Rev. B*, 73:205302, May 2006. 3

[69] A. Kogan, S. Amasha, D. Goldhaber-Gordon, G. Granger, M. A. Kastner, and Hadas Shtrikman. Measurements of kondo and spin splitting in single-electron transistors. *Phys. Rev. Lett.*, 93:166602, Oct 2004. 2

[70] Andrei Kogan, Sami Amasha, and M. A. Kastner. Photon-induced kondo satellites in a single-electron transistor. *Science*, 304(5675):1293–1295, 2004. 2

[71] J. König, H. Schoeller, and G. Schön. Cotunneling at resonance for the single-electron transistor. *Physical review letters*, 78(23):4482–4485, 1997. 23, 39

[72] Markus König, Hartmut Buhmann, Laurens W. Molenkamp, Taylor Hughes, Chao-Xing Liu, Xiao-Liang Qi, and Shou-Cheng Zhang. The quantum spin hall effect: Theory and experiment. *Journal of the Physical Society of Japan*, 77(3):031007, 2008. 89

[73] F. H. L. Koppens, C. Buizert, K. J. Tielrooij, I. T. Vink, K. C. Nowack, T. Meunier, L. P. Kouwenhoven, and L. M. K. Vandersypen. Driven coherent oscillations of a single electron spin in a quantum dot. *Nature*, 442(7104):766–771, 2006. 2, 18, 19, 20, 25, 27, 29, 55

[74] F. H. L. Koppens, J. A. Folk, J. M. Elzerman, R. Hanson, L. H. W. van Beveren, I. T. Vink, H. P. Tranitz, W. Wegscheider, L. P. Kouwenhoven, and L. M. K. Vandersypen. Control and Detection of Singlet-Triplet Mixing in a Random Nuclear Field. *Science*, 309:1346–1350, 2005. 3, 19, 24, 27, 30, 55, 60, 61, 63, 70

[75] F. H. L. Koppens, K. C. Nowack, and L. M. K. Vandersypen. Spin echo of a single electron spin in a quantum dot. *Phys. Rev. Lett.*, 100:236802, Jun 2008. 18

[76] A. N. Korotkov. Intrinsic noise of the single-electron transistor. *Phys. Rev. B*, 49:10381–10392, April 1994. 69, 74

[77] L. P. Kouwenhoven, C. M. Marcus, P. L. McEuen, S. Tarucha, R. M. Westervelt, and N. S. Wingreen. Electron transport in quantum dots. In L. L. Sohn, L. P. Kouwenhoven, and G. Schön, editors, *Mesoscopic Electron Transport*. Kluwer Academic Publishers, Dordrecht, Boston, London, 1997. 1

[78] M. Kroutvar, Y. Ducommun, D. Heiss, M. Bichler, D. Schuh, G. Abstreiter, and J. J. Finley. Optically programmable electron spin memory using semiconductor quantum dots. *nature*, 432:81–84, November 2004. 2

[79] N. S. Lai, W. H. Lim, C. H. Yang, F. A. Zwanenburg, W. A. Coish, F. Qassemi, A. Morello, and A. S. Dzurak. Pauli Spin Blockade in a Highly Tunable Silicon Double Quantum Dot. *Sci. Rep.*, 1:110, 2011. 3, 4, 14, 30, 31, 47, 52, 70

[80] D. Leonard, M. Krishnamurthy, C. M. Reaves, S. P. Denbaars, and P. M. Petroff. Direct formation of quantum-sized dots from uniform coherent islands of InGaAs on GaAs surfaces. *Applied Physics Letters*, 63:3203–3205, December 1993. 1

[81] L. S. Levitov. *The Statistical Theory of Mesoscopic Noise*, volume 97 of *NATO Science Series*. Springer eBook, 2003. 77

[82] W. H. Lim, F. A. Zwanenburg, H. Huebl, M. Möttönen, K. W. Chan, A. Morello, and A. S. Dzurak. Observation of the single-electron regime in a highly tunable silicon quantum dot. *Applied Physics Letters*, 95(24):242102, December 2009. 57

[83] H. W. Liu, T. Fujisawa, T. Hayashi, and Y. Hirayama. Pauli spin blockade in cotunneling transport through a double quantum dot. *Phys. Rev. B*, 72(16):161305, 2005. 3, 19, 23, 30, 31, 40

[84] H. W. Liu, T. Fujisawa, Y. Ono, H. Inokawa, A. Fujiwara, K. Takashina, and Y. Hirayama. Pauli-spin-blockade transport through a silicon double quantum dot. *Phys. Rev. B*, 77(7):073310, 2008. 3, 19, 30, 55, 61

[85] D. Loss and D. P. Divincenzo. Quantum computation with quantum dots. *Phys. Rev. A*, 57:120–126, 1998. 2, 19, 29, 55, 68

[86] D. Loss, F. L. Pedrocchi, and A. J. Leggett. Absence of Spontaneous Magnetic Order of Lattice Spins Coupled to Itinerant Interacting Electrons in One and Two Dimensions. *Physical Review Letters*, 107(10):107201, September 2011. 3, 16

[87] S. Loth, M. Etzkorn, C. P. Lutz, D. M. Eigler, and A. J. Heinrich. Measurement of fast electron spin relaxation times with atomic resolution. *Science*, 329(5999):1628, 2010. 29, 68

[88] N. Mason, M. J. Biercuk, and C. M. Marcus. Local gate control of a carbon nanotube double quantum dot. *Science*, 303(5658):655–658, 2004. 1

[89] Yigal Meir, Ned S. Wingreen, and Patrick A. Lee. Low-temperature transport through a quantum dot: The anderson model out of equilibrium. *Phys. Rev. Lett.*, 70:2601–2604, Apr 1993. 2

[90] I. A. Merkulov, Al. L. Efros, and M. Rosen. Electron spin relaxation by nuclei in semiconductor quantum dots. *Phys. Rev. B*, 65:205309, Apr 2002. 63

[91] B. T. Miller, W. Hansen, S. Manus, R. J. Luyken, A. Lorke, J. P. Kotthaus, S. Huant, G. Medeiros-Ribeiro, and P. M. Petroff. Few-electron ground states of charge-tunable self-assembled quantum dots. *Phys. Rev. B*, 56:6764–6769, Sep 1997. 1

[92] F. Molitor, S. Dröscher, J. Güttinger, A. Jacobsen, C. Stampfer, T. Ihn, and K. Ensslin. Transport through graphene double dots. *Applied Physics Letters*, 94(22):222107, June 2009. 1

[93] Joel E. Moore and Xiao-Gang Wen. Anomalous magnetic splitting of the kondo resonance. *Phys. Rev. Lett.*, 85:1722–1725, Aug 2000. 2

[94] Andrea Morello, Jarryd J. Pla, Floris A. Zwanenburg, Kok W. Chan, Kuan Y. Tan, Hans Huebl, Mikko Mottonen, Christopher D. Nugroho, Changyi Yang, Jessica A. van Donkelaar, Andrew D. C. Alves, David N. Jamieson, Christopher C. Escott, Lloyd C. L. Hollenberg, Robert G. Clark, and Andrew S. Dzurak. Single-shot readout of an electron spin in silicon. *Nature*, 467(7316):687–691, 10 2010. 55

[95] S. Nadj-Perge, S. M. Frolov, E. P. A. M. Bakkers, and L. P. Kouwenhoven.

Spin-orbit qubit in a semiconductor nanowire. *Nature*, 468(7327):1084–1087, 12 2010. 55

[96] S. Nadj-Perge, S. M. Frolov, J. W. W. Van Tilburg, J. Danon, Y. V. Nazarov, R. Algra, E. Bakkers, and L. P. Kouwenhoven. Disentangling the effects of spin-orbit and hyperfine interactions on spin blockade. *Physical Review B*, 81(20):201305, 2010. 30

[97] K. C. Nowack, F. H. L. Koppens, Yu. V. Nazarov, and L. M. K. Vandersypen. Coherent control of a single electron spin with electric fields. *Science*, 318(5855):1430–1433, 2007. 18, 19

[98] K. Ono, D. G. Austing, Y. Tokura, and S. Tarucha. Current rectification by pauli exclusion in a weakly coupled double quantum dot system. *Science*, 297(5585):1313, 2002. 2, 14, 19, 29, 55, 69, 70

[99] K. Ono and S. Tarucha. Nuclear-spin-induced oscillatory current in spin-blockaded quantum dots. *Phys. Rev. Lett*, 92(25):256803, 2004. 3, 19, 29, 30, 88

[100] A. Pályi and G. Burkard. Hyperfine-induced valley mixing and the spin-valley blockade in carbon-based quantum dots. *Phys. Rev. B*, 80(20):201404, 2009. 31, 57, 61

[101] A. Pályi and G. Burkard. Spin-valley blockade in carbon nanotube double quantum dots. *Phys. Rev. B*, 82(15):155424, 2010. 31

[102] J. R. Petta, A. C. Johnson, J. M. Taylor, E. A. Laird, A. Yacoby, M. D. Lukin, C. M. Marcus, M. P. Hanson, and A. C. Gossard. Coherent manipulation of coupled electron spins in semiconductor quantum dots. *Science*, 309(5744):2180, 2005. 2, 18, 29, 55, 70

[103] J. R. Petta, A. C. Johnson, A. Yacoby, C. M. Marcus, M. P. Hanson, and A. C. Gossard. Pulsed-gate measurements of the singlet-triplet relaxation

time in a two-electron double quantum dot. *Phys. Rev. B*, 72(16):161301, 2005. 29, 69

[104] J. R. Petta, H. Lu, and A. C. Gossard. A Coherent Beam Splitter for Electronic Spin States. *Science*, 327:669–, February 2010. 3

[105] A. Pfund, I. Shorubalko, K. Ensslin, and R. Leturcq. Suppression of spin relaxation in an inas nanowire double quantum dot. *Phys. Rev. Lett*, 99(3):36801, 2007. 24, 27, 30, 70

[106] M. Pioro-Ladriere, M. Ciorga, J. Lapointe, P. Zawadzki, M. Korkusiński, P. Hawrylak, and A. S. Sachrajda. Spin-blockade spectroscopy of a two-level artificial molecule. *Phys. Rev. Lett*, 91(2):26803, 2003. 29

[107] M. Pioro-Ladriere, T. Obata, Y. Tokura, Y.S. Shin, T. Kubo, K. Yoshida, T. Taniyama, and S. Tarucha. Electrically driven single-electron spin resonance in a slanting zeeman field. *Nature Physics*, 4(10):776–779, 2008. 18, 19, 20, 29

[108] M. B. Plenio and P. L. Knight. The quantum-jump approach to dissipative dynamics in quantum optics. *Rev. Mod. Phys.*, 70:101–144, Jan 1998. 81

[109] F. Qassemi, W. A. Coish, and F. K. Wilhelm. Stationary and transient leakage current in the pauli spin blockade. *Phys. Rev. Lett*, 102(17):176806, 2009. 3, 30, 31, 36, 38, 39, 40, 42, 50, 51, 63, 65, 70, 71, 74, 80, 84, 85

[110] Iuliana P. Radu, J. B. Miller, C. M. Marcus, M. A. Kastner, L. N. Pfeiffer, and K. W. West. Quasi-particle properties from tunneling in the v = 5/2 fractional quantum hall state. *Science*, 320(5878):899–902, 2008. 27

[111] I. E. Rashba. Properties of semiconductors with an extremum loop .1. cyclotron and combinational resonance in a magnetic field perpendicular to the plane of the loop. *Sov. Phys. Solid State*, (2):1109, 1960. 14, 15

[112] P. Recher, E. V. Sukhorukov, and D. Loss. Quantum Dot as Spin Filter and Spin Memory. *Physical Review Letters*, 85:1962–1965, August 2000. 2, 22

[113] D. J. Reilly, J. M. Taylor, J. R. Petta, C. M. Marcus, M. P. Hanson, and A. C. Gossard. Suppressing spin qubit dephasing by nuclear state preparation. *Science*, 321(5890):817–821, 2008. 18

[114] M. S. Rudner, F. H. L. Koppens, J. A. Folk, L. M. K. Vandersypen, and L. S. Levitov. Nuclear spin dynamics in double quantum dots: Fixed points, transients, and intermittency. *Physical Review B*, 84(7):075339, August 2011. 16, 88

[115] M. S. Rudner and L. S. Levitov. Self-polarization and dynamical cooling of nuclear spins in double quantum dots. *Phys. Rev. Lett*, 99(3):36602, 2007. 3, 16, 19, 30, 88, 89

[116] M. S. Rudner and L. S. Levitov. Phase transitions in dissipative quantum transport and mesoscopic nuclear spin pumping. *Physical Review B*, 82(15):155418, October 2010. 3

[117] M. S. Rudner, L. M. K. Vandersypen, V. Vuletić, and L. S. Levitov. Generating Entanglement and Squeezed States of Nuclear Spins in Quantum Dots. *Physical Review Letters*, 107(20):206806, November 2011. 3

[118] Pablo San-Jose, Gergely Zarand, Alexander Shnirman, and Gerd Schön. Geometrical spin dephasing in quantum dots. *Phys. Rev. Lett.*, 97:076803, Aug 2006. 3

[119] R. Sánchez, S. Kohler, and G. Platero. Spin correlations in spin blockade. *New Journal of Physics*, 10(11):115013, November 2008. 80

[120] Sami Sapmaz, Carola Meyer, Piotr Beliczynski, Pablo Jarillo-Herrero, and Leo P. Kouwenhoven. Excited state spectroscopy in carbon nanotube double quantum dots. *Nano Letters*, 6(7):1350–1355, 2006. 1

[121] Eran Sela, Yuval Oreg, Felix von Oppen, and Jens Koch. Fractional shot noise in the kondo regime. *Phys. Rev. Lett.*, 97:086601, Aug 2006. 27, 80

[122] N. Shaji, C. B. Simmons, M. Thalakulam, L. J. Klein, H. Qin, H. Luo, D. E. Savage, M. G. Lagally, A. J. Rimberg, R. Joynt, et al. Spin blockade and lifetime-enhanced transport in a few-electron si/sige double quantum dot. *Nature Physics*, 4(7):540–544, 2008. 19, 30, 57

[123] C. B. Simmons, J. R. Prance, B. J. Van Bael, Teck Seng Koh, Zhan Shi, D. E. Savage, M. G. Lagally, R. Joynt, Mark Friesen, S. N. Coppersmith, and M. A. Eriksson. Tunable spin loading and T_1 of a silicon spin qubit measured by single-shot readout. *Phys. Rev. Lett.*, 106:156804, Apr 2011. 55

[124] C. B. Simmons, Madhu Thalakulam, Nakul Shaji, Levente J. Klein, Hua Qin, R. H. Blick, D. E. Savage, M. G. Lagally, S. N. Coppersmith, and M. A. Eriksson. Single-electron quantum dot in si/sige with integrated charge sensing. *Applied Physics Letters*, 91(21):213103, 2007. 67

[125] F. M. Souza, J. C. Egues, and A. P. Jauho. Quantum dot as a spin-current diode: A master-equation approach. *Phys. Rev. B*, 75(16):165303, April 2007. 80

[126] F. M. Souza, A. P. Jauho, and J. C. Egues. Spin-polarized current and shot noise in the presence of spin flip in a quantum dot via nonequilibrium Green's functions. *Phys. Rev. B*, 78(15):155303, October 2008. 80

[127] G. A. Steele, G. Gotz, and L. P. Kouwenhoven. Tunable few-electron double quantum dots and Klein tunnelling in ultraclean carbon nanotubes. *Nature Nanotechnology*, 4:363–367, June 2009. 2

[128] Charles Tahan, Mark Friesen, and Robert Joynt. Decoherence of electron spin qubits in si-based quantum computers. *Phys. Rev. B*, 66:035314, Jul 2002. 55

[129] S. Tarucha, D. G. Austing, T. Honda, R. J. van der Hage, and L. P. Kouwenhoven. Shell filling and spin effects in a few electron quantum dot. *Phys. Rev. Lett.*, 77:3613–3616, Oct 1996. 1

[130] N. C. van der Vaart, S. F. Godijn, Y. V. Nazarov, C. J. P. M. Harmans, J. E. Mooij, L. W. Molenkamp, and C. T. Foxon. Resonant tunneling through two discrete energy states. *Phys. Rev. Lett.*, 74:4702–4705, Jun 1995. 23

[131] W. G. van der Wiel, S. De Franceschi, J. M. Elzerman, T. Fujisawa, S. Tarucha, and L. P. Kouwenhoven. Electron transport through double quantum dots. *Rev. Mod. Phys.*, 75:1–22, Dec 2002. 8, 10, 58, 59

[132] A. B. Vorontsov and M. G. Vavilov. Spin relaxation in quantum dots due to electron exchange with leads. *Phys. Rev. Lett*, 101(22):226805, 2008. 3, 19, 23, 30, 31, 40

[133] S. K. Watson, R. M. Potok, C. M. Marcus, and V. Umansky. Experimental Realization of a Quantum Spin Pump. *Physical Review Letters*, 91(25):258301, December 2003. 2

[134] Ireneusz Weymann. Effects of different geometries on the conductance, shot noise, and tunnel magnetoresistance of double quantum dots. *Phys. Rev. B*, 78:045310, Jul 2008. 19

[135] Wayne M. Witzel, Malcolm S. Carroll, Andrea Morello, Łukasz Cywiński, and S. Das Sarma. Electron spin decoherence in isotope-enriched silicon. *Phys. Rev. Lett.*, 105:187602, Oct 2010. 55

[136] S. A. Wolf, D. D. Awschalom, R. A. Buhrman, J. M. Daughton, S. von Molnár, M. L. Roukes, A. Y. Chtchelkanova, and D. M. Treger. Spintronics: A Spin-Based Electronics Vision for the Future. *Science*, 294:1488–1495, November 2001. 68

[137] M. Xiao, M. G. House, and H. W. Jiang. Measurement of the spin relaxation

time of single electrons in a silicon metal-oxide-semiconductor-based quantum dot. *Phys. Rev. Lett.*, 104:096801, Mar 2010. 55

[138] G. Yamahata, T. Kodera, H. O. H. Churchill, K. Uchida, C. M. Marcus, and S. Oda. Magnetic field dependence of Pauli spin blockade: A window into the sources of spin relaxation in silicon quantum dots. *Phys. Rev. B*, 86(11):115322, September 2012. 3, 14, 69

[139] S. Yang, X. Wang, and S. Das Sarma. Generic Hubbard model description of semiconductor quantum-dot spin qubits. *Phys. Rev. B*, 83(16):161301, April 2011. 10

[140] O. Zarchin, M. Zaffalon, M. Heiblum, D. Mahalu, and V. Umansky. Two-electron bunching in transport through a quantum dot induced by Kondo correlations. *Phys. Rev. B*, 77(24):241303, June 2008. 80

[141] P. Zoller, M. Marte, and D. F. Walls. Quantum jumps in atomic systems. *Phys. Rev. A*, 35:198–207, Jan 1987. 81